THESIS

METHOD DEVELOPMENT FOR LONG-TERM LABORATORY STUDIES EVALUATING CONTAMINANT ASSIMILATION PROCESSES

Submitted by

Rachael Lynne McSpadden

Department of Civil and Environmental Engineering

In partial fulfillment of the requirements

For the Degree of Master of Science

Colorado State University

Fort Collins, Colorado

Fall 2016

Master's Committee:

Advisor: Tom Sale

Jens Blotevogel
Greg Butters

ABSTRACT

METHOD DEVELOPMENT FOR LONG-TERM LABORATORY STUDIES EVALUATING CONTAMINANT ASSIMILATION PROCESSES IN LOW-K ZONES

Remediation technologies for soil and groundwater that are impacted by chlorinated solvents are limited when reducing contaminant concentrations below maximum contaminant levels (MCLs) established by the US Environmental Protection Agency (EPA). The limited effectiveness of current technologies is partly due to well-documented contaminant back diffusion from low-permeability (k) zones causing long-term impacts on water quality. Back diffusion out of low-k zones for extended periods of time, give strong evidence that assimilation processes are driving the fate and transport of chlorinated solvents within low-k zones. The direct impacts assimilation processes, such as sorption and degradation, have on contaminant concentrations may be slow and negligible on shorter time scales. But for longer time scales assimilation processes could have consequential effects on sites where groundwater concentrations are predicted to exceed MCLs for decades to centuries. Research studies located in the field have been carried out to study assimilation processes in low-k zones. The challenge of such field studies is capturing complete data sets from complex field environments. The challenges include inability to close the mass balance, confidently identifying assimilation mechanisms at work, and are limited to short term studies. Thus, the overall objective of this research is to advance the current knowledge of assimilative processes within low-k zones through the application of long-term (~5-10years) laboratory studies.

The goal of the research presented herein, is to create a starting point for long-term laboratory studies in the hopes to quantify assimilation processes within low-k zones. Prior to conducting long-term laboratory experiments, a necessary step of establishing and testing methods need to be conducted. The research described within this thesis applies the use of short-term laboratory studies conducted over a 2 to 3 month time span to test preliminary methods, establish baseline data, and test applicability of mathematical models.

The model contaminant used for the short-term laboratory experiments was tetrachloroethene (PCE). For the beginning stages of method development, the assimilation process that was isolated and focused on was sorption. Sorption was evaluated in porous media of differing properties, which included four field soils (Soil A, B, C, and D) and one lab grade soil (LGS). Two short-term column studies were tested to evaluate for viability in collecting data to be used in capturing transport and assimilation processes for use in long-term laboratory studies. The two short-term column study methods are identified throughout this document as headspace vials and ampules. The design setup for both column studies were constructed to utilize diffusive transport of contaminant with a saturated lower boundary layer of PCE, an initially clean water saturated soil column, and headspace at the upper boundary layer. For each column study design, the contaminant is transported via passive diffusion, starting from a volume of high concentration (at the lower boundary layer) to a place of low concentration (throughout the clean soil and the top of the headspace to the clean upper boundary layer). The difference between the two short-term column studies is the method of data collection. The headspace vial method allows for non-destructive sampling of the headspace over time to quantify the diffusive transport of PCE through the soil column. The ampule method utilizes a completely closed system with a destructive sampling technique where the entire ampule is extracted within

methanol to help eliminate the potential for mass lost from the system due to volatilization. In addition to the two short-term column studies, batch sorption studies were conducted to gain independent measurements of sorption parameters for the four field soils used throughout the column experiments. Lastly, a numerical solution to the diffusive transport partial differential equation was developed using Mathcad^{TM}. Three sorption models are employed: linear, Freundlich and Langmuir models. The parameter values from the batch sorption study were used as inputs for the mathematical model and results were compared to the short-term column study headspace vial experiment.

Results from the short-term column studies show that losses from headspace vials may limit the values of the method over time periods greater than one week, but ampules are more stable than headspace vials and show the most potential for application in long-term laboratory studies. Batch sorption studies can complement the diffusive-transport studies by allowing for resolution of sorption parameter values that are independent of transport rates. The validity of the model appears to be challenged by unaccounted losses from the headspace vials, and was therefore unable to estimate experimental data results.

The results of the ampules and batch sorption studies are suggested to be used to aid in the design of the long-term studies. The laboratory experiments and modeling described herein will, in hopes, be a step closer to advance the knowledge of assimilative processes and assist in determining the assimilative capacity of low-k zones. Ultimately, this work will hopefully contribute to improved decision-making at contaminated sites, possibly allowing money spent on ineffective remedies to be directed toward more productive solutions.

ACKNOWLEDGEMENTS

I would like to acknowledge the following groups and individuals for their part in supporting the work of this thesis:

First, I would like to thank my advisor Tom Sale for helping me understand the purpose and drive for my research. Knowing the larger applications of my research helped bring passion and drive that may otherwise have been lost.

I would also like to thank my unofficial co-advisor Mitch Olson. Mitch had many useful insights for my research. He was always there to guide, support, provide knowledge, as well as a bottomless pit of patience throughout this entire research journey. I would also like to thank my committee members Jens Blotevogel and Greg Butters, for continually teaching me both in and out of the classroom.

I would also like to thank the following people for their input and suggestions throughout the research development: Fred Payne, John Wilson, Thomas Borch, and Michael Olson. This work would not have been possible without the Arcadis research gift to CSU.

I owe so much gratitude to all the people that I worked with at the Center for Contaminant Hydrology. My colleagues, who were also my lab mates, friends, psychologists, running partners, tennis Tuesday pals, and hiking buddies: Eric Emerson, Marc Chalfant, Zoe Bezold, Molly McLaughlin, Missy Tracy, Calista Campbell, Maria Irianni-Renno, Gary Dick, Kevin Saller, Helen Dungan, Christina Ankrom, Nolan Platt.

I would like to thank Alex Amchislavskiy for putting up with my antics, you are so supportive with everything I do, and this was no exception.

And last but certainly never least, I would like to thank my wonderful, supportive family for making me the person I am today. You all have taught me so much and have encouraged me to strive and push toward all of my goals. I love you all so much. B”H for amazing people to be by my side through it all.

TABLE OF CONTENTS

LIST OF TABLES

LIST OF FIGURES

1. INTRODUCTION

The following provides an introduction to this thesis document including a problem statement, background on subsurface releases of chlorinated solvents, hypotheses for this research, and the overall organization for this document. Information presented in this section provides a foundation for subsequent chapters.

1.1. Problem Statement

Chlorinated solvents such as tetrachloroethene (PCE) and trichloroethene (TCE) can be persistent groundwater contaminants (Stroo et al.2012). PCE and TCE have been used in applications such as dry cleaning and degreasing operations. Although production and use of chlorinated solvents have decreased, while the implementation of better management practices has increased, spills that occurred prior to these changes are still causing major impacts to groundwater. The Environmental Protection Agency (EPA) as well as state regulatory departments have implemented remedial programs with the goal of preventing exposure, reducing risk, and restoring sites to beneficial use. Even with intense remedial efforts, chlorinated solvent plumes have remained persistent and affect groundwater quality many years after release and treatment (Mackay and Cherry 1989, NRC 2013).

A recent survey, addressing the efficacy of current and past remediation efforts to measure success in the closing of chlorinated solvent sites (Geosyntec 2004), revealed that out of 139 remediation sites none of the sites were deemed fully successful in proper closure (with >80% reduction in mass flux, >80% mass removal, and no rebound) . Two sites were deemed "successful" only when the criteria were lowered to >61% reduction in mass flux, >80% mass removal, and no rebound. Both of these sites were pilot-scale applications in homogeneous sand.

The study found that the inability to close a site was due in part to the heterogeneous nature of the subsurface media and the limited effectiveness of current remediation technologies within heterogeneous media.

Field and laboratory studies have looked into different remediation technologies to find the most effective remediation treatment in heterogeneous materials (Goldstein et al. 2004, Saller 2014). Both studies found that treatments were effective in reducing concentrations to non-detect levels, but shortly after treatment ended, there was a rebound of concentrations that eventually rose to pre-treatment levels. Rebound commonly found within contaminated sites is often caused by back diffusion out of low-permeability (k) zones (Liu and Ball 2002, Parker et al. 2004, Chapman and Parker 2005, Sale et al. 2008, Parker et al. 2008, Wahlberg 2012, and Chapman et al. 2012). Recontamination of the transmissive zones in aquifers due to back diffusion from low-k zones can have substantial impacts on groundwater for extended periods of time (Stroo et al. 2012, Newell and Sale 2010). The slow release of contaminants from low-k zones challenges current concepts about cleanup standards, risks, and management of contaminated sites.

A key knowledge gap involves the sorption and degradation processes that control long-term release from low-k zones. The use of predictive models to estimate appropriately long-term impacts of plumes is common. A general lack of understanding in what drives the transport and flux into and out of low-k zones restricts our predictive models' ability to forecast future behavior. Limitations of predictive models will further affect the management of sites and will increase ineffective site management decisions. Without appropriate decision-making tools to manage contaminated sites, NRC (2012) estimates that by 2033 expenditures for soil and groundwater cleanup alone will exceed over $200 billion. The central theme of this work is to develop experimental methods in support of long-term studies to better understand the processes

that drive contaminant fate and transport within low-k zones. This knowledge will support rational decisions to manage chlorinated solvent sites and will encourage more effective and sustainable contaminant site management.

The process referred to as assimilative capacity is defined by the ability of subsurface media, under natural conditions, to sorb and/or degrade the original contaminant. Assimilative capacity can have substantial impacts on the overall longevity of the contaminant plume and may reduce the contaminant mass that needs to be treated within the site. Over long periods of time, the most important process in plumes may be occurring in low-k zones (Takeuchi et al. 2011, Wahlberg 2012,). Although assimilative processes (sorption and degradation) are recognized to occur within the subsurface, the extent of their impacts on contaminant fate and transport within low-k zones are poorly understood.

1.2. Hypotheses

Building on the above statement, subsurface media have an assimilation capacity for chlorinated solvents that can have a substantial impact on contaminant concentrations in the transmissive zone. The assimilation capacity of low-k zones involves potentially slow processes, including sorption and degradation (abiotic and biotic).

The overarching goals of the research are to establish long-term laboratory (~5-10 years) study methods to capture and quantify the slow processes that are currently poorly understood. The longer time frames will help to reveal critical processes missed by conventional laboratory and field studies with shorter duration. To enhance our likelihood of success, we must ensure that laboratory experiments have stable controls. Short-term laboratory studies will provide a guide to experimental design, sampling methods, and baseline data.

The hypotheses for research concerning details within this document are:

- Headspace vials using Mininert® valve caps can be used to take non-destructive, headspace samples to establish the aqueous concentration at the top of a soil column to understand transport of PCE through the soil.
- Ampules can reduce volatile losses and increase recovery of mass within the system.
- Batch sorption studies applying varying PCE concentration to porous media can be used to independently resolve appropriate model and sorption parameter values, and find the best model type to fit the headspace vial data.
- Numerical mathematical models can help in understanding the headspace vial system and bring to light other issues with headspace vials methods that the simple data collection may not bring to light.

1.3. Objectives

The overarching goals of this research are to develop methods that can be used to:

- Advance our knowledge of assimilative capacities in low-k zones
- Improve our understanding of the factors that govern plume longevity
- Provide decision-making tools to manage contaminated sites

Goals and objectives specific to the research presented in this document are to:

- Ensure rigorous mass balances, sampling methods, and experimental design
- Establish baseline data and loss rates
- Apply preliminary data to a working model

- Apply models to larger spatial and temporal analyses

1.4. Organization and Content

This work is organized into four chapters. The first chapter contains the introduction. Chapter 2 is a literature review, which presents related work. Chapter 3 describes laboratory experiments, outlining the six different laboratory experiments used to help develop methods for long-term laboratory studies of low-k zones processes with results. Chapter 4 presents the mathematical modeling, which will be applied to experimental data gathered from Chapter 3 to help gain insight into characterizing, quantifying, and predicting processes that dominate within the soil. Lastly, Chapter 5 concludes with the key findings of the research presented herein, implications, and suggestions for future work.

2. LITERATURE REVIEW

This chapter introduces key concepts that pertain to this thesis. The Literature Review serves to build a foundation for the research contained within this document, as well as expose any knowledge gaps. Sections within this chapter include: Conceptual Overview, Current Models, and Long-Term Processes. The Conceptual Overview presents the current understanding of contaminant fate and transport of chlorinated solvents in heterogeneous media. Section 2.2 discusses how models predict and approximate contaminant flux due to processes within low-k zones. Lastly, Section 2.3 discusses the two main processes, sorption and degradation, which control the flux of contaminants within low-k zones.

2.1. Conceptual Overview

Natural subsurface media have a large amount of heterogeneity affecting the fate and transport of contaminants. Specifically, concerning chlorinated solvents within the subsurface media, elements of heterogeneity include permeability, sorption capacity, mineralogy, and redox conditions. Historically, studies of contaminant transport were based on the assumption that the subsurface was homogenous (Bear 1988); whereas, modern contaminant hydrology embraces the importance of subsurface heterogeneity (Chapman and Parker 2005, Sale et al. 2013). Rigorous characterization of heterogeneous subsurface with a high amount of detail is rarely possible. Instead, a common practice is to develop a site conceptual model that captures the critical elements of a system in a stylistic fashion.

A simple conceptual model is that of transmissive and low-permeability (k) zones. Transmissive and low-k zones can be defined in terms of mobile and immobile pore space, respectively (Payne et al. 2008). We can further delineate and define transmissive and low-k zones in more relative

terms by the depositional energy that formed each zone. Generally, transmissive zones were deposited under higher depositional energy, creating bodies with coarser materials. The physical attributes of transmissive zones lead to characteristics where advective transport primarily dominates, provides for more oxidized environments, and tends to have a lower fraction of organic carbon per volume porous media. Commonly, higher depositional energies do not occur as regularly as lower depositional energies causing transmissive zones to construct a smaller fraction of the total subsurface. Low-k zones are formed under conditions of lower depositional energy, creating units with finer materials. The physical attributes due to lower energy deposition are: limited advection with diffusion possibly dominating within low-k zones; more reduced environments; and a higher fraction of organic carbon per surface area. Lower energy states are easier to obtain and, therefore, lead to low-k zones commonly constituting a large fraction of the total subsurface.

The proposed conceptual model we will be focusing on is a simplified heterogeneous system consisting of the two zones following Sale and Newell (2010): transmissive zone and low-k zone. Figure 1 displays our current understanding of contaminant transport concerning dense non-aqueous phase liquid (DNAPL) and its dissolved phase constituents within heterogeneous subsurface media. During the early stage, DNAPL may be present in pools or ganglia within the transmissive zone (not pictured within the figure), where the DNAPL does not enter the low-k zone due to the low-k media's higher entry pressures (Parker et al. 2004). A concentration of aqueous flow exists within the transmissive zones that are the more permeable segments of the formation. The dissolved phase constituents move away from the DNAPL source zones, due to the effects of advective flow, dispersion, and diffusion that assists in creating a dissolved phase plume (indicated by red within the Figure 1).

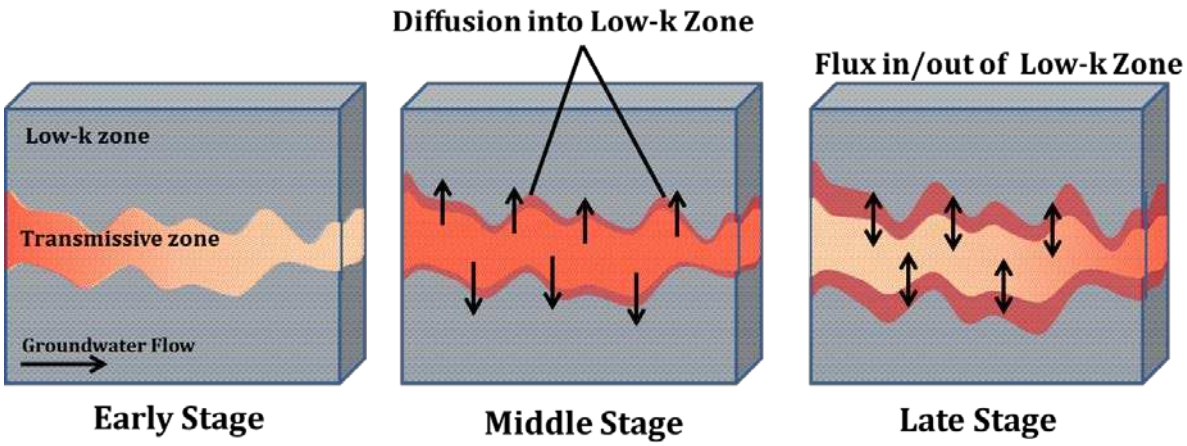

Figure 1. Evolution of chlorinated solvent release (indicated by red) in a simplified heterogeneous system of transmissive zone and low-k zones.

During the early and middle stages, the dissolved phase plume will continue to develop as long as the DNAPL source continues to remain (NRC 2004). Where fractures are not present within the low-k matrix, the concentration gradient between the dissolved phase plume and the low-k zone begins to drive the dissolved contaminant into the low-k zone with the only driving force being diffusive transport into the matrix (Parker et al. 2004, Johnson et al. 1989). The zones are then charged up with contaminant and start to act as secondary storage for the aqueous and sorbed-phase contaminants.

From middle to late stages, the finite DNAPL source and dissolved-phase plume disappear or are cut off (either due to remediation treatment, full dissolution and mobilization downgradient out of the system, or migration further into the low-k matrix), resulting in the contaminant mass found mainly within the low-k zone. Eventually, the transmissive porous media aqueous contaminant concentration declines, due to natural gradients, pumping, or successful remediation treatments within the transmissive zones, which reverses the contaminant concentration gradient. Reversing the concentration gradient causes the dissolved-phase contaminant within the low-k

zones to diffuse outward from the low-k matrix back into the transmissive zones known as “back diffusion” (Parker et al. 1994). This back diffusion is commonly a slower process due to lower concentration gradients and causes relatively slow release rates into the transmissive porous media, making contaminant plumes remain persistent (Parker et al. 1994, Feenstra et al. 1996, Seyedabbasi et al. 2012) and therefore sustaining contaminant concentrations in transmissive zones for an extended time.

Within low-k zones, assimilation processes may occur due to degradation and/or sorption of chlorinated-solvent plumes (Luthy et al. 1997, Johnson et al. 2001a, Field and Sierra-Alvarez 2004). Evidence of sorption and degradation have been found within field and laboratory studies (Parker et al. 2008, Lui et al. 1997). Therefore, this conceptual model (Figure 1) must include assimilative processes (Figure 2) that will ultimately affect the long-term fate and transport of contaminants in transmissive zones.

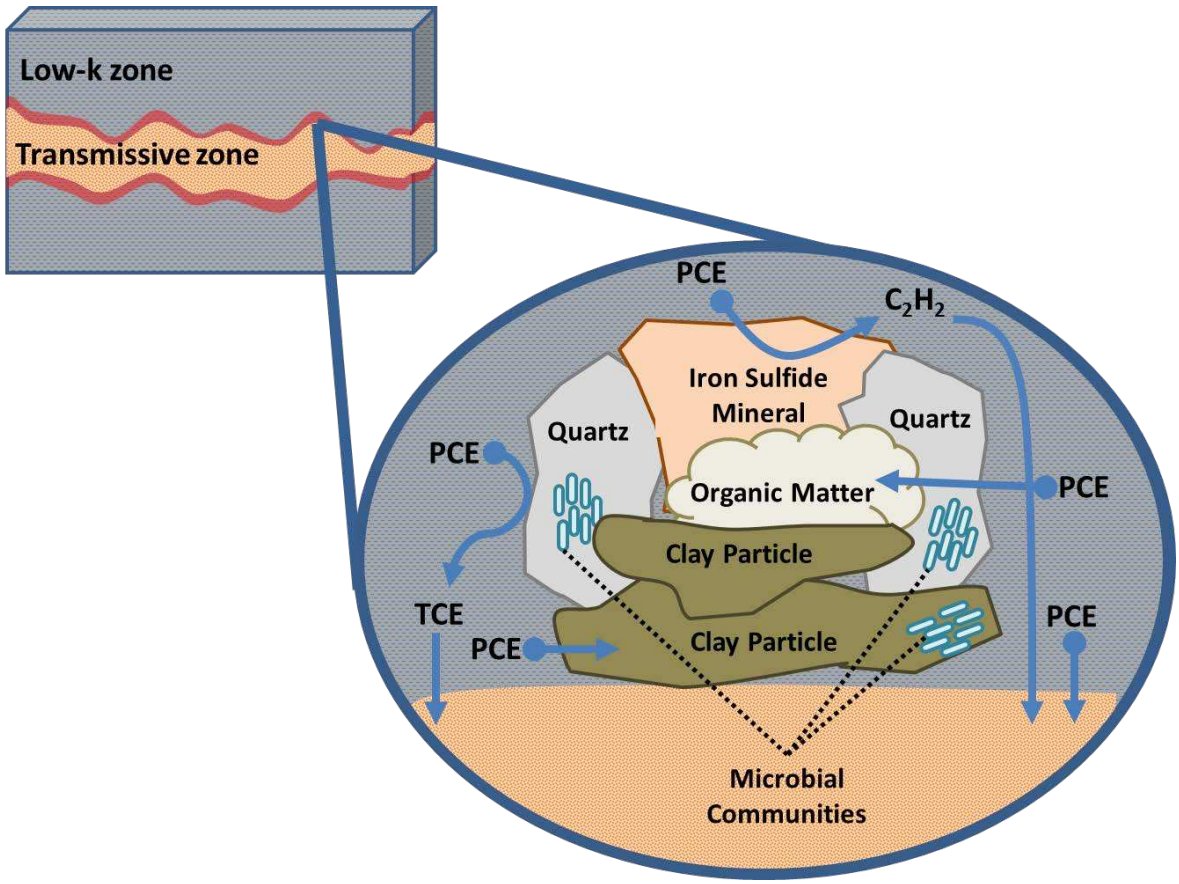

Figure 2. Contaminant fate and transport between transmissive and low-zones during middle and late stages. Image adapted from Purves et al (1994).

The processes shown within Figure 2 are sorption and abiotic/biotic degradation. Specific examples of each process include:

- Sorption or entrapment of PCE shown through the use of organic matter and clay particles that can remove the contaminant from the system either reversibly or irreversibly.
- Abiotic degradation due to an iron-sulfide mineral surface that has been reported in laboratory studies to have the ability to transform PCE to acetylene (C_2H_2).
- Biotic degradation that converts PCE to TCE (and possibly further to ethene via sequential hydrogenolysis) in microbial communities.

The impact that sorption and degradation processes have on contaminant plumes may be small over brief duration (days/months). Over longer time spans (years/decades) assimilative processes, will ultimately control the overall longevity of plumes in transmissive zones. Several different studies show that assimilative processes could play a large role in affecting plume longevity. Liu and Ball (2002a) recognized that although sorption was a controlling process within their in-situ field experiments, the time scale of 35 months was not long enough to rule out significant degradation for longer time scales. In another study, field data from Parker et al. (2004) showed no TCE degradation but recognized that even over long time frames, degradation could play an important role in affecting contaminant transport. Modeling has progressed to incorporate assimilative processes to include degradation, as seen in Wahlberg (2012), which expanded upon the Sale et al. (2008a) two-layer model.

2.2. Current Models

Correctly predicting the impact of low-k zones on long-term water quality of transmissive zones requires a more complete understanding of the small-scale heterogeneity within low-k zones (Luthy et al. 1997, Kalinovich et al. 2012, Sale et al. 2013). Models have been developed for higher resolution, such as Sale et al. (2008a), Chapman et al. (2012), Wahlberg (2012), that capture mass flux out of low-k zones at small-scale concentration gradients, but many of the challenges have occurred in accurately capturing the long-term processes that affect contaminant storage, release, and transformation within the low-k zones.

2.2.1. Sorption

Sorption is a common and simple modeling paradigm used to describe the partitioning of contaminants onto or into (adsorption or absorption) soil particles. Using the partitioning

coefficient (K_d) to capture the equilibrium of contaminant within sorbed and aqueous phase, Schwarzenbach et al. (2003) used the following relationships:

$$C_s = K_d C_w \tag{1}$$

$$K_d = f_{oc} K_{oc} \tag{2}$$

where C_s ($M \cdot M^{-1}$) is the total sorbed concentration, K_d ($L^3 \cdot M^{-1}$) is the partitioning coefficient and C_w ($M \cdot L^{-3}$) is the total aqueous concentration at equilibrium, f_{oc} ($M \cdot M^{-1}$) is the fraction of organic carbon, K_{oc} ($L^3 \cdot M^{-1}$ of organic carbon) is the organic carbon partitioning coefficient. In Equation 1, sorption onto the solid is directly proportional to the fraction of organic carbon of the soil. This direct proportion is known as "linear sorption".

Determination of the retardation factor (R), which is the ratio of average linear velocity of the groundwater to the velocity of the contaminant at the leading edge of the plume, can be estimated by the following equation from Freeze and Cherry (1979):

$$R = 1 + \frac{\rho_b}{\phi} K_d \tag{3}$$

where ρ_b ($M \cdot L^{-3}$) is the bulk density of the soil, and ϕ (dimensionless) is the porosity of the soil.

Linear sorption has been known to occur for hydrophobic organic compounds when the molecular propensity towards mineral sorption is low and the amount of organic carbon (Allen-King at al. 1997) is high and within smaller ranges of contaminant concentration (Ball and Roberts 1991). Absorptive partitioning into a material (e.g., natural organic matter) is often characterized by linear isotherms in which the ratio of sorbed to aqueous concentration is

independent of concentration (Allen-King et al. 2002) and when the matrix is dominated by sorbent organic matter (SOM) (Luthy et al. 1997).

Although linear sorption is commonly assumed with modeling, subsurface sorption may not occur linearly due to: 1) the variable distribution of organic carbon within the geologic media due to heterogeneous depositional energies, 2) adsorptive properties of organic carbon and inorganic matter (e.g. minerals), and lastly, 3) the sorptive properties of swelling clays not affected by the f_{oc} (Allen-King et al. 1996). Sorption may not occur on a linear scale due to concentration-dependent retardation which in turn affects diffusion within micropores. This concentration-dependency also affects desorption mechanisms where slow processes of diffusion within sediment particles are further retarded by sorption nonlinearity (Allen-King et al. 2002).

Equations 1 and 2 tend to under predict the magnitude of sorption for hydrophobic organic compounds (HOCs) on soils (Allen-King et al. 2002), partly due to the omission of adsorption onto the matrix surfaces. The most dramatic effects on sorptive properties occurs when contaminant concentrations are low and the soil contains a small quantity of high surface area carbonaceous material (HSACM) (Allen-King et al. 2002). Other linear free energy relationships (LFERs) also have limitations if dominant adsorptive processes or site-specific materials exist (Kalinovich et al. 2012). Accurately modeling adsorptive properties within the matrix may be difficult, since the matrices may exhibit some combination of linear and nonlinear isotherms depending on the surface properties (Luthy et al. 1997).

Common non-linear isotherms used to capture adsorptive properties within the matrix are the Freundlich and Langmuir isotherm. The Freundlich isotherm (Equation 4) is commonly used to

relate sorbed and aqueous-phase HOC concentrations within a naturally heterogeneous geologic system. The isotherm uses adjustable parameters to describe sorption:

$$C_s = K_f C_w^n \quad (4)$$

where K_f ($(L^3 \cdot M)^{-n}$) is the Freundlich constant or capacity factor, n (dimensionless) is the Freundlich exponent.

The Langmuir Isotherm is used to describe constant sorption energy with limited sorption sites on the sorbent surface. The Langmuir isotherm (Equation 4) is described as:

$$C_s = \frac{\Gamma_{max} K_L C_w}{1 + K_L C_w} \quad (5)$$

where Γ_{max} ($M \cdot M^{-1}$) represents the total number of surface sites per mass of sorbent, K_L ($L^3 \cdot M^{-1}$) is the Langmuir constant and assumes a constant sorbate affinity for all surface sites.

2.2.2. Degradation

As is common with regard to degradation, the model uses first-order rate laws and uniform degradation to represent the processes occurring within the subsurface matrix (Bodin et al. 2003, Falta 2005, and Sale et al. 2008). The first-order degradation equation is shown:

$$\frac{dC}{dt} = -\lambda C \quad (6)$$

Where λ (T^{-1}) is the decay constant, which can be defined by the half-life period ($t_{1/2} = \ln(2) \cdot \lambda^{-1}$). However, this uniform degradation does not accurately capture the effects of different types of degradation and the dependence of environmental conditions, distribution of degrading material

(minerals and/or specific degraders) as well as other constraints that limit the rate of reactions. Models that have been used to incorporate the complex limiting constraints to predict a more accurate degradation rate within the subsurface are geochemical speciation modeling (abiotic degradation) and Monod kinetic models (biotic degradation) (EPA/600/R-09/115, Chambon et al. 2010).

Lastly, after all processes have been considered the model must capture the effects and influences sorption and degradation processes have on each other. The two layer model developed by Sale et al. (2008) explored the different applications of adsorption, retardation, and degradation and the ultimate physics of contaminant transport. Although this model used a highly idealized scenario, the longevity of the plumes may be driven by the storage and release processes within low-k zones. To further our understanding, we should consider more complex settings and incorporate multiple-layer scenarios with field-scale data for support.

2.3. Long-Term Processes

This section expands further on the processes described above (Section 2.2.1 and 2.2.2). This section includes specific examples of the field and laboratory studies that give evidence to the assimilative processes that may be found within low-k zones. This section also shows how assimilation processes can affect contaminant fate and transport within low-k zones.

2.3.1. Sorption

As described in Section 2.2.1, sorption is a process that can have substantial impacts on the longevity of the contaminant plume. Sorption can occur in several different ways within the low-k zone subsurface media, which include many heterogeneous materials. Heterogeneous

materials include inorganic surfaces (e.g., clays and minerals), organic matter surfaces, microbially-alterated biomass, as well as thermally alterated carbaceous matter (TACM). This section will discuss in detail how each of these materials has the propensity to sorb HOCs.

Inorganic surfaces such as clays and minerals surfaces sometimes do not naturally sorb HOCs readily, but when certain conditions are present other sorbed molecules onto surfaces may be able to lead to a modification of sorbents, favoring further sorption (Schwarzenbach et al. 2003). In clays and minerals, this modification occurs when intercalation of specific cations promotes sorption of non-ionic HOCs that would not have occurred previously. Swelling of clay matrices, also known as organoclays, allow for sorption of HOCs to occur on the surface and interlayers of the clay minerals. An example of expanding clay minerals is montmorillonite. Montmorillonite has a high cation exchange capacity (CEC) with large expansive properties and high surface areas, but is hydrophilic and, therefore, will not have any affinity for HOCs (Park et al. 2013). However, the properties of the clay minerals can be modified to hydrophobic conditions by replacing inorganic exchangeable cations and intercalating organic quaternary ammonium or pyridium cations creating organoclays. This exchange allows the organoclays to have a strong capacity to sorb non-ionic and hydrophobic compounds from aqueous solutions (Sheriff et al. 1987, Groisman et al. 2004, Park et al. 2013).

Groisman et al. (2004) found that non-ionic HOCs are better sorbed to longer chain organoclay octadecyltrimethylammonium bentonite with respect to short-chain organoclays, such as tetramthyltriammonium bentonite. The organic cation chains, depending on length and affinity of HOCs, may lead to a promotion of more linear (partitioning due to long alkyl chains) or non-linear (adsorption with short alkyl chains) sorption (Lee et al. 2004).

Organic matter surfaces have also been found to play a large role in sorption within surbsurface media. Organic matter may include portions with both fluid and rigid properties (also known as "rubbery and glassy" in the chemical world, or "soft and hard carbon" in the geosciences). Nonionic HOCs may both absorb into fluid organic matter and adsorb onto a rigid surface or micropore (Schwarzenbach et al. 2003). Humic substances (e.g., kerogen, coal, graphite) have a large range of different sorptive properties that can affect the overall amounts of sorbate on the surface. Diagenesis and weathering of organic matter may also have some effect on the affinity of SOM for sorption of HOCs (Luthy et al. 1997). Allen-King et al. (1997) also found that the age and source of the organic carbon also affects the sorption process of HOCs by several orders of magnitude.

TACM typically creates non-polar surfaces of potentially high specific surface area and porosity that include micropores. These conditions promote adsorption and can lead to non-linear HOC sorption isotherms that allow for high sorption capacity at low aqueous concentrations. The total HOC sorption on TACM is a superposition of partitioning and adsorption. Adsorption tends to dominate at low concentrations, and partitioning dominates at high aqueous concentrations. The greatest non-linearity was shown by the dark calcareous lithocomponents found from marine-derived carbonate (Kalinovich et al. 2012).

2.3.2. Biotic Degradation

Chlorinated compounds, such as PCE and TCE, can be degraded via anaerobic conditions through the ability of the microorganism to gain beneficial use of the contaminant as an electron donor and carbon source to stimulate growth (Field and Sierra-Alvarez 2004). Early research focused on biotic reductive transformation of chlorinated solvents, such as halorespiration and

cometabolism (Lee and Batchelor 2002). Halorespiration occurs when the chlorinated compound serves as an electron acceptor, resulting in reductive dehalogenation (McCarty et al. 1997, Field and Sierra-Alvarez 2002). Cometabolism occurs when the microorganism transforms the chlorinated compounds while degrading other substrates (Wackett 1995). New sustainable remediation technology to help facilitate and enhance biodegradation, such as the use of enhanced reductive dechlorination (ERD) (Sutherson et al. 2002), biogeochemical reductive dechlorination (BiRD) (Magar et al. 2001), and thermal remediation (Zeman 2013) is in the development stages.

2.3.3. Abiotic Degradation

After recognizing the substantial, but still limited potentials of biotic reductive transformation, scientists have begun to develop a better understanding of abiotic transformation/degradation. Kreigman-King and Reinhard (1992) found that reductive dehalogenation was possible within subsurface media using mineral surfaces (e.g., biotite and vermiculite) as electron donors and/or reaction mediators to increase the rate of the transformation process. Transformations can ultimately affect the fate and transport of the contaminant within aqueous environments. Common minerals, such as iron sulfides, iron oxides, green rust and iron-bearing clays, have been found to transform or degrade chlorinated compounds. The use of these common minerals have demonstrated complete or near complete transformation of chlorinated solvents. Lee and Batchelor (2002) found that abiotic reductive dechlorination of PCE, TCE, *cis*-dichloroethene (cis-DCE), and vinyl chloride (VC) can occur on mineral surfaces of pyrite and magnetite and were able to increase the rate of transformation using adsorbed Fe(II), known to be a facilitator on other mineral surfaces, to increase reaction (EPA 2009). Some of the methods used to discover if aquifers contain these minerals are mineralogical analyses, geochemical modeling,

monitoring of groundwater for reaction products that are unique to abiotic reactions, and fractionation of stable isotopes (EPA 2009).

2.4. Knowledge Gaps

Knowledge gaps regarding processes in within the low-k zones include:

- How do assimilative processes affect the overall flux into and out of low-k zones?
- What is the rate of these assimilative processes?
- How do sorption and degradation processes interact with each other?
- What conditions are necessary for sorption and degradation interactions to occur?
- How do sorption and degradation interactions affect the rate of degradation and transport of the contaminant?
- What is the transport of both parent and degradation products in low-k zones?

This thesis focuses on further developing laboratory methods in the hopes that the methods developed and used for future studies will be able to address some of these knowledge gaps.

3. LABORATORY EXPERIMENTS

This chapter describes the laboratory experiments that were conducted to develop methods for evaluating chlorinated compounds fate and transport in low-k zones. Employed methods include 1) headspace vials and 2) ampules (Figure 3). This section focuses first on the headspace vials. Four separate experiments were conducted to assist in establishing methods for the headspace vials. The experiments used to develop methods for the headspace vials include: a stability experiment to study the Mininert® valves' ability to reduce volatile losses, sorption study to observe the effects that fiber filters have on PCE concentrations, a headspace vial experiment using field soil, and batch sorption experiments using field soils. Then the section will discuss the method employed for using the ampules. The experiment used for the ampule is the methanol extraction method. This methanol extraction method is then applied to the headspace vials with field soil to compare the ampules and the headspace vials. Each experiment is described with experimental objectives, methods, and results. The results of each experiment provide guidance and direction for developing methods for subsequent experiments.

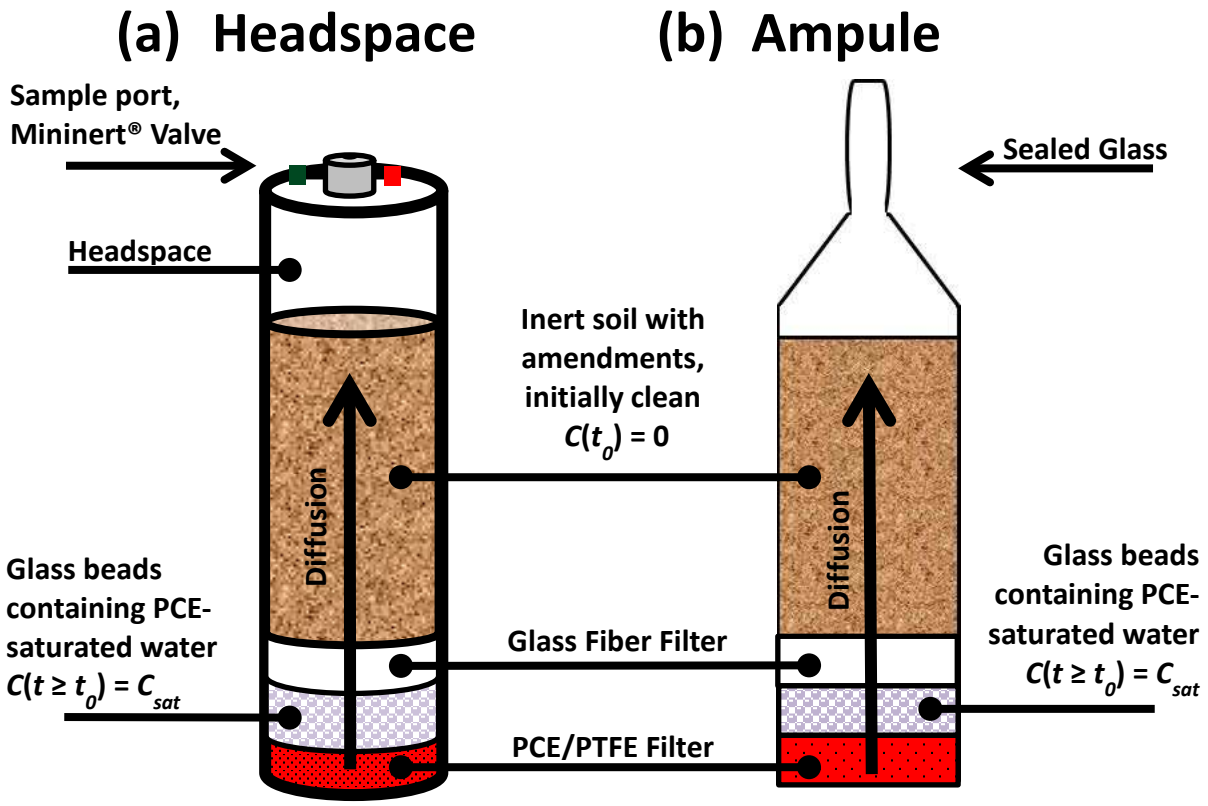

Figure 3. Column study design for (a) headspace vial and (b) ampules.

3.1. Headspace Stability Experiment

The headspace stability experiment was used to help determine the best way to seal the headspace vial to limit the potential losses that could occur from sampling of the headspace vials. Different sealing methods have been used to help limit losses but have not been tested with the sampling methods used throughout the headspace vial experiment. Sections 3.1.1 through 3.1.3 discuss the experimental objectives, methods, and results all which helped to determine the best method for sealing the headspace vials and reducing mass losses due to sampling.

3.1.1. Experimental Objectives

In long-term experiments, controlling mass loss through the apparatus is important. Past experiments used lead foil tape and a PTFE liner with crimp tops to reduce sorption and leakage from the vial. Using crimp tops only allows for one sampling event to occur before the cap is no longer effective in controlling volatile losses. A key challenge is the need to maintain a closed system while being able to obtain multiple sampling events over time. The use of a Mininert® valve screw thread cap (Sigma Aldrich, Supelco, Bellefonte, PA) (Figure 4a) was considered as a solution, since the Mininert® valve has an open and close valve as well as a rubber septum to reduce volatile losses during sampling events. The rubber septum is removable and can be replaced with a new unused rubber septum, allowing for multiple sampling events to occur over time. The objective of this experiment was to evaluate different modifications to the Mininert® valve cap that would still allow for repeatable sampling and also minimize the rate of mass lost from the apparatus (Figure 4). This experiment provides information to determine the best way to seal and store headspace vials for future long-term experiments. All Mininert® valve screw caps within this experiment were modified by replacing the silicone septum with a 4 inch length by a 1 mm diameter section of Viton core (Figure 4b). The reason for this modification was to use chemically resistant septum for the experiment and to reduce contaminant loss between sampling events and increase ease in replacement of the septum. After each sampling event, which involves piercing the Viton core, the Viton core was shifted over to where the sample was only exposed to an unpierced section of the core. The two treatments that were tested in this stability experiment were PTFE liner with lead foil tape (Figure 4 c, d, and e) and underwater storage. The results from this experiment will guide decision making for the design of future headspace vial experiments as well as the long-term diffusion reactor vessels.

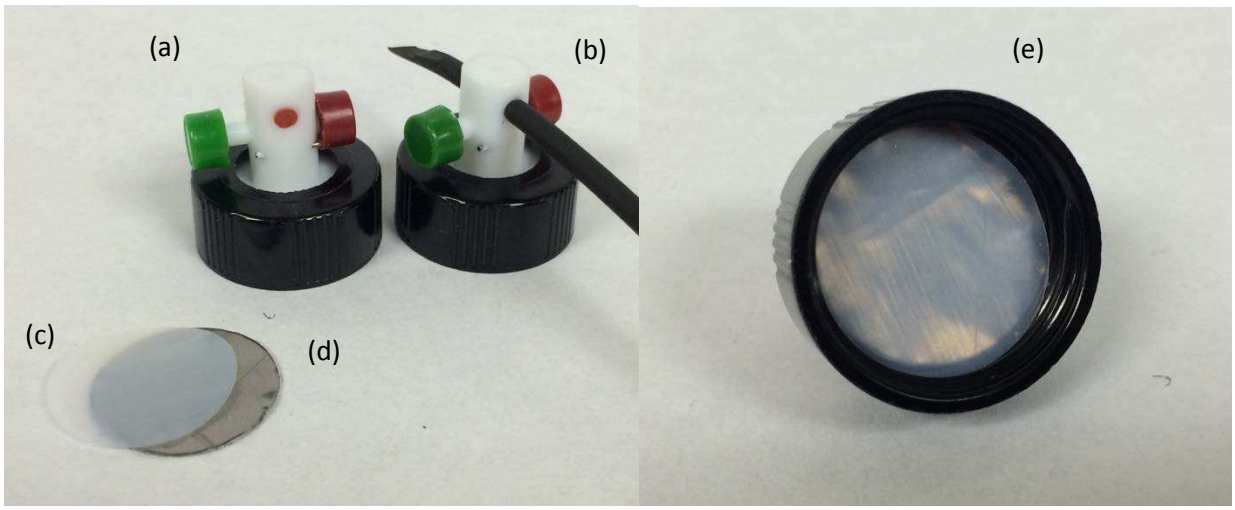

Figure 4. Mininert® valve screw caps with (a) original silicone septum (b) modified Viton septum (c) PTFE liner (d) lead foil tape and (e) PTFE with lead foil tape inserted underneath the Mininert ® valve screw cap.

3.1.2. Methods

The experimental design of stability experiment and the materials used for the physical setup of the vial are described. Next, a description of the sampling procedures is presented. Finally, analytical techniques are discussed.

Experimental Design

The first treatment tested in this experiment was to determine if the application of PTFE liner and lead foil tape on Mininert® valves would reduce mass lost through the sampling port as compared to the Mininert® valves without the modification. The second treatment that was tested was underwater storage of the headspace vials. Storage of vessels underwater has been used to reduce volatile losses from vessels (Olson 2014). Testing treatments together were necessary to identify which treatment combination would be the most effective at reducing overall mass loss within the headspace vials. Table 1 is the experimental design for the stability experiment including four treatments: no liner, liner, no water, and water storage. Each

treatment was performed in triplicate with the exception of the combination of treatments with liner and stored under water which was carried out with a range of high, medium, and low PCE concentrations (1, 10, and 100 mg $\cdot L^{-1}$).

Table 1. Experimental Design for Stability Laboratory Experiment with Concentrations and number of vials produced for each treatment.

Treatment*	**Stored in Water**	**PTFE Liner and Lead Foil Tape**	**Concentration (mg PCE$\cdot L^{-1}$)**
W-Lined	Yes	Yes	1, 10, 100
W-Unlined	Yes	No	10
NW-Lined	No	Yes	10
NW-Unlined	No	No	10

*NW = No water, W = water

Materials

The following materials were used in the setup of the headspace vials: 20 mL borosilicate glass vial, Mininert® Valve screw thread cap (Sigma Aldrich, Supelco, Bellefonte, PA) modified with Viton cord (size 16, Masterflex), PCE (99+% UltraPure, Alpha Aesar, Ward Hill, MA), Sudan IV (dye content 81%, Aldrich Chemical Co., Milwaukee, WI), magnetic PTFE stir bars (2 mm bar diameter, Sigma Aldrich®, Milwaukee, WI), PTFE liner (0.0025-in thickness, Modified PTFE Bag, Fluoro Lab, Dover, NH), lead foil tape (0.1 mm, 3M™,St. Paul, MN), laboratory grade acetone (Mallinckrodt Chemicals, Phillipsburg, NJ), and a magnetic stir bar plate (Micro-V™, Cole-Parmer, Barrington, IL).

Vial Setup

Each vial was filled with 15 mL of deaired water and a 2 mm (bar diameter) stir bar placed at the bottom of the vial. Then, 100 µL of PCE-acetone solution (details of acetone solution are summarized in Appendix B) was injected at the bottom of each vial. Three PCE-acetone solutions were used to achieve high (100 mg$\cdot L^{-1}$), medium (10 mg$\cdot L^{-1}$) and low (1 mg$\cdot L^{-1}$) PCE

concentrations within the vials. PCE-acetone stock solutions were prepared with concentrations of 14,980 $mg \cdot L^{-1}$, 1665 $mg \cdot L^{-1}$, 185 $mg \cdot L^{-1}$ where 100 µL of each solution was injected into 15 mL of water to create a PCE concentration in a water solution of 100 $mg \cdot L^{-1}$, 10 $mg \cdot L^{-1}$, and 1 $mg \cdot L^{-1}$ respectively. The vials were spiked with their respective stock solutions using a 100 µL Syringe (Hamilton®). The solution was injected at the bottom of the vial, which was immediately closed with a Mininert® valve threaded screw cap modified with Viton core and other treatments were applied. PTFE liner and lead foil tape were cut with a 25 mm punch out and placed within the Mininert® valve underneath the cap prior to the sealing of the vials.

Sampling Procedures

Samples were collected after 2, 9, 23, 47, and 146 days. A headspace sampling procedure was used to sample 100µL of each headspace vial. Prior to sampling, the vial was placed on a magnetic stir bar plate set to level 5 for 10 minutes. Sampling of Headspace vials was completed using a 500 µL Sample Lock syringe (Hamilton®) with a rounded-tip needle (Hamilton®). The syringe was filled with 100 µL of atmospheric gas and the valve on the syringe was closed. The Mininert® valve was switched to open and the syringe needle was used to poke through the sample port. After 3 seconds, the syringe was then unlocked, and the atmospheric gas was purged into the vial. Three quick pumps of the syringe plunger were completed to ensure full mixing of the headspace. Then 100 µL of the headspace was pulled into the syringe, and the syringe valve was closed. The sample was analyzed as described in the following section.

Analytical Techniques

The 100 µL sample was manually injected into a gas chromatograph. Samples were analyzed on an Agilent (Santa Clara, CA) 6890 gas chromatograph (GC) equipped with a FID and a Restek

Rtx-5 column (30 m length × 0.32 mm I.D. × 0.25 μm film thickness). The oven program maintained a constant temperature of 40°C for 6.0 minutes. Sample injection settings included a split ratio of 10:1 at a column flow rate of 3.0 $mL \cdot min^{-1}$.

3.1.3. Results

This section discusses the results for the stability experiment using headspace sampling. The entire stability design (as described in Table 1) was sampled at 2, 9, 23, 47, and 146 days after initial setup of the vials.

Figure 5 displays the headspace vials containing the PCE concentration of 10 $mg \cdot L^{-1}$ with data normalized to the initial concentration over time in days. Each data point represents the average between three distinctly separate samples gathered from the same headspace vial that were taken during a sampling event. Five sampling events occurred over the 146 day experiment. Figure 5 displays an overall decreasing trend for each of the treatments showing that losses occur with each treatment; the underwater treatment has fewer losses than the lined treatment. Figure 5 also displays a change in loss rate from early time points (2-9 days) versus late time points (47-146 days). Table 2 displays the quantified difference of early loss rates (2-9 days) and late loss rates (47-146 days). The highest early loss rates occurred for lined vials that were not stored underwater with a 74.9% loss of PCE. Conversely, the lowest early loss rates occurred in unlined vials that were underwater with a loss rate of 26.1%. Later time loss rates from 47 to 146 days, showed lined vials not stored underwater had the lowest loss rate of 4.7%. The lined vials were found to have a large amount of loss occurring in the early stages of the experiment with the losses reducing during the late stages. The reduction of the late stage loss rate may be due to less PCE within the vial, reducing the driving force that would cause volatile losses to occur. Losses

early in the experiment will further affect the long-term results; therefore, the best treatment option is the one that has the least amount of losses at the start of the experiment. Results from this experiment suggest that the treatment of storing vials underwater reduces volatile losses over time during the early stage of the experiment.

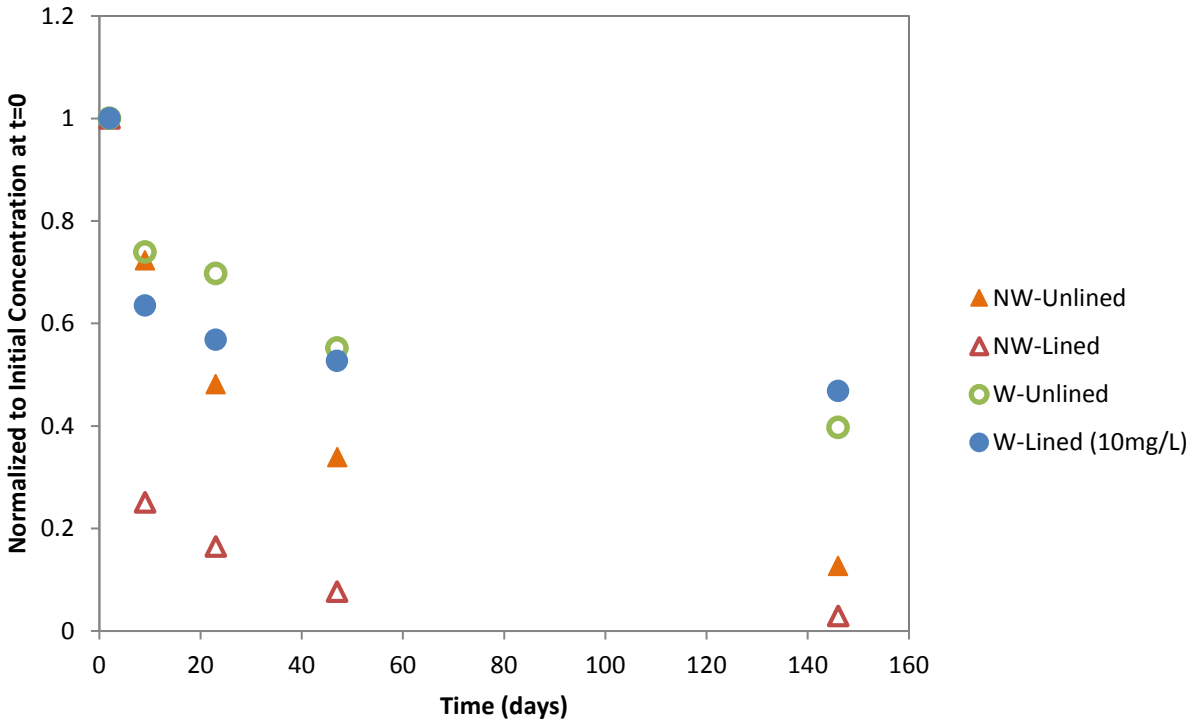

Figure 5. Normalized plot of vials with 10mg·L^{-1} PCE concentration over time.

Table 2. Percentage of early and late loss rates of PCE.

Treatment	Percent of Early Loss Rates (%) (2-9 days)	Percent of Late Loss Rates (%) (47-146 days)
NW-Unlined	27.7	21.2
NW-Lined	74.1	4.7
W-Unlined	26.1	15.5
W-Lined (1mg·L^{-1})	44.7	27.1
W-Lined (10 mg·L^{-1})	36.5	5.99
W-Lined (100 mg·L^{-1})	30.9	8.33

Figure 6 plots concentration versus time for vials with concentrations of 1 mg PCE·L^{-1}, 10 mg PCE·L^{-1} and 100 mg PCE·L^{-1} of PCE normalized to the initial PCE concentration over time. The percent loss from the vials progresses in order of high concentration to low concentration, with the 100 mg·L^{-1} vial having the highest loss of 62.5%, the 10 mg PCE·L^{-1} with 47.9%, and lastly the 1 mg PCE·L^{-1} with 47.1% (Table 4). A Student t-Test two-sample assuming equal variances was conducted to determine if the normalized losses were significantly different from each other. Using an alpha value of 0.05, all t-test values comparing each of the groups was found to be less than 0.05 (Table 3). This result shows that the groups do not have equal losses and therefore are significantly different from each other. This exercise shows that the losses from the vials are dependent on initial concentration of the vial (see Appendix A for t-Test details).

Table 3. t-Test results comparing the normalized concentration of the lined 1, 10, and 100 mg·L^{-1} vials

t-Test: Two-Sample Assuming Equal Variances		
1 mg·L^{-1} and 10 mg·L^{-1}	**10 mg·L^{-1} and 100 mg·L^{-1}**	**1 mg·L^{-1} and 100 mg·L^{-1}**
0.036301	0.001009	0.007991

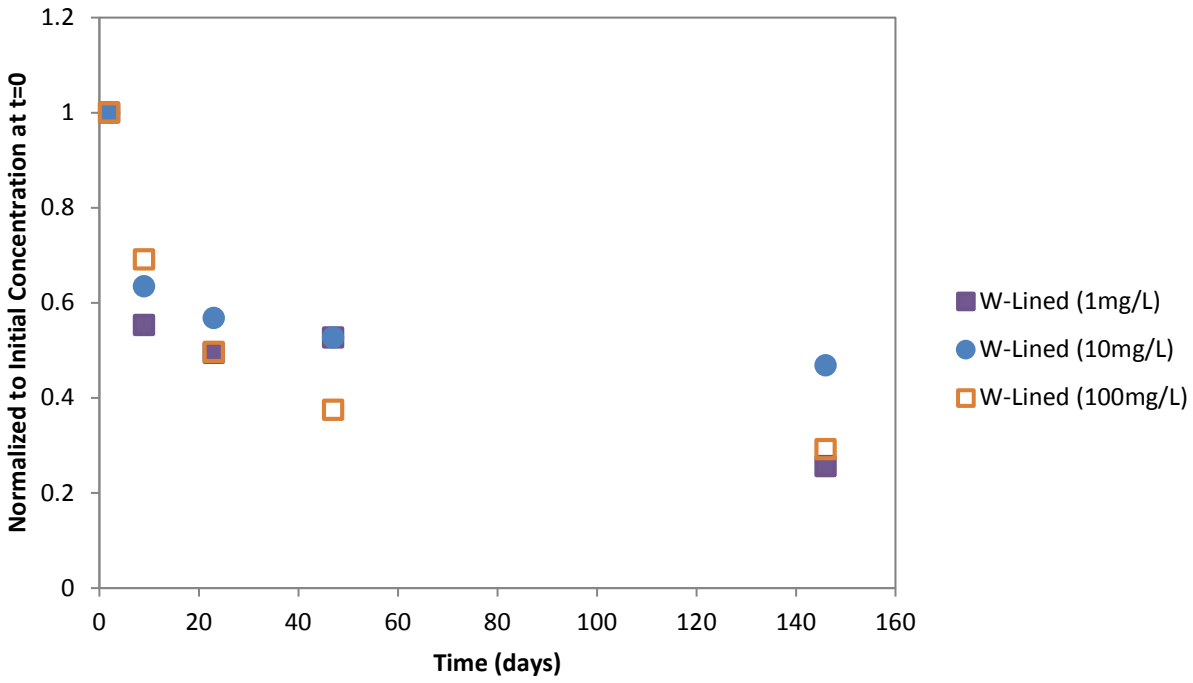

Figure 6. Normalized plot of PCE concentrations with respect to initial concentration over time with treatments of starting concentration at 10mg·L^{-1}

Overall, this stability experiment assumes the most significant losses from the vials are due to diffusion out of the seal and/or during sampling procedures. Other losses to also be considered are due to incorporation of PCE mass to the PTFE liner, the glass vial, and the stir bar within the vial. Table 4 shows a summary of the average overall losses from each vial for corresponding treatments. The treatment with the least amount of losses from the experiment was the unlined and stored under water treatment with the overall loss being 44.1% with respect to the initial concentration.

Table 4. Summary table of stability experiment losses

Treatment	Total Average PCE Concentration Lost (mg·L^{-1})	Percent Lost from Initial Concentration (%)
NW-Unlined	6.60	66.1
NW-Lined	9.18	92.3
W-Unlined	4.44	44.1
W-Lined (1 mg·L^{-1})	0.58	47.3
W-Lined (10 mg·L^{-1})	4.80	47.9
W-Lined (100 mg·L^{-1})	50.9	62.5

Figure 7 shows the total PCE concentration losses over time and displays the correlation of concentrations with higher loss rates within the vials. Error bars represent the standard deviation of the sample groups (n = 3).

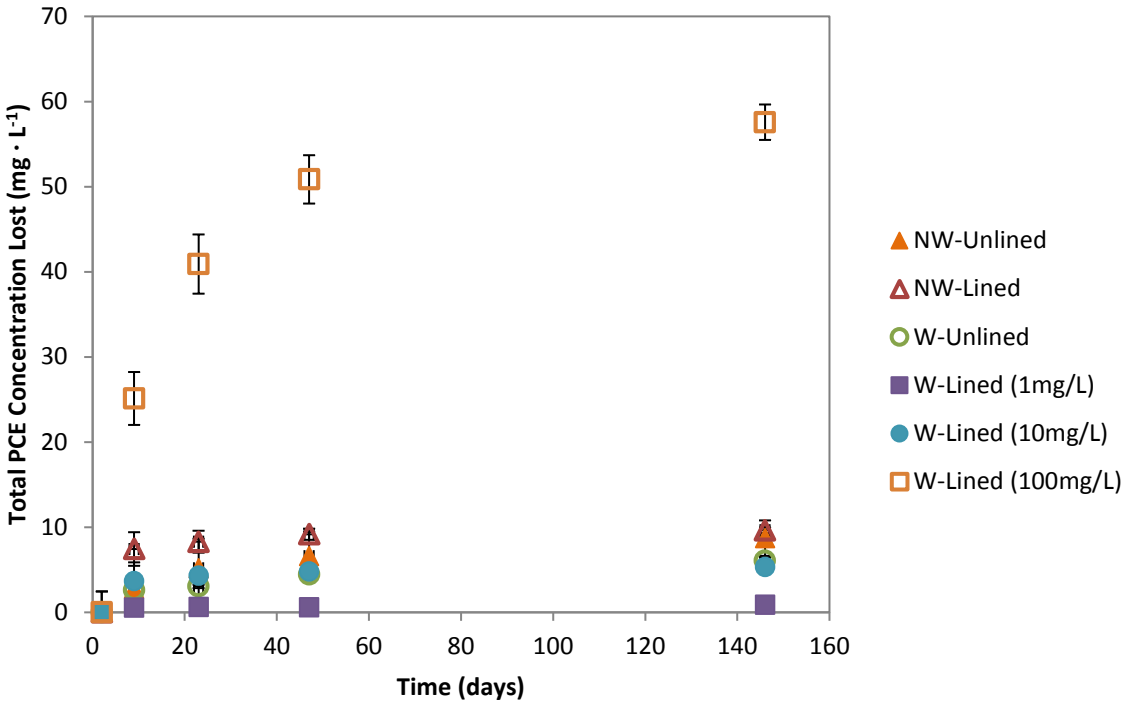

Figure 7. Total PCE concentration lost ($mg \cdot L^{-1}$) over time in days

From the stability experiment results, for future setup we anticipate losses ranging from 8.26% to 44.9% over time, depending on the aqueous concentration within the vial. To minimize losses, headspace vials should be stored underwater and without a liner. The greatest amount of losses occurs during the early stages of the experiment, and that losses appear to stabilize over time during the late stages of the experiment. Early losses may be attributed to incorporation of volatile mass into the Mininert® valve into the septum/cap via irreversible sorption. Late losses could be attributed to sampling methods and procedures. Losses from the headspace vials are assumed to occur due to diffusion through the Mininert® valve, but other losses may occur due to

sorption to the stir bars, and the glass vials. The stir bars may also cause an increase in agitation within the vial which increases the mass within the headspace and, therefore, increases the mass lost from the system through the headspace. Given loses without porous media, there are unknown issues causing losses, the next step would be to see how losses occur with the porous media. For future implementation of these Mininert® valves, to limit losses from the system, no liner is suggested. For long term laboratory experiments, the Mininert® valve is not suggested to help in minimizing losses from the system.

3.2. Sorption Experiment with Fiber Filters

With the design of the headspace vials, two fibers were used: PTFE fiber filter and a glass fiber filter (Figure 3). Both fiber filters serve crucial roles in allowing the headspace vial to maintain proper boundary and initial conditions. This section explains the location the filter used within the headspace vial and the purpose of each filter.

The PTFE fiber filter sits at the bottom of the vial and allows for the PCE (when injected in NAPL form) to spread out evenly across the filter due to the PTFE fiber filter and the PCE both having non-polar physical qualities. To ensure that beading or globulation does not occur the PCE must spread evenly across the bottom of the vial. A non-homogenous layer of contaminant may cause gradients in contaminant entry into the soil column which would not satisfy the ideal homogenous, saturated boundary condition. The PTFE fiber filter ensures that a saturated bottom boundary condition remains intact.

The glass fiber filter separates the soil from the glass beads. This fiber filter prevents the soil from falling through the glass beads and keeps the soil from having direct contact with the PCE in NAPL form. The glass fiber filter also helps in keeping the soil initially clean when the soil is

being added into the column during the setup of the headspace vial; having a clean soil column throughout the entire length of the soil column is another necessary component for maintaining proper initial conditions.

3.2.1. Experimental Objectives

The objective of the sorption experiment for the fiber filters used in the headspace vials was to quantify if any significant PCE sorption occurred onto the glass fiber filter or PTFE fiber filter. If significant sorption occurred, this experiment would help to quantify sorption of each fiber filter.

3.2.2. Methods

The following section discusses the methods used to conduct the sorption fiber filter experiment, including a description of the experimental design, materials, vial setup and the analytical techniques used.

Experimental Design

Table 5 displays the experimental design for the sorption study for the two different fibers used within the headspace vials. Three treatments were explored in this experiment: a control, PTFE fiber filters, and glass fiber filters. A solution consisting of water saturated with PCE (200mg $PCE \cdot L^{-1}$) and injected into the reactor vials. The control for the sorption of fiber filters consisted of only the 10 mL of PCE solution.

Table 5. Experimental Design for Sorption Study with Fiber Filters

Treatment	Control	Glass Fiber Filter	PTFE Filter
Number of Vials	6	3	3

Materials

The following materials were used in conducting the sorption experiment on the fiber filters for the headspace vials: 20 mm Crimp-Top Headspace Vials (20 mL, MicroLiter, VWR®, Radnor, PA), tetrachloroethylene (PCE) (99%, Alfa Aesar®, Ward Hill, MA), Sudan IV (dye content 81%, Aldrich Chemical Co. Milwaukee, WI), luer lock glass syringe (10 mL, Hamilton®, Reno, NV), glass microfiber filter (25 mm, Grade GF/F, Whatman®, Pittsburgh, PA), 25 mm polytetrafluoroethylene (PTFE) fiber filter (45 mm Advantec PF100, Cole-Parmer, Vernon Hill, IL).

Vial Setup

For the sorption study for fiber filters each crimp-top headspace vial was filled with a PTFE fiber filter or a glass fiber filter, and 10 mL of PCE solution (details on solution is found in Appendix B).

All vials were continuously mixed using a tumbler (fabricated at Colorado State University) rotating at level 2 (12 rpms). The samples were tumbled for 38 days before analysis.

Analytical Techniques

Headspace samples were analyzed using a Tekmar™ 7000 headspace autosampler (Teledyne Temar, Mason, OH). Vials were equilibrated in the autosampler at 40°C for 8 minutes. For the sorption study for fiber filters, samples were analyzed by gas chromatograph equipped with a

flame ionization detector (GC-FID) (Agilent Technologies 6890N Network GC System, Agilent Technologies, Incorporated, Santa Clara, CA) operated with a split ratio of 20:1 with an Agilent Rt®-Q Bond (30 m x 0.32 mm I.D.x 10 µm). The oven program maintained 200ºC temperature with no ramp for a total runtime of 6.0 minutes. A 5-point calibration curve was used to convert GC peak area responses to percentage of PCE at solubility using a PCE and water solution (see Appendices A and B for graphs and calculations).

3.2.3. Results

This section discusses the results of the sorption study for fiber filters, which was conducted for 38 days. Figure 8 presents the concentration of PCE within the vial of each treatment (full design described in Table 5). The glass fiber filters and PTFE filters show a decrease of PCE concentration as compared to the control. With standard error bars, the glass fiber filters show overlap with the control; whereas, the PTFE fiber filters standard error bars show no overlap with the control (see Table 6 for values). To further resolve significant differences between the fiber filters and the control, a Student t-Test was conducted using a null hypothesis that assumed equal sample variances between the groups. The results from the t-Test showed that the two-tail p-value for glass fiber filters and the PTFE fiber filters results were 0.095 and 0.019 respectively (see Appendix A for full analysis). The t-Test concludes that any number less than 0.05, one must reject the null hypothesis of assuming sample populations are not significantly different; the glass fiber filters are similar to the sample population of the control, but the PTFE fiber filters sample population was shown to be significantly different.

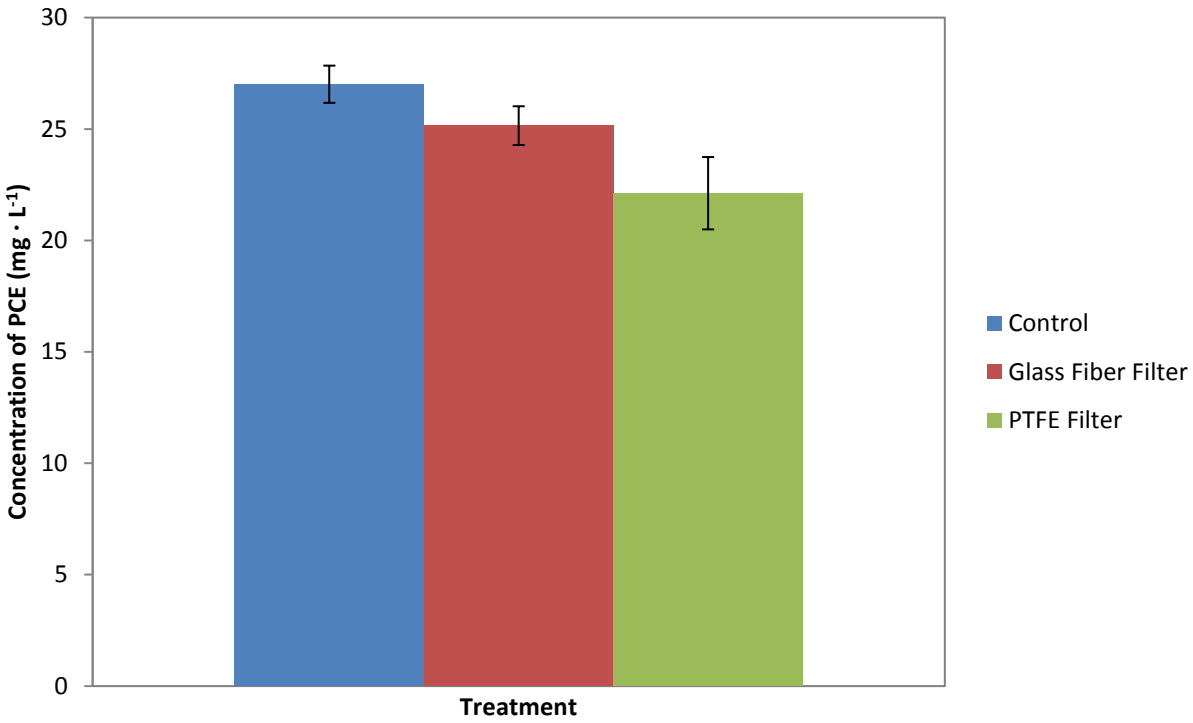

Figure 8. Total headspace concentration of PCE within vial with different treatments (Control, Glass Fiber Filter, and PTFE Fiber Filter)

Table 6. Average PCE concentration for headspace values for each treatment and the standard deviation.

Treatment	Average PCE concentration ($mg \cdot L^{-1}$)	Standard Deviation ($mg \cdot L^{-1}$)
Control	27.01	0.84
Glass Fiber Filter	25.15	0.87
PTFE Fiber Filter	22.12	1.62

From this study, the PTFE fiber filter and the control showed significantly different concentrations. The difference in concentration is assumed to be caused by sorption of PCE to the fiber filter. Due to the function of the PTFE filter and its location within the vial setup, the PTFE filter will not affect the overall distribution and transport of the contaminant. The glass fiber filter does not indicate any significant sorption occurring over the course of the 38-day experiment. Therefore, the glass fiber filter does not affect the overall distribution/transport of

the contaminant into the soil column. Future work should consider conducting longer sorption experiments with a range of contaminant concentration to quantify the range of effects the fibers could have within the system and to account properly for sorption losses from the fibers.

3.3. Headspace Vial Experiment

This section will discuss the full headspace vial experiment. The full headspace vial experiment involves utilizing the Mininert® valve, PTFE and glass fiber filters (as discussed in previous Section 3.2) together along with field soil to complete the full headspace vial design (Figure 9). This section first provides an overview of the experimental design for the headspace vial. Subsequently, the experimental objectives, methods, and lastly, results are presented.

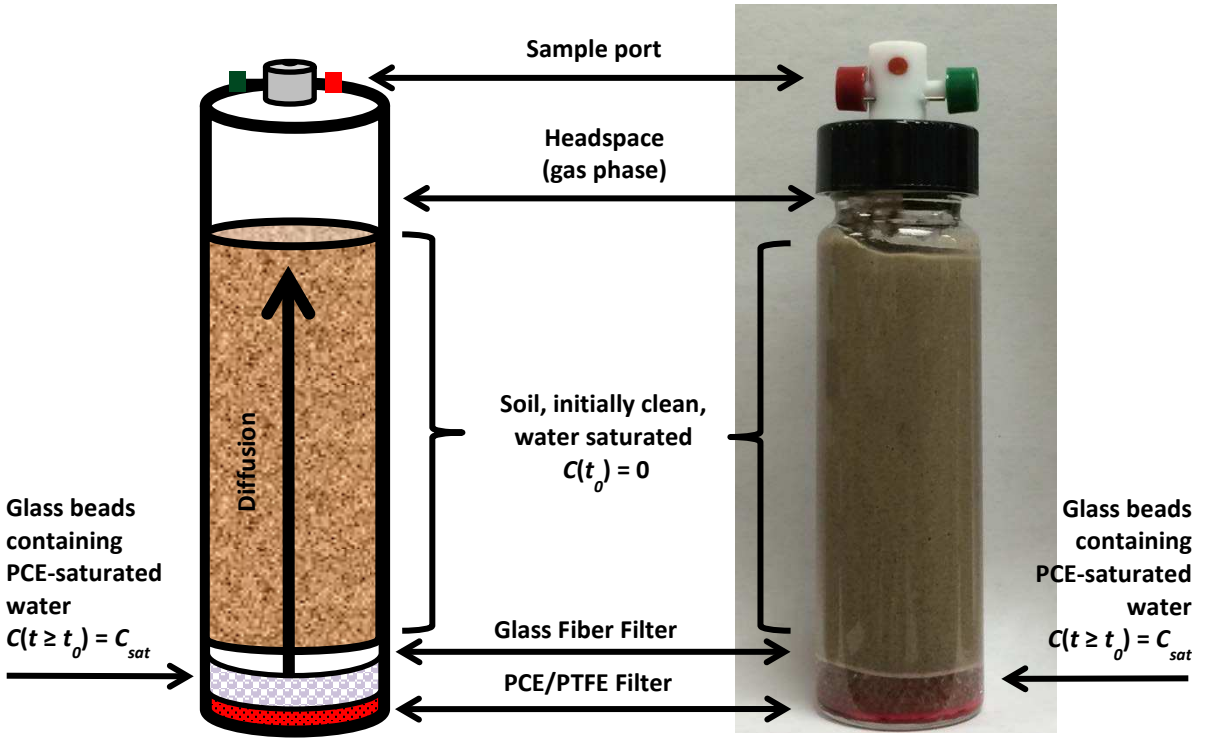

Figure 9. Headspace Vial design

3.3.1. Experimental Design

As discussed in Section 3.1, the headspace vial method uses the Mininert® valve, which allows for the collection of repeatable non-intrusive headspace sampling of the column study while still gaining sufficient and meaningful data. Figure 9 shows the headspace vial design. The headspace vial is set up with a zero-flux boundary layer located at the bottom of the glass vial. Above this layer is a saturated boundary layer (saturated with a NAPL), formed by a PTFE fiber filter. The model contaminant used within this study is PCE, which is injected within the PTFE filter to allow for a uniform layer of PCE at the bottom of the vial. Small glass beads rest on top of the PCE saturated PTFE fiber filter. Glass beads provide both a spacer and barrier to 1) separate the NAPL from the soil to prevent potential uneven distribution of the contaminant and 2) allow for NAPL to dissolve into aqueous phase and enter the geologic matrix in its dissolved phase. This setup allows for diffusion driven processes to drive the contaminant vertically upward toward the zero-flux boundary condition at the top of soil column. The glass fiber filter rests on top of the glass beads. The glass fiber filter allows for the geologic material to rest on top of the glass beads without falling through the pores of the beads and still allows for ease in diffusion of the dissolved phase contaminant through the glass fiber filter and into the geologic material. A clean soil column is then set on top of the glass beads with a small headspace at the top of the soil column where sampling occurs. The entire vial is then sealed with a Mininert® valve modified with Viton core and stored underwater to help reduce volatile losses from the headspace vial.

3.3.2. Experimental Objectives

The experimental objective for the headspace experiment is to test our current experimental design for feasibility and ease of capturing sufficient and meaningful data by establishing baseline data. These short term laboratory tests will set a foundation for the experimental design of the long-term experiments necessary to capture critical processes missed by conventional laboratory and field studies.

3.3.3. Methods

This section discusses the methods used to conduct the headspace vial experiment with porous media. This section includes details about the experimental design, soil characteristics, materials, preparation of materials, vial setup, sampling procedures, and analytical techniques.

Experimental Design

Table 7 is the experimental design used for the Headspace Vials. This design includes the four field soils and one laboratory grade soil (LGS). Details on the soil characteristics for each of the field soils are denoted in the following section. The LGS soil was used as a control which consisted of 50% US silica sand (>0.075mm) and 50% kaolin clay (<0.002mm) by weight.

Table 7. Experimental Design for Diffusion Reactor Vessels

Soil Name	20 mL Vial	40 mL Vial	60 mL Vial
LGS	3	3	3
Soil A		3	
Soil B		3	
Soil C		3	
Soil D		3	

Soil Characteristics

Four field soils were used in both the headspace vials (as noted above). Characteristics of these field soils were examined to consider the processes dominating within these soils. Two analyses were carried out: particle distribution and total carbon. Prior to any soil analysis, all soils were sent through a 30 mesh sieve (0.589 mm opening size) to ensure a low-k soil environment. Soils were also baked at 110°C for 24 hours to ensure all previous water and possible volatile contaminants were sufficiently baked off of the geologic material.

Particle Distribution Analysis

For the particle distribution analysis, two methods were used to delineate soil particle size: sieve shaker method and hydrometer testing. The sieve shaker was used to gain distribution of larger particle size distribution, where 5 sieves were used: 50, 80, 100, 140, and 200 mesh sieves with 0.295, 0.177, 0.147, 0.106, 0.075 mm sieve openings respectively (Figure 10). The sieves with soil were shaken on the sieve shaker at level 6 for 60 minutes.

The hydrometer analysis was used to quantify the distribution of finer particle size for the four field soils (Figure 11). To conduct the hydrometer test, ASTM (2007) Standard Test Method for Particle-Size Analysis of Soils protocol was used.

Figure 12 displays the combination of the two soil analyses performed: sieve and hydrometer.

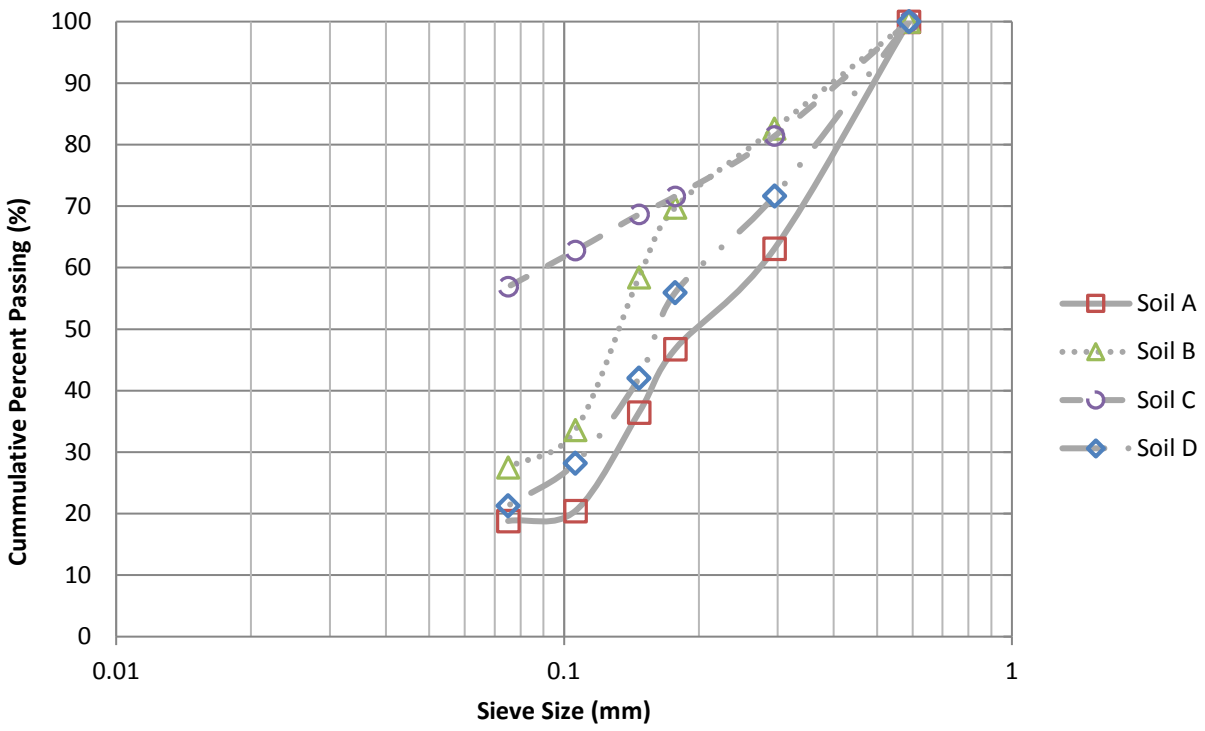

Figure 10. Particle distribution analysis of field soils used within laboratory studies

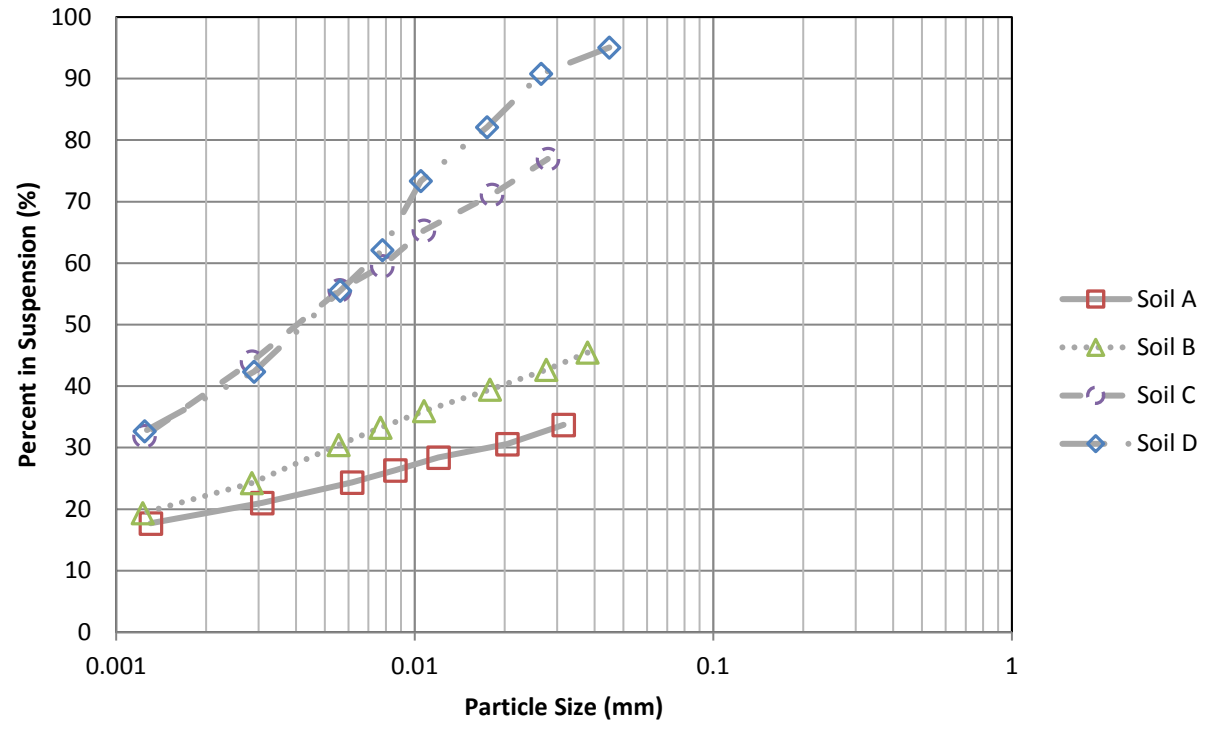

Figure 11. Hydrometer analysis of the four field soils

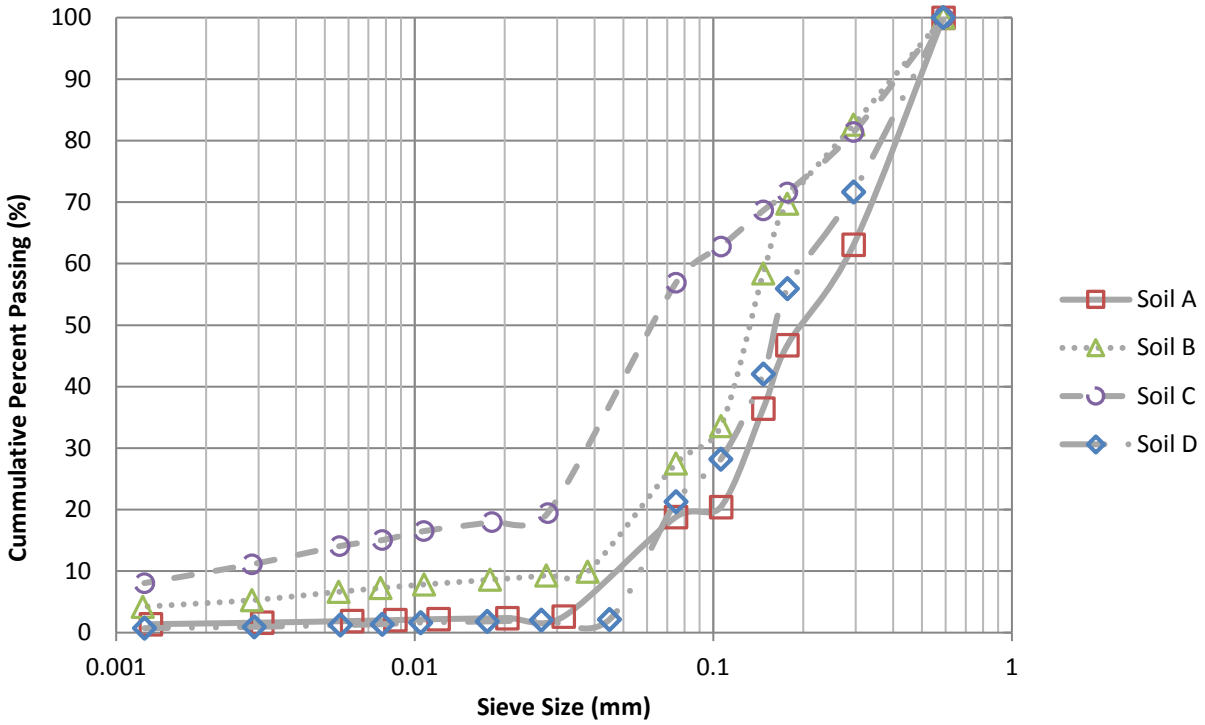

Figure 12. Total percent passing combining both the sieve and hydrometer analyses

Total Carbon Analysis

EcoCore (Colorado State University, Plant Sciences) conducted the total carbon analysis. Total carbon analysis was analyzed on a LECO Tru-Spec CN analyzer (Leco Corp., St. Joseph, MI) and produced direct concentrations of inorganic carbon, total carbon and nitrogen which were conducted in triplicates. Organic carbon concentrations were calculated by difference from the off-line inorganic carbon analysis.

Table 8. Total carbon analysis for field soils and lab grade soil

ID#	%C	Average %C	OC	Average %OC	Notes
Soil A - 1	2.132	2.351	0.066	0.309	
Soil A - 2	2.474		0.434		
Soil A - 3	2.447		0.426		
Soil B - 1	2.184	2.186	0.187	0.210	
Soil B - 2	2.163		0.193		
Soil B - 3	2.21		0.251		
Soil C - 1	0.7195	0.713	0.619	0.616	
Soil C - 2	0.7043		0.607		
Soil C – 3	0.7141		0.621		
Soil D – 1	0.1599	0.162	0.175	0.178	below limit of detection
Soil D – 2	0.1648		0.180		below limit of detection
Soil D – 3	0.1619		0.177		below limit of detection
LGS – 1	0.054	0.052	0.073	0.073	below limit of detection
LGS – 2	0.0502		0.069		below limit of detection
LGS – 3	0.0505		0.078		below limit of detection

The K_{ow}-K_{oc}-f_{oc} relationship, as referenced in Cwiertny and Scherer (2010), describes the relationship between the partitioning coefficient between octanol and water (K_{ow}), the organic carbon-water partitioning coefficient (K_{oc}), and the fraction of organic carbon (f_{oc}). The K_{ow}-K_{oc}-f_{oc} relationship was used to calculate the partitioning coefficient (K_d), the final equation used is shown in Appendix B by Equation 15 (Section 8.3.2). Table 9 shows the K_d values calculated using Equation 15. The K_d values calculated below will later be applied to establish sorption values to represent soil characteristics. For details on finding K_{oc} values, see Appendix B.

Table 9. Calculated K_d for PCE sorption on the field soils using the relationship between K_{oc} and f_{oc}

Sample Name	f_{oc} (g OC·g sample^{-1})	K_d (L·kg OC^{-1})	Average K_d Value (L·kg OC^{-1})
Soil A - 1	0.001	0.13	
Soil A - 2	0.004	0.87	0.62
Soil A - 3	0.004	0.85	
Soil B - 1	0.002	0.37	
Soil B - 2	0.002	0.39	0.42
Soil B - 3	0.003	0.50	
Soil C - 1	0.006	1.24	
Soil C - 2	0.006	1.22	1.23
Soil C - 3	0.006	1.24	
Soil D - 1	0.002	0.35	
Soil D - 2	0.002	0.36	0.36
Soil D - 3	0.002	0.36	
LGS - 1	0.001	0.15	
LGS - 2	0.001	0.14	0.15
LGS - 3	0.001	0.16	

Materials

The following materials were used in the setup of the headspace vials: borosilicate glass vial (20 mL, 40 mL, 60 mL VWR® TraceClean®), Mininert® Valve screw thread cap (20 mm, Supelco® Sigma-Aldrich®) with modified Viton core (3.5 mm, Dupont), 25 mm Polytetrafluoroethylene (PTFE) fiber filter (45 mm Advantec PF100 Cole-Parmer), borosilicate glass beads (1.5 mm, Germinator 500™ Glass Bead Sterilizer, CellPoint Scientific), glass microfiber filter (25 mm, Grade GF/F, Whatman®), compressed carbon dioxide (CO_2) gas (Research Grade 5.0 Carbon Dioxide, size 150A Aluminum Cylinder, Airgas®), PCE (99%, Alfa Aesar®), sudan IV (dye content 81%, Aldrich Chemical Co., Milwaukee, WI), silica sand (F95 series, U.S. Silica), kaolin clay (B-80 Grade, Thiele Kaolin Co.), four field soils (Soil A, B, C, D), 500 µL PTFE luer lock glass syringe (Hamilton®), Luer Lock blunt-tipped hypodermic needle (Chemistry Stockroom CSU), 60 mL Luer Lock tip plastic syringe (BD, Franklin Lakes, NJ), glass tubing (4 mm I.D.), and deaired tap water (City of Fort Collins, 630 mm Hg for 1 hour per 1L of water).

Preparation of Materials

Prior to vial setup, the following materials were sterilized: borosilicate glass vials, glass beads, syringe needles, deaired tap water, glass tubing, spatulas, and all geologic media. The sterilization process was conducted using the autoclave liquid setting with a 15 minute steam time and 30 minute dry time, reaching a maximum temperature of 121^{o}C and minimum pressure of 0 bars. Materials were covered in aluminum foil to ensure sterility once removed from the autoclave. The sterilization process was used to reduce the potential for biological activity and/or growth within the headspace vials. After sterilization, all geologic material was baked at 120^{o}C.

Vial Setup

The following contents are all contained within one borosilicate glass vial (20 mL, 40 mL, 60 mL) (Figure 9). The PTFE fiber filter was cut out to 25 mm and placed at the base of the vial with 3.5 grams of glass beads poured on top of the PTFE fiber filter, and a glass microfiber filter was placed on top of the glass beads. The glass vial was then purged of all oxygen using pressurized CO_2 gas, introduced at the bottom of the vial at the PTFE fiber filter surface using the blunt-tipped hypodermic needle. Once all oxygen was purged (approximately 5 minutes of purging), 2 mL of deaired tap water was added to the vial at the bottom of the glass beads to reduce introduction of air bubbles. After the addition of water vials are exposed back to an aerobic environment (approximately 2 hours). Prior to contaminant introduction, the bottom of the vial was surrounded by ice to obtain low temperatures to reduce potential volatile losses of contaminant. Using the 500 µL gastight Luer Lock syringe and Luer Lock hypodermic needle, 300 µL of PCE tagged with Sudan IV was injected at the glass bead interface. The mass of PCE

injected was recorded by weight. The geologic-material paste was loaded into the 60 mL syringe and glass tubing attachment. The syringe was used to apply the geologic material paste directly to the surface of the glass fiber filter and the vial was filled with the geologic material up to the bottleneck portion of the glass vial. The mass of geologic material paste was recorded by weight. A Mininert® valve cap modified with Viton core was used to seal the vials. All Mininert® valve caps were then covered with a rubber sleeve stopper to cover the sample opening, and vials were then placed under water with a stable temperature of 21 ± 1°C.

The control consisted of 36.9 mL of deaired tap water (City of Fort Collins), injected with 100µL of the PCE-methanol solution that had a concentration of 37,200 mg of PCE·L of methanol^{-1}. The concentration in the control was calculated to be at approximately 50.4% solubility or 101 mg·L^{-1} of PCE (see Appendix B for calculations).

Sampling Procedures

Sampling of headspace vials was completed using a 500 µL sample lock syringe (Hamilton®) with a rounded tip needle (Hamilton®). The syringe was filled with 100 µL of atmospheric gas and locked. The Mininert® valve cap was switched to open, and the needle inserted into the Viton septum. After 3 seconds, the syringe was then unlocked, and the atmospheric gas was purged into the sample vial. Three quick pumps of the plunger ensured mixing of the headspace. Then, 100 µL of the headspace from the sample vial was pulled into the syringe, and the syringe was re-locked. The sample was then manually injected into the gas chromatograph. The addition of 100 µL of atmospheric gas was to ensure no negative pressure gradient (or "pumping effect") was being induce within the sample vial.

Analytical Techniques

Two analytical techniques were employed in the sample analysis for the headspace vials. The first technique strictly detected PCE in the headspace and was used for all data analysis days (1, 7, 14, 28, 42, 89, and 193) except for day 50. These samples were analyzed by a gas chromatograph equipped with a flame ionization detector (GC-FID) (Agilent Technologies 6890N Network GC System, Agilent Technologies, Incorporated, Santa Clara, CA) operated with an inlet temperature of 250°C and a split ratio of 10:1 with a Restek 10224 Rtx®-5 column (30 m x 0.32 mm I.D. x 0.25 µm). The oven program maintained 40°C temperatures with no ramp for a total runtime of 6.0 minutes. The sample was manually injected into the FID inlet of the gas chromatograph using 100 µL of gas from the headspace vials. GC peak area responses were converted to aqueous PCE concentration ($mg \cdot L^{-1}$) through a 5-point calibration curve, using known PCE concentrations in methanol (see Appendix B for calculations and mass details). Therefore, PCE aqueous concentration was indirectly measured through the sampling of the headspace of the sampling vial.

The second analytical technique was used to detect degradation products within the headspace vials. The switch in analytical techniques occurred on Day 50 of the sampling times. The samples on Day 50 were analyzed using a gas chromatograph equipped with a flame ionization detector (GC-FID) (Agilent Technologies 6890N Network GC System, Agilent Technologies, Incorporated, Santa Clara, CA) operated with an inlet temperature of 250°C and a split ratio of 10:1 with a Agilent Rt®-Q Bond column (30 m x 0.32 mm I.D. x 10 µm). The oven program initially was set to 45°C with one ramp set to increase by 20°C to a final temperature of 250°C with a runtime of 15.25 minutes. The sample was manually injected into the inlet with 100 µL of gas sample from the headspace vials.

Accounting for Partitioning

Once results were obtained from the analytical method, the last step was to adjust results adjusted using a simple partitioning equation to account for mass in both gaseous and aqueous phases. The partitioning equation was applied to the calibration curve, where the calibration curve was then used to establish concentrations based off of peak area results from the analytical method. The partitioning equation applied is described as follows:

$$M_w = \frac{M_{total}}{\left(\left(\frac{V_g}{V_w} \cdot H_D\right) + 1\right)}$$

Where M_w, is the adjusted aqueous mass (M), M_{total}, is the total mass within the vial that was calculated on a mass basis (M), V_g is the volume of air within the vial which was assumed to be 1.25 mL, V_w is the volume of water within the vial which was 1 mL, H_D is the Henry's dimensionless constant which was established by Pankow and Cherry (1996) for PCE to be 0.712. For the derivation of this equation see Appendix B.

3.3.4. Results

This section presents the results of the laboratory study for the headspace vial experiment. Sampling events occurred at Day 1, 7, 14, 28, 42, 50, 89, and 193. The following data show results from these sampling events with PCE concentration at the top of the soil column over time (days). All graphs within this section display error bars that include the standard deviation of the three samples for each field and LGS.

Degradation products were sampled at 50 days using the same sampling technique as all other previous samples, but using a different analytical technique which utilized the GC/FID with

Agilent Rt®-Q Bond column. The degradation products that were tested were TCE, 1,2-1,2-DCE, 1,1-DCE, VC, ethane, and methane. During the longer analysis, no degradation products were detected, therefore, the following graphs omit the sampling point at 50 days.

Focusing first on the control that consisted of water and PCE-methanol solution, Figure 13 shows the concentration of PCE within the control solution over time. The injected amount of PCE resulted in a concentration of 101 mg PCE·L^{-1} (see Appendix B for calculations). The headspace concentration should equilibrate with the aqueous concentration and remain constant if no volatile losses occurred due to the Mininert® valve or the sampling procedures. Figure 13 suggests the headspace concentration increases in the control vial at early time points, and then begins to equilibrate back to the initial concentration sample reading. The difference between the initial concentration (91.0 mg·L^{-1}) and the final concentration (87.4 mg·L^{-1}) was 3.56 mg·L^{-1}. The error bars indicate variance due to sampling where triplicate sampling was conducted on the control. Figure 13 does not show the losses from the stability experiment shown in Section 3.1. The inconsistent results of the control in the headspace vial and the stability study may be because stir bars were not used in the headspace vial control. The stir bar within the stability studies could have acted as sink where PCE within solution may have sorbed onto the stir bar. The stir bar may also have caused enough agitation within the solution to increase the concentration in the headspace, therefore, increasing the mass lost through the Mininert® valve cap and Viton core. Another reason the control from the headspace vial and the stability experiment do not show the same losses could be due to improvements in the sampling method. Further investigation is necessary to identify the correct capture of losses due to sampling methods. Suggestions for future work include multiple controls setup to allow for an average loss rate.

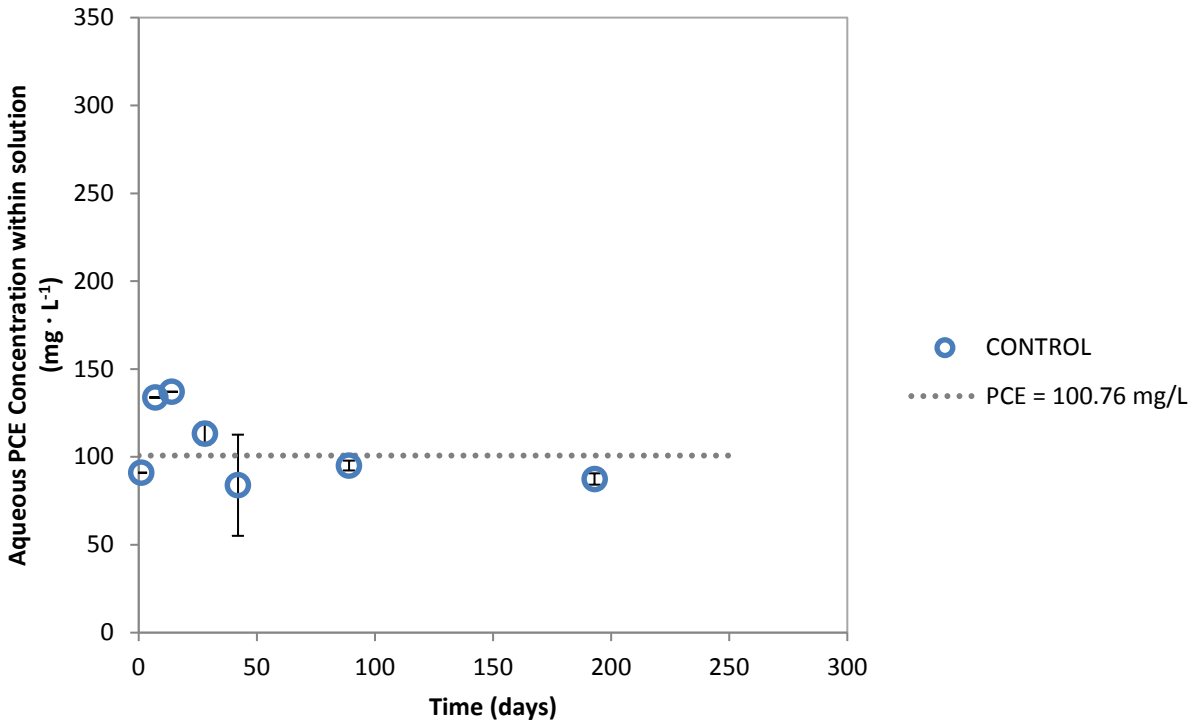

Figure 13. Control for diffusion reactor headspace vial experiment with PCE concentration: 101 mg·L^{-1} stored at 21± 1˚C .

Figure 14 displays PCE concentrations for LGS with varying soil column length of (3, 6, and 11.5 cm) from the headspace vial experiment. The graph displays the varying contaminant breakthrough at the top of the varying soil column lengths. The 3 cm soil length shows early breakthrough of contaminant at the top of the soil column, with breakthrough time being longer for the 6 cm soil length and extending further with the 11.5 cm soil length relative to the 3 cm soil length. The 3 cm soil length reaches approximately 90 mg·L^{-1}at 42 days just below half of PCE solubility, where solubility of PCE is defined as 200 mg·L^{-1} in pure water as cited in Pankow and Cherry 1996, before dropping top soil concentration at 89 days. This measurement appears anomalous and could indicate either volatile losses due to sampling error/ syringe leakage. At the last sampling event on Day 193, recovery of the aqueous PCE concentration at

the top of the soil column reaches concentrations of just below solubility in the 3 cm soil column. At 89 days the 6 cm soil column length reaches half of solubility (approximately 106 $mg \cdot L^{-1}$) at the top of the soil column, and the 11.5 cm soil column length reaches just below half of solubility (84 $mg \cdot L^{-1}$) at 89 days. The use of Pankow and Cherry's definition of PCE solubility was used as an approximate measurement of solubility of PCE, it is necessary to obtain solubility ranges of PCE for each soil mixture. Future work should measure experimental solubility using the soil matrix, since soil composition (i.e. salt ions) could potentially affect the range of solubility of PCE and other constituents of concern. Another reason why concentrations are approximate is due to the use of a pre-defined Henry's dimensionless coefficient (of 0.712 as defined by Pankow and Cherry) to correct aqueous concentrations when applying the calibration curve to convert peak area responses from the GC to aqueous PCE concentrations at the top of the soil (see Appendix A and B for supporting information). It would be appropriate to experimentally resolve the Henry's dimensionless coefficient for PCE, due to a variance in literature values.

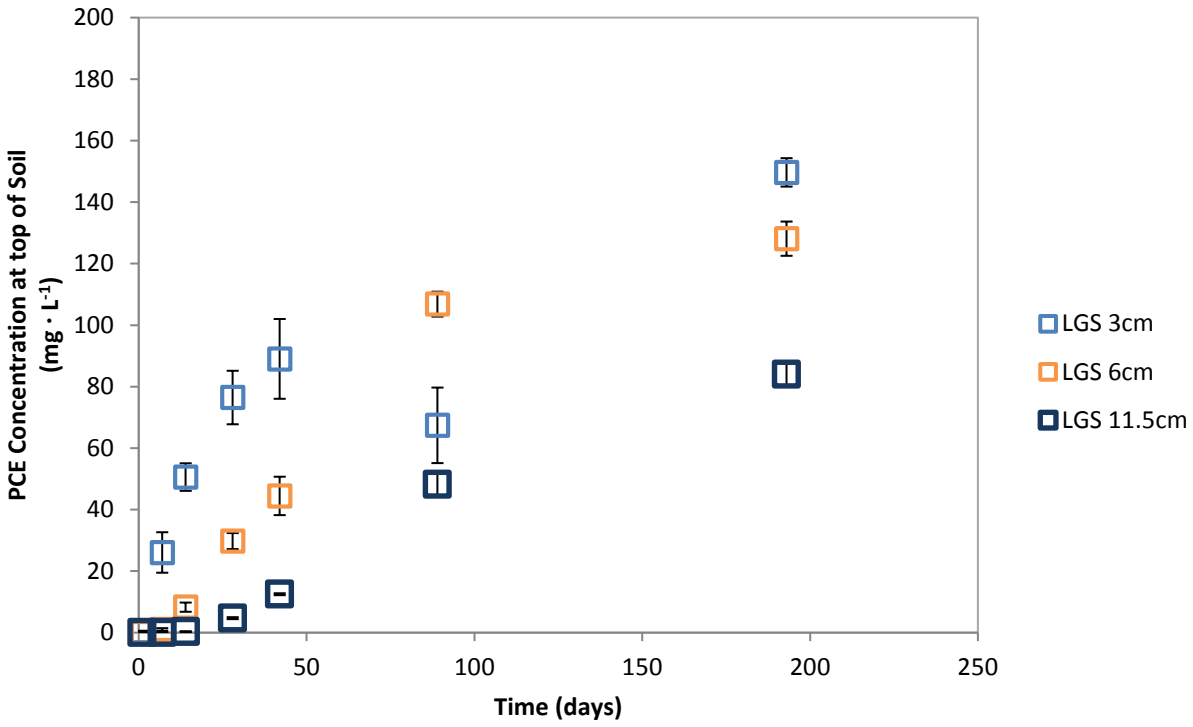

Figure 14. Headspace vial PCE concentration ($mg \cdot L^{-1}$) over time (Day 1, 7, 14, 28, 42, 89, 193) with varying soil length of LGS

Figure 15 displays the headspace vials with the same soil length of 3 cm. LGS has the fastest transport rate of PCE concentration through the soil column. At early time, Soil B shows the second fastest transport rate of PCE concentration through the soil column, with Soil D, Soil A, and then Soil C showing declining transport rates (Table 10). At later time steps, Soils A and B shows a decrease in transport rates through the soil, where Soils C and D have an increase in the transport rate of the contaminant. Soil C shows the slowest rate of flux at the top of the soil column at the earliest time point with 475 $mg \cdot m^{-2} \cdot day^{-1}$. This slower flux rate is most likely due to the high amount of organic carbon with respect to the other field soils (Table 8). Soil C also has a large increase in flux rates at later time points. The switch from a slow flux rate to a high flux rate could be due to a high amount of adsorption occurring at the beginning causing a retardation in the transport of the PCE, but once the adsorption sites are full, the transport of PCE

becomes much faster since it is no longer retarded due to sorption occurring at the surface. As for the complementary sample, Soil A shows a high early transport rate of 1107 $mg \cdot m^{-2} \cdot day^{-1}$, but at the later sampling points, the transport rate declines to 504 $mg \cdot m^{-2} \cdot day^{-1}$. The decline in flux could be due to the aqueous concentration approaching solubility of PCE.

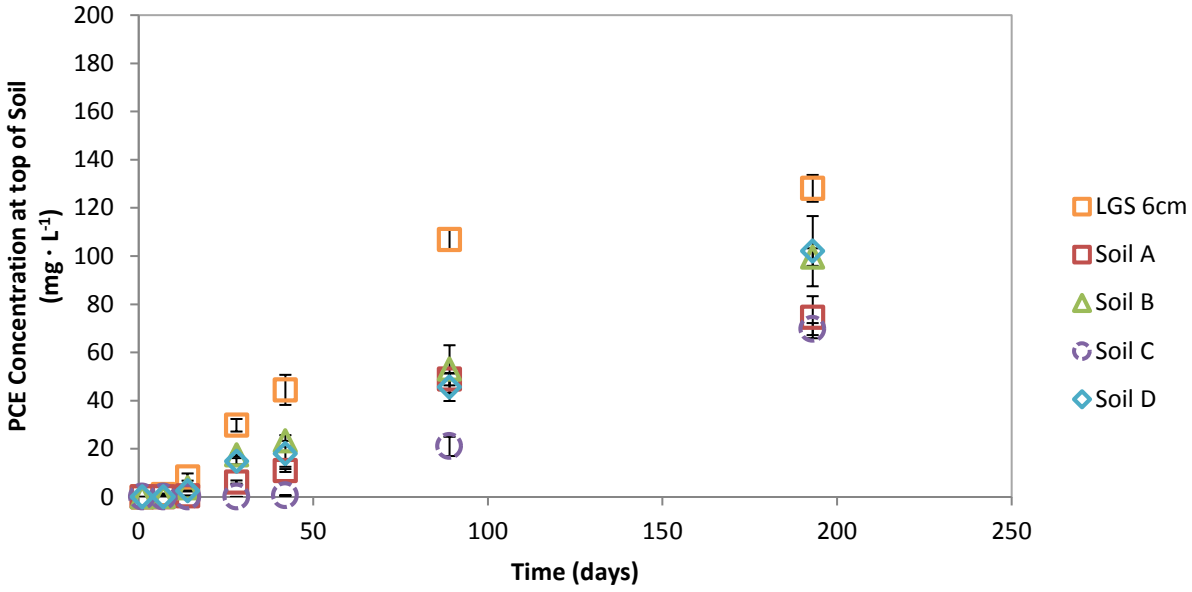

Figure 15. Headspace vial PCE concentration ($mg \cdot L^{-1}$) over time with 6 cm soil length

Table 10. Early and late flux rates for field soil breakthrough at the top of the soil column

Soil Type	Early Rates ($mg \cdot m^{-2} \cdot day^{-1}$) 1-89 days	Late Rates ($mg \cdot m^{-2} \cdot day^{-1}$) 89-193 days
Soil A	1107	504
Soil B	1202	910
Soil C	475	954
Soil D	1030	1106

3.4. Batch Sorption Experiment for Field Soils

This laboratory experiment was performed to determine the sorption of each of the field soils while removing variable factors that may affect the rate of sorption. These variables include concentration and exposure. Batch studies were used to control and/or reduce the impacts these factors may have on determining the true rate of sorption of the field soils. The following section discusses the experimental objectives, methods, and results that were achieved from the batch sorption study of field soils.

3.4.1. Experimental Objectives

The overall objective of the sorption experiment was to study the significance of sorption on the different field soils. These batch studies were used to limit the effects that mass transfer, concentration, and exposure have on the rate of sorption. This sorption experiment will help in resolving retardation parameters for different field soils. The parameters gained from the batch sorption study of field soils are used as input parameters for the mathematical model (Chapter 4) which will be used to match the model to the experimental data gathered from the headspace vials.

3.4.2. Methods

The following method section includes a description of the experimental design, materials, vial setup, and analytical techniques used for the batch sorption for field soils experiment.

Experimental Design

The following is the experimental design used for the batch sorption studies on field soils for headspace vials. The control for the sorption study for field soils was lab grade soil. The study was carried out over 28 days with sampling events occurring on days 1, 5, 9, 14, 20, and 28. Table 11 shows the experimental design for the sorption experiment which was conducted with variable concentration and time to help determine the sorption of each of the field soils. To resolve the effects sorption processes have over time on the field soils, a constant concentration of 10 $mg \cdot L^{-1}$ of PCE was used within all of the field soils for every sampling event. To resolve the effects that varying concentration has on sorption processes within the field soils at one time sample (14 days), five different concentrations (90, 30, 10, 3, and 1 $mg \cdot L^{-1}$) were used.

Table 11. Sorption study for field soils design where triplicates were conducted for each treatment

Soil Type	**Treatment Concentration for Each Time Step Analyzed ($mg \cdot L^{-1}$)**									
	Day 1	**Day 5**	**Day 9**			**Day 14**			**Day 20**	**Day 28**
LGS	10.0	10.0	10.0	90.0	30.0	10.0	3.0	1.0	10.0	10.0
Soil A	10.0	10.0	10.0	90.0	30.0	10.0	3.0	1.0	10.0	10.0
Soil B	10.0	10.0	10.0	90.0	30.0	10.0	3.0	1.0	10.0	10.0
Soil C	10.0	10.0	10.0	90.0	30.0	10.0	3.0	1.0	10.0	10.0
Soil D	10.0	10.0	10.0	90.0	30.0	10.0	3.0	1.0	10.0	10.0

Materials

The following materials were used in the setup of the sorption experiments for soil and fiber filters: 20 mm crimp-top headspace vials (20 mL, MicroLiter, VWR®), tetrachloroethylene (PCE) (99%, Alfa Aesar®), sudan IV (dye content 81%, Aldrich Chemical Co. Milwaukee, WI), methanol (high purity, 99.9%, Burdick & Jackson®, Radnor, PA).

Vial Setup

The sorption study for soil each crimp-top headspace vial was filled with 5.0 grams of geologic material, 10 mL of deaired water, 10 µL of PCE-methanol solution (see Appendix B for details about the solution). All vials were continuously mixed using a tumbler (fabricated at CSU) rotating constantly at level 2 (12 rpm).

Analytical Techniques

Headspace samples were analyzed using a Tekmar^{TM} 7000 headspace autosampler (Teledyne Temar, Mason, OH). Vials were equilibrated in the autosampler at 40°C for 8 minutes. Samples were analyzed by gas chromatograph equipped with a flame ionization detector (GC-FID) (Agilent Technologies 6890N Network GC System, Agilent Technologies, Incorporated, Santa Clara, CA), operated with a split ratio of 20:1 with a Restek Q-Bond column (30 m length × 0.32 mm I.D. × 10 µm film thickness). The oven program maintained a 40°C temperature with no ramp for a total runtime of 6.0 minutes. An 11-point calibration curve was used to convert GC peak area responses to aqueous concentration of PCE (mg·L-1) (see Appendices A and B for calibration graphs and calculations). The calibration curve allows for indirect measurements of the aqueous concentration of PCE by using calibration standards with a known amount of PCE in the sampling vials. Therefore, when measuring the headspace, one is indirectly measuring the aqueous concentration of PCE.

3.4.3. Results

The following presents the results obtained from the batch sorption study of field soils. This section describes results from the two sorption tests as described in the above experimental

design: 1) sorption over time for each field soil and 2) effects of sorption due to a range of concentration levels applied to each field soil.

First, results from the sorption experiment to capture sorption over time will be discussed where data is displayed as aqueous concentration of PCE (C_{aq}) over time. Then, results from the sorption experiment to capture the effects of sorption due to varying concentration is discussed. The following results are portrayed as sorbed PCE concentration (C_s) versus aqueous concentration of PCE (C_{aq}) with varying isotherm trendlines fitted to the experimental data. The isotherm trendline fittings explored herein include: linear, Freundlich, and Langmuir isotherm fits. The Henry's dimensionless coefficient, $H_D = 0.712$, was used to calculate the estimated sorbed PCE mass onto each of the field soils (Pankow and Cherry 1996).

For both sorption experiments, the LGS is not displayed in the following results. This is due to 1) our assumption that the soil is inert, therefore, no sorption should occur, and 2) sampling difficulties that did not allow for similar sampling methods to take place.

Sorption Over Time

The following section discusses the results of the sorption study for soils and the rate of sorption of PCE to field soils over time. Figure 16 displays data for sorption over time by comparing the change in aqueous concentration of PCE over time of incubation (20 days). The aqueous concentration of PCE was indirectly measured using the calibration curve as described in the analysis technique in the previous method section. The results do not show any apparent trend over the 20 day incubation time, made evident by small R^2-values (Table 12) and large error bars. The lack of trend may be due to the timing of the sampling events unable to capture the sorption window. For future work, ensuring appropriate sampling time points is vital in capturing

the rate of sorption of the soils over time. Recommendations for capturing the sorption rates would be to have earlier time sampling events.

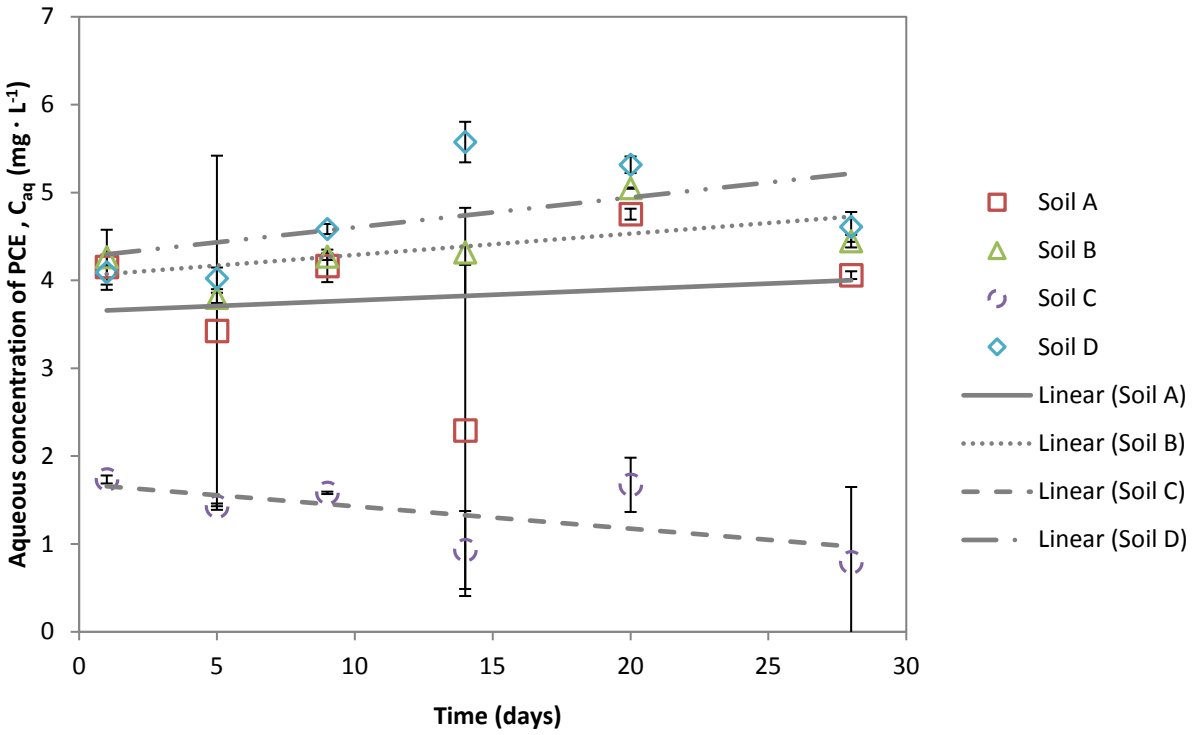

Figure 16. Aqueous concentration of PCE over time with linear trendlines for each field soil.

Table 12. Linear trendline equation and R^2-value for the aqueous concentration of PCE over time for each field soil.

Soil Name	Equation Parameters		R^2-value
	Slope (mg·L^{-1}·day^{-1})	y-int (mg·L^{-1})	
Soil A	0.0127	3.645	0.0221
Soil B	0.0242	4.0476	0.3583
Soil C	-0.0254	1.6818	0.4026
Soil D	0.034	4.263	0.2901

Linear Isotherm

The following section discusses two methods in which the K_d value was established for the linear sorption relationship. The first method utilizes the plotting of aqueous concentration of PCE versus the sorbed mass of PCE onto the field soils (Equation 1) to establish the K_d value using assuming a linear relationship. To establish the value of sorbed PCE mass onto each of the field soils was calculated using the Henry's dimensionless coefficient (H_D = 0.712) from the previous section.

Figure 17 and Table 13 display the linear trend and the K_d values, where Soil C has the largest K_d value, suggesting that this soil possesses higher affinity to sorbing PCE than the other field soils.

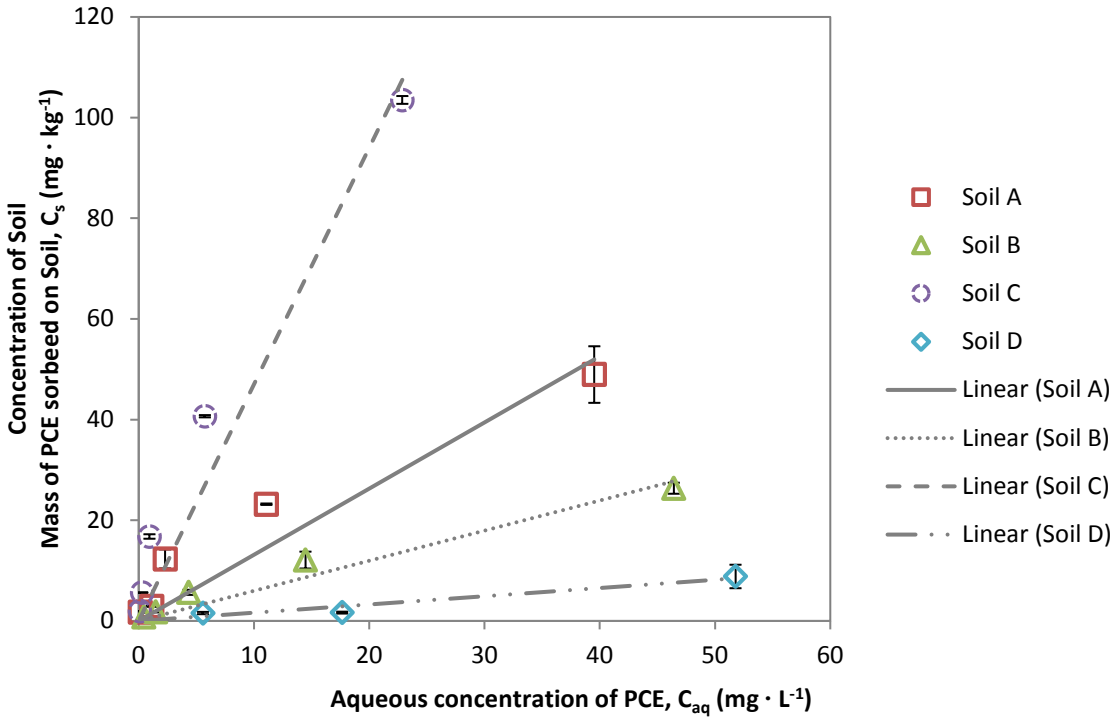

Figure 17. Linear trendlines to obtain parameter values using linear sorption relationship with concentration of soil values calculated using H_D = 0.712

Table 13. Linear isotherm value, K_d, and trendline significance values, R^2-value, using sorption values calculated using H_D=0.712

Soil Type	K_d (L·kg^{-1})	R^2-value
Soil A	1.314	0.946
Soil B	0.598	0.884
Soil C	4.700	0.944
Soil D	0.163	0.958

Freundlich Isotherm

The following graphs and tables show the results for establishing the Freundlich isotherm parameters *n* and K_f.

Figure 18 shows the concentration of PCE mass sorbed onto field soils (calculated using H_D=0.712) versus aqueous concentration of PCE (mg·L^{-1}) with all of the field soils A, B, C, and D after 14 days of incubation. Table 14 displays the Freundlich isotherm variables obtained from the power trendlines. Field soils A, B, and C were able to have power trendlines fit to the data series. Soil D has an incomplete data series for Figure 18 and Figure 19 due to negative values resulting from the calculated sorbed soil mass. From the power trendlines, Soil C has the largest K_f values, suggesting that Soil C has a higher sorptive capacity relative to the other soils used within the experiment.

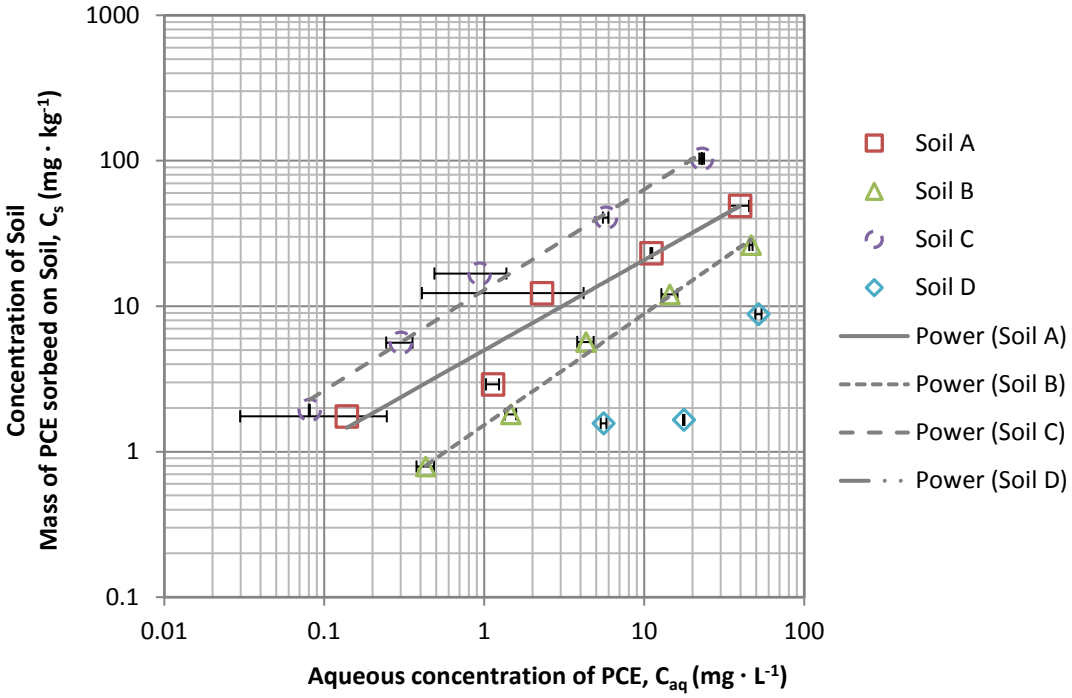

Figure 18. Concentration of sorbed mass PCE (calculated using Henry's Dimensionless Coefficient (H_D = 0.712)) versus aqueous PCE concentration

Table 14. Freundlich isotherm variables for K_f and n values from power trendlines

Soil Name	Freundlich Isotherm Variables		
	K_f $(L \cdot kg^{-1})^n$	n (dimensionless)	R^2-value
Soil A	4.99	0.62	0.927
Soil B	1.528	0.76	0.992
Soil C	12.95	0.69	0.987
Soil D	-	-	-

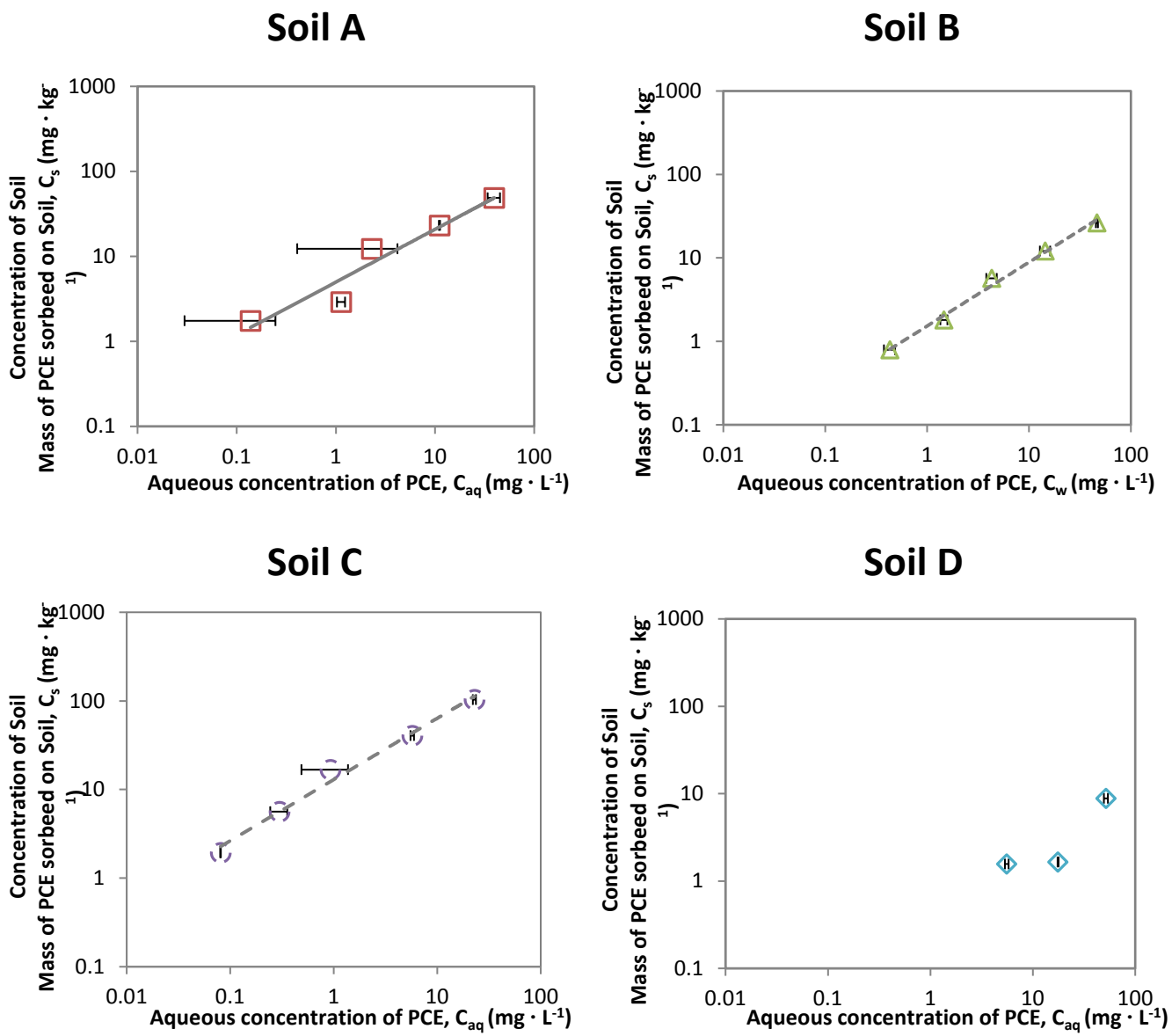

Figure 19. Concentration of sorbed mass of PCE versus aqueous PCE concentration (mg·L^{-1})

Langmuir Isotherm

The following section extracts the Langmuir isotherm variables K_L and Γ_{max} through plotting values from the sorption experiment with varying concentration. Using Langmuir's Isotherm equation (Equation 4) and rearranging the variables to obtain values from the linear trendlines to calculate parameters K_L and Γ_{max} results in Equation 6:

$$\frac{1}{C_s} = \frac{1}{C_{aq}}\left(\frac{1}{\Gamma_{max}K_L}\right) + \frac{1}{\Gamma_{max}} \tag{6}$$

Figure 20 **Error! Reference source not found.**displays the linear relationship between the inverse of the aqueous PCE concentration (C_{aq}^{-1}) versus the inverse of the concentration of PCE mass sorbed to the field soil (C_s^{-1}). The sorbed values were calculated using the Henry's dimensionless coefficient, $H_D = 0.712$. Table 15 show the values for the Langmuir Isotherm variables, K_L and $\Gamma_{max,}$ for each of the sorption values.

Table 15. Langmuir isotherm variables for K_L and Γ_{max} for calculated sorption values using $H_D = 0.712$

Soil Name	**Langmuir Isotherm Variables**		
	K_L ($L \cdot mg^{-1}$)	**Γ_{max} ($mg \cdot kg^{-1}$)**	**R^2-value**
Soil A	1.35	10.79	0.794
Soil B	0.14	13.97	0.982
Soil C	0.48	51.02	0.996
Soil D	0.09	4.22	0.520

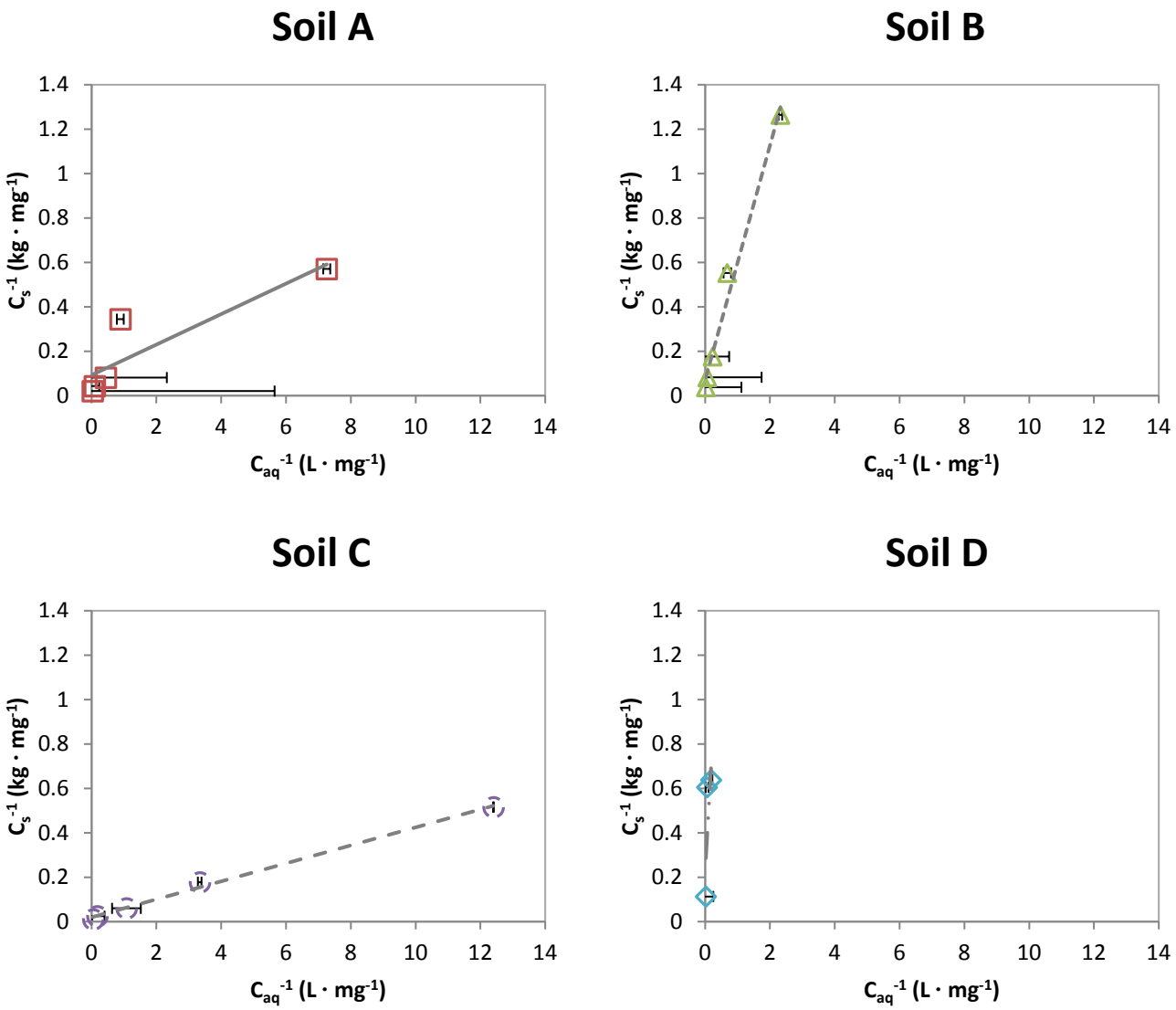

Figure 20. Plot of the inverse sorbed concentration (C_s^{-1}) versus aqueous PCE concentration (C_{aq}^{-1}) to establish Langmuir variables K_L and Γ_{max} from linear trendlines

From Table 15, Soil C has the largest amount of sorption sites (Γ_{max}) with respect to the other field soils, suggesting that Soil C has more potential for adsorptive sites than the other soils, increasing its potential to sorb PCE more readily with respect to the other field soils.

The linear, Freundlich, and Langmuir isotherms all suggest Soil C has the most sorptive capacity in comparison to the other field soils. Other experimental data, referencing the particle distribution analysis and the total carbon analysis, suggest similar conclusions. The larger amount of organic carbon may be one reason why Soil C sorbs a greater fraction of contaminants. Another reason why Soil C may have a larger amount of sorptive properties could be due to the particle size distribution of the soil, having higher fraction of clay than the other soils. Combined, the organic carbon and the finer clay materials increase the sorptive capacity of the soils. From the previous headspace vial experiment, Figure 15, displays Soil C as having the slowest transport rate relative to the other field soils, with breakthrough of the contaminant not occurring until day 89. Soil C's slow transport rate could be due to its high sorptive capacity and a larger tortuosity than the other field soils.

From the R^2-values that Soil A and B's sorption were best fit by the Freundlich Isotherm. Soil C was best fit by the Langmuir isotherm. And Soil D was best fit by the linear isotherm. The parameter values established from the linear, Freundlich, and Langmuir isotherms were used to establish the retardation factor, *R*, input value to test the mathematical model used in Chapter 4.

3.5. Methanol Extraction of Ampule

Due to potential losses that were shown from the stability and headspace vials study, closing the mass balance and recovering the original mass left within the vial over a long period of time remains a major challenge. A sealed glass ampule was viewed a plausible solution to avoid the

apparent losses that were observed through the Mininert® valve. The ampules approach follows the same conceptual design as the headspace vials, where there is an initially clean soil column that rests on top of a saturated boundary layer of PCE. Although vertical diffusion does occur within the soil column, the focus of this experiment is to measure recovery of the total mass from the vial and soil. To reduce volatile losses and gain measurable data from ampules, the ampules were broken while submerged in methanol to ensure the contents inside the ampule were not exposed to the outside environment except for methanol. The challenge with the ampule method during this initial stage of development is that the method only provides data at one point in time. Ideally, soils would be analyzed in vertical segments to gain information on transport of contaminant through the soil column. But as a first step, this work simply considers analysis of total mass in the entire soil system. The extraction of the whole ampule and its contents will provide data to establish initial recovery using this methanol extraction method.

3.5.1. Experimental Objectives

The experimental objective of the ampules was to demonstrate the ability and feasibility of closing the mass balance over an extended period of time. Furthermore, our objective was to establish methods for extraction of the ampules that results in sufficient recovery.

3.5.2. Methods

The method section includes a discussion on the experimental design, materials, preparation of materials, vial setup, extraction method, sampling procedures, and lastly, analytical techniques.

Experimental Design

The four field soils introduced in Section 3.3.3 and the lab grade field soil (control) were used within this experiment. The experimental design (Figure 21) consisted of triplicates of each field soil and eight lab grade field soils.

Figure 21. Ampule vial setup with field soils and lab grade soil.

Materials

The Materials used within the ampules were the same as those of the headspace vials: PTFE fiber filter, borosilicate glass beads, glass microfiber filter, compressed carbon dioxide gas, PCE, sudan IV, silica sand, kaolin clay, 500 µL PTFE luer lock glass syringe, luer lock blunt-tipped hypodermic needle, 60 mL luer lock tip plastic syringe, glass tubing, and deaired tap water. Other materials used were glass ampules (20 mL vials, Wheaton®, Millville, NJ), butane micro-torch (Bernzomatic, Home Depot™, Fort Collins, CO), glass jars with PTFE lined caps (125 mL, VWR®), lab grade methanol, hammer, screw driver and rubber stopper.

Preparation of Materials

The ampules were sterilized beforehand using the same methods as the headspace vials sterilization methods. The same materials were sterilized as with the headspace vials experiment which within this experiment excludes headspace vials and includes the glass ampules. For this experiment, the same soils, preparation, sterilization, and geologic-material paste were involved; only the ampules replaced the headspace vials.

Vial Setup

Ampules have the same vials setup as headspace vials (as described in previous section) except for a few minor differences in PTFE and glass fiber filter diameter sizes and the closing of the vial. The PTFE and glass fiber filters were cut to 20 mm sizes. The same protocols were used in filling the ampules as the headspace vials except in the replacement of a Mininert® cap to take mass measurements the use of a rubber septum cap was used in order to reduce any volatile losses during the vial setup procedure.

After the final step of measuring the glass ampule with geologic-material paste, the rubber septum cap was removed to allow for the closing of the glass ampule. To close the glass ampule, the top edge of the glass ampule and the glass rod were heated with a butane micro-torch (Figure 22a). Once the glass rod and glass ampule sufficiently heated, the glass rod and glass ampule were removed from the heat and were then fused together as one unit (Figure 22b). The flame of the butane mini-torch was placed back on the neck of the glass ampule just below the fused portion of the unit. The unit was then rotated to allow for the flame to evenly heat the neck of the glass. Once deformation of glass began to show (Figure 22c), the fused glass rod was then pulled upward and twisted. The walls of the ampule neck began to collapse and seal due to

deformation from the flames heat. Once the walls collapsed the fused glass rod is then pulled separately from the rest of the glass ampule (Figure 22d). The vials were then stored in a dark, dry, cool place for 124 days at room temperature ranging from 21 to 25^{o}C.

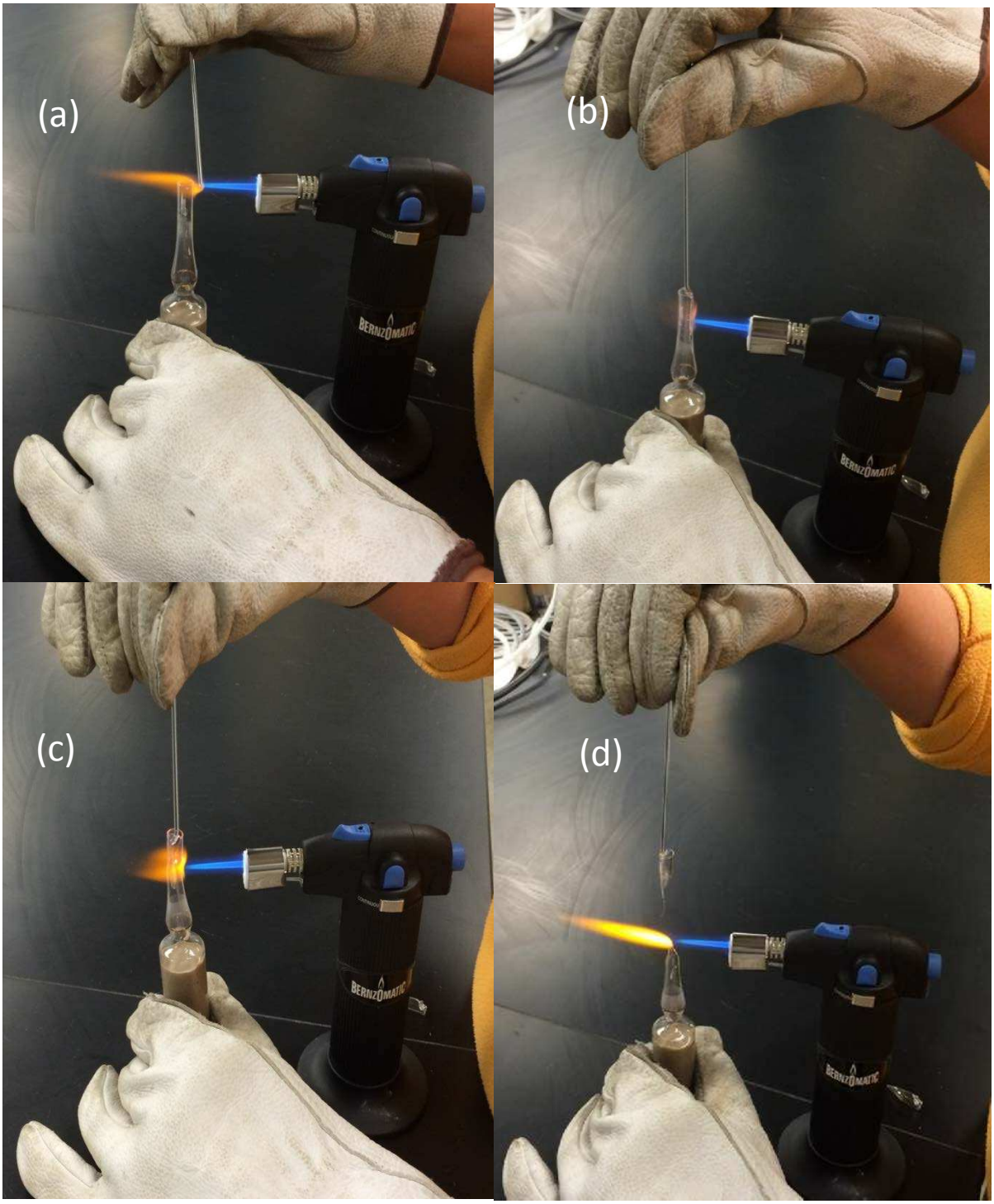

Figure 22. Steps to closing glass ampules (a), (b), (c), and (d)

Extraction Method

After 124 days, the vials were broken open and extracted into lab-grade methanol to recover the contaminant mass injected into the vials. Materials used specifically in the extraction method were sealed glass ampules, glass jar with 80 mL of lab-grade methanol, hammer, rubber stopper, and screw driver (Figure 23). Glass jars were used to extract the entire glass ampule into 80 mL of lab-grade methanol.

Figure 23. Materials used for methanol extraction of ampules.

First, the glass ampule was inverted with the scored portion of the glass submerged under methanol (Figure 24a). Then, by using the hammer to tap on the rubber stopper (placed on the bottom of the ampule) the scored portion of the glass ampule was broken (Figure 24b). The rubber stopper softens the force of the hammer and prevents the hammer from breaking the bottom of the glass vial. The hammer is tapped on the rubber stopper until the rubber stopper and the bottom of the glass ampule were submerged in the methanol. The screwdriver and

hammer were then used to break the bottom of the glass ampule to ensure the methanol made contact with the PTFE and glass fiber filters (Figure 24c).

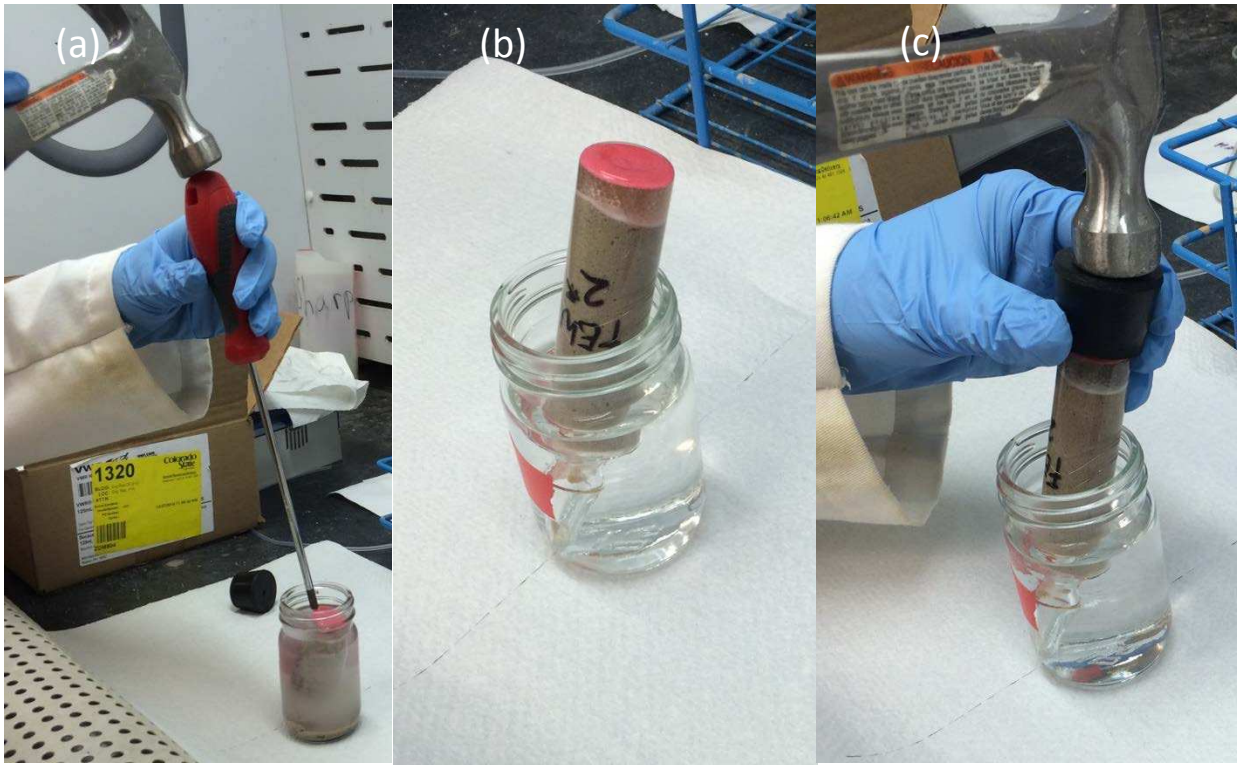

Figure 24. Steps for completing methanol extraction of ampules (a), (b), and (c)

Once the top and bottom of the glass ampule were broken, the glass jar was then closed using a PTFE-lined threaded cap. The extraction solution (methanol and glass ampule contents) were then shaken for 10 minutes on the vortex shaker at level 6 and then sonicated for 30 minutes in a 35°C water bath. The extraction solution was left to settle for 7 days before sampling.

Sampling Procedures

Sampling occurred 7 days after the initial extraction of ampules to ensure small particles were not suspended within the solution. Using a 100 µL manual pipette, 100 µL of the extraction sample were injected into 900 µL of lab-grade methanol within a GC vial.

Analytical Techniques

Samples were analyzed by gas chromatograph equipped with a flame ionization detector (GC-FID) (Agilent Technologies 6890N Network GC System, Agilent Technologies, Incorporated, Santa Clara, CA) operated with an inlet temperature of 250^{o}C and a split ratio of 20:1 with a Restek 10224 Trx-5 column. The oven program maintained 40^{o}C for 3 minutes, and then up to 150^{o}C, which was reached after 1 minute, with a total runtime of 6.75 minutes. GC peak area responses were converted to PCE concentration ($mg \cdot L^{-1}$) through a 5-point calibration curve, using a known PCE concentration in methanol (see Appendix A and B for calibration curve and calculations), which was further converted to PCE in grams. The calibration curve for the methanol extraction for ampules had a sampling error, therefore, the use of the headspace calibration curve was used for the conversion from peak area to PCE in grams.

3.5.3. Results

Table 16 shows the percent recovery of PCE from the methanol extraction method of the ampules, where Soil D had the highest recovery at 101.5% recovery. Figure 25 shows that given the methods employed, no significant difference of the other four field soils from the lab-grade control soil.

Table 16. Percent recovery of PCE from methanol extraction of ampules

Soil Name	Percent Recovery (%)	Standard Deviation
LGS	99.78	0.048
Soil A	93.15	0.049
Soil B	95.26	0.030
Soil C	97.91	0.020
Soil D	101.51	0.105

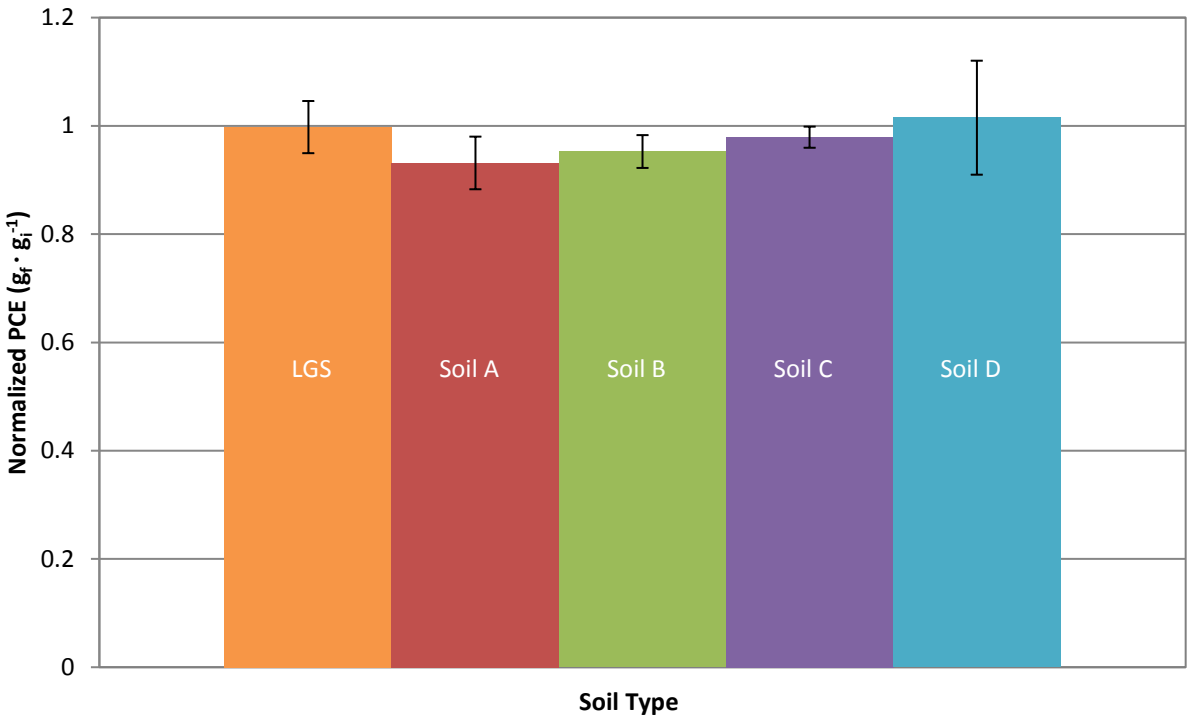

Figure 25. Normalized PCE recovery with final mass in grams over initial mass in grams ($g_f \cdot g_i^{-1}$) from ampules methanol extraction method with LGS and the four field soils

3.6. Methanol Extraction of Headspace Vials

The data from the ampules and the headspace experiment were not comparable, since one experiment measured total mass within the system and the other measured concentration at the top of the soil column, respectively. To allow for a comparison of results, the methanol extraction method used on the ampules was applied to the headspace vials. The following sections describe of the objective, methods, and results.

3.6.1. Experimental Objective

The objectives of the methanol extraction experiment is to compare the headspace vial experiment to the ampule experiment, and to determine PCE mass lost from the system.

3.6.2. Methods

The methods used are similar to the methods applied to the ampules in Section 3.5.2. The method section includes a discussion of the experimental design, materials, preparation of materials, vial setup, extraction method, sampling procedures, and lastly, analytical techniques.

Experimental Design

This experimental design includes the four field soils and one lab-grade soil (used as the control group). The experimental design is the same as the headspace vial experiment shown in Table 7. The entire headspace vial experiment will be used in conducting the methanol extraction.

Materials

Similar materials used for the methanol extraction of the ampules were also used for the methanol extraction of the headspace vials: wide-mouthed glass jars with black phenolic screw caps (125 mL and 250 mL, Qorpak®, VWR®), amber wide-mouthed jars with caps (500 mL, I-Chem, VWR®), lab grade methanol, hammer, screw driver and rubber stopper.

Vial Setup

Each jar was filled with 80 mL, 150 mL, and 250 mL of methanol for each headspace vial 20 mL, 40 mL, and 60 mL respectively. The jars were weighed and recorded throughout the process: empty jar and cap, jar and cap with methanol, and lastly, jar and cap with methanol and headspace vial.

Extraction Method

The same extraction method used on the ampules was applied to the extraction method of the headspace vials. See Methanol Extraction Method in Section 3.5.2 for ampules with more detail.

Sampling Methods

Sampling occurred 7 days after initial extraction of the headspace vials to ensure small particles were not suspended within the solution. Using a 1000µL manual pipette, 1000µL of the extraction sample were injected into a GC vial.

Analytical Techniques

Samples were analyzed by gas chromatograph equipped with a flame ionization detector (GC-FID) (Agilent Technologies 6890N Network GC System, Agilent Technologies, Incorporated, Santa Clara, CA) operated with an inlet temperature of 250^{o}C and a split ratio of 20:1 with a Restek 10224 Trx-5 column. The oven program maintained 40^{o}C for 3 minutes, and then up to 150^{o}C, which was reached after 1 minute, with a total runtime of 6.75 minutes. GC peak area responses were converted to PCE concentration ($mg \cdot L^{-1}$) through a 5-point calibration curve, using a known PCE concentration in methanol (see Appendix A and B for calibration curve and calculations), which was further converted to PCE in grams.

3.6.3. Results

The following results display the total mass recovered from the headspace vials using the methanol extraction as described in the previous sections. Table 17 and Figure 26 displays results from the four field soils and one LGS, all with the same soil column length of 6 cm.

Figure 26 shows the average normalized PCE mass for each soil, which is the ratio of the final mass of PCE measured to the initial mass of PCE, with the final measurement being taken after 8 sampling events over 208 days submerged underwater. The graph shows that no significant difference exists between each of the soils in the recovery of the PCE mass from the system, due to the error bars all overlapping. The soil with the largest percent of PCE recovery was Soil C with 91.2% mass recovery. The reason why Soil C had the highest recovery is most likely due to its higher ability to sorb the contaminant in the aqueous phase, as shown from the previous experiments (Section 3.3 and 3.4). The higher sorption characteristic of Soil C reduces the concentration at the top of the soil column reducing volatile losses that occur due to sampling, since most of the contaminant is in the sorbed phase. The soil group with the lowest recovery was the LGS. One reason for the decrease in recovery for LGS can be due to the soil being inert and was unable to sorb any of the contaminant, allowing more of the contaminant to be more susceptible to volatilizing and escaping the system. Since the top of the soil column for LGS has a higher contaminant concentration due to lack of sorption, an increase in the loss of PCE mass occurs as compared to the other soils with a higher ability to sorb the aqueous concentration.

Table 17. Percent recovery of PCE for field soils and LGS for 6 cm soil column length

Soil Type	Percent Recovery of PCE (%)	Standard Deviation (%)
LGS	84.2	13.7
Soil A	87.1	4.59
Soil B	90.0	2.52
Soil C	91.2	3.50
Soil D	88.0	0.92

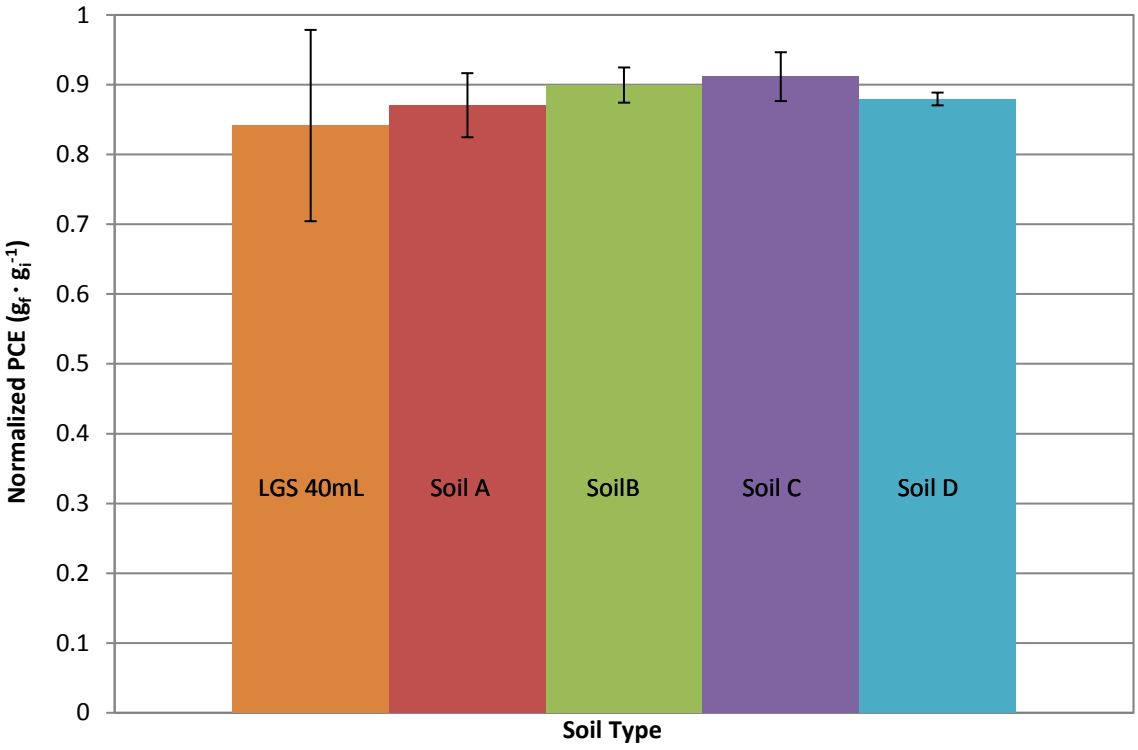

Figure 26. Normalized PCE recovery from methanol extraction for 6 cm field and lab grade soil columns.

Figure 27 shows the normalized PCE mass recovered of the three different soil column lengths for the LGS (3 cm, 6 cm, and 11.5 cm). Although the error bars do not show any significant difference between the three soil lengths, the longest soil column (11.5 cm) has the least amount of mass loss compared with the other soil lengths with a 99.1% recovery. The reason for longer soil columns to have a higher amount of recovery is most likely due to the contaminant having to travel a longer length and not reaching the top of the soil column as fast as the shorter soil columns. Less mass traveling to the top of the soil column reduces the overall loss of PCE due to sampling methods.

Table 18. Percent recovery of PCE for varying soil column length for LGS

Soil Length	Percent Recovery of PCE (%)	Standard Deviation (%)
3 cm	84.5	11.3
6 cm	84.2	13.7
11.5 cm	99.1	3.87

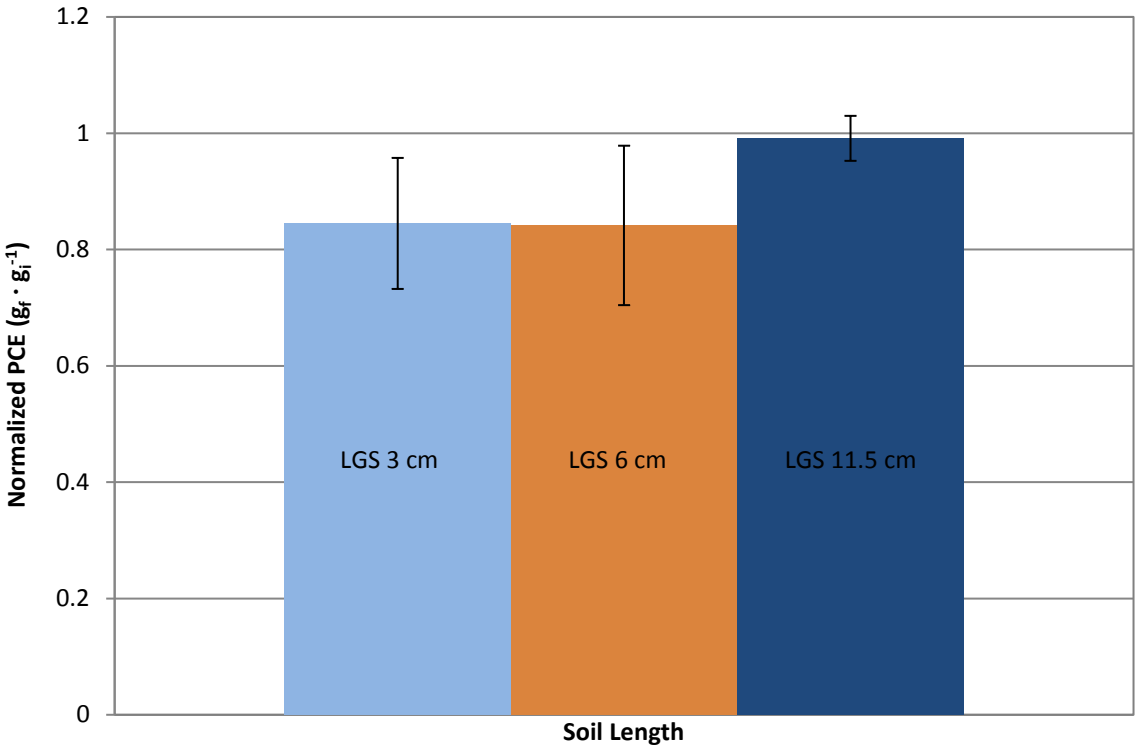

Figure 27. Normalized PCE mass ($g \cdot g^{-1}$) comparing final and initial mass of PCE, final measurements were gathered from the methanol extraction for LGS 3 cm, 6 cm, and 11.5 cm headspace vials

4. MATHEMATICAL MODELING

The following section describes the model used to represent contaminant transport through low-k media. Processes considered in the model include diffusion, sorption and degradation. The inputs for the model were obtained from the batch sorption experiment (Section 3.4). The model output produces results that are similar to the headspace vial experiment (Section 3.3), which displays concentration at the top of the soil column over time. The mathematical model will allow for the results from the batch sorption study to be compared to the headspace vial experiment, by using the batch sorption parameters as inputs to the model. The comparison of the results from the two studies will test the hypothesis that batch sorption studies can be used in conjunction with the headspace vial matrix to allow for a broader matrix for future long-term studies. The contents of this section include objectives, methods, and results.

4.1.Objectives

The purpose of the model is to test processes considered in the model, such as sorption, and compare the model to experimental conditions to ensure consistency. Another objective is to compare results obtained from batch sorption to headspace vial experiments to see if the two experiments can complement and enhance data gathered between these two experiments. The last goal of the model is to see if the experimentally obtained effective diffusion coefficient values for PCE (D_{exp}) is a practical approximation of the physical soil column within headspace vials.

4.2.Methods

The model uses a diffusion/reaction transport equation with boundary conditions and initial conditions set to reflect the headspace experiment system discussed in the previous laboratory experiments (Section 3.3). The following method section presents the key model assumptions, equations and methods used to develop the model output. Figure 28 shows the physical system used to represent the laboratory studies (see section 4.2.3 for variable definitions).

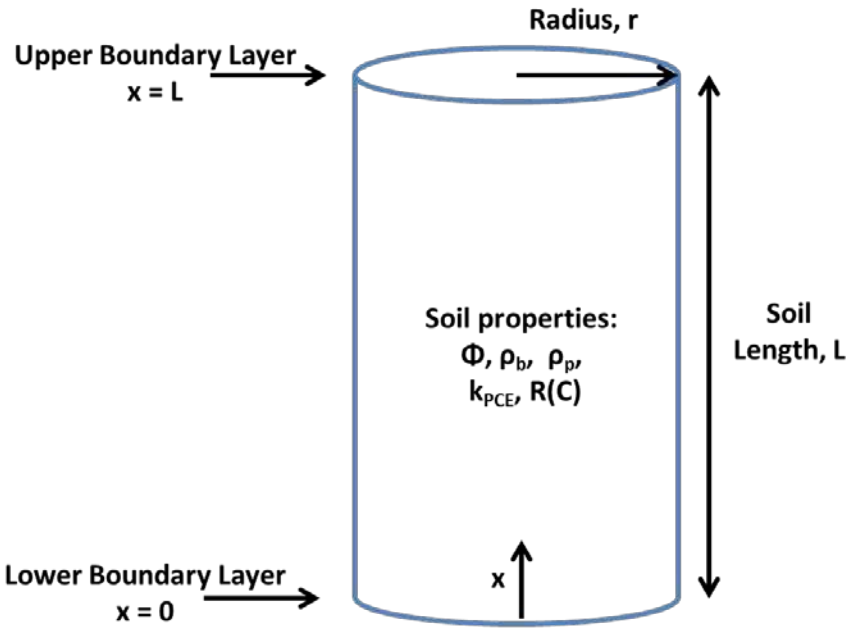

Figure 28. Physical system used for the model

4.2.1. Assumptions

Key assumptions for the model include:

1. Diffusion is the sole transport process within the soil column
2. Soils within the column are initially clean (uncontaminated)

3. The concentration at the lower boundary, in proximity to the NAPL is held constant at solubility.
4. The flux of contaminant is uniform across the lower boundary layer
5. Only aqueous phase contaminant is transported throughout the soil column
6. Aqueous and gas phase at the top of the soil column reaches equilibrium instantaneously
7. The headspace has a small enough mass where the flux is negligible from the top of the soil into the headspace.

4.2.2. Equations

The following partial differential equation was used to describe the transport of aqueous phase contaminant within the headspace experimental vials.

Governing Equations

The governing equation for this model is a simple diffusive transport equation:

$$R(C_{aq})\frac{\partial C_{aq}}{\partial t} = D\frac{\partial^2 C_{aq}}{\partial x^2} - kC_{aq} \quad (7)$$

Where, $R(C_{aq})$ (dimensionless) is the retardation factor as a function of concentration, C_{aq} ($M \cdot L^{-3}$) is the aqueous concentration of contaminant, t (T) is time, D ($L^2 \cdot T^{-1}$) is the effective diffusion coefficient of PCE, x (L) is the position of the soil column, and k (T^{-1}) is the degradation coefficient.

Boundary/Initial Conditions

Boundary conditions are as follows:

- At all time, *t*, the PCE concentration at the lower boundary (x = 0) is equal to the solubility of PCE in the aqueous phase. This follow from assumption (3) from the list presented above. The solubility value was obtained from Pankow and Cherry 1996.

$$C_{aq}(0,t) = 200\frac{mg}{L} \quad (8)$$

- At all time, the aqueous PCE concentration gradient ($M{\cdot}L^{-2}{\cdot}T^{-1}$) at the upper boundary layer (i.e., where L = 3 cm, 6 cm, or 11.5 cm) is zero. This follows from assumptions (7) from the list presented above.

$$\frac{\partial C_{aq}(L,t)}{\partial x} = 0 \quad (9)$$

Initial conditions are as follows:

- At initial time, *t = 0*, at all length, *x*, there is an aqueous concentration ($M{\cdot}L^{-3}$) of zero throughout the soil column. The entire soil column is considered "clean" and uncontaminated. This follows from assumption (2) from the list presented above.

$$C_{aq}\,(x,0) = 0\frac{mg}{L} \quad (10)$$

4.2.3. Solutions

The model simulates the experimental headspace vial system, wherein the main contaminant transport process is diffusion within the aqueous phase through the soil. The focus is on the rate of contaminant transport through the soil column and the measurable effects of sorption and degradation on contaminant transport. A closed analytical solution (van Genuchten 1982) was considered, but was found to be limiting in abilities to add increased complexities within the

system (i.e. non-linear sorption and degradation). To overcome this limitation, the selected modeling approach was a numerical model used to estimate the transport of the aqueous phase contaminant through the soil.

The calculations for the numerical solution for estimating aqueous phase transport through the soil column were carried out using Mathcad^{TM} 15.0 software (PTC, Inc., Neeham, MA). The governing equation (Equation 7) was solved numerically using the Mathcad^{TM} Partial Differential Equation (PDE) solve function.

Dimensions of column length, L, and radius, r, were used to define the boundaries of the system. The input parameters that may be changed within the model are porosity (ϕ), saturation concentration (C_{sat}), effective diffusion coefficient for PCE (D), retardation factor as a function of concentration ($R(C)$), and degradation coefficient (k).

Porosity, ϕ, was calculated using the relationship between particle density ρ_p ($M \cdot L^{-3}$) and bulk density ρ_b ($M \cdot L^{-3}$) where $\phi = 1 - \rho_p \cdot \rho_b^{-1}$, using a particle density of 2.65 $g \cdot m^{-3}$, and bulk density values measured from experimental data (Appendix D). The saturation concentration was kept constant at 200 $mg \cdot L^{-1}$ since only one contaminant, PCE, was introduced to the system. The experimentally calculated effective diffusion coefficient (D_{exp}) was defined by the relationship between the free diffusion of PCE in water $D_0 = 10.1 \times 10^{-3}$ $cm^2 \cdot sec^{-1}$ as defined by Pankow and Cherry (1996), porosity (ϕ), and tortuosity (τ) by the equation: $D_{exp} = D_0 \phi \tau$.

Tortuosity is further defined as a function of porosity and is calculated following Boudreau (1996):

$$\tau = \frac{1}{1 - \ln(\phi^2)} \tag{11}$$

Due to uncertainties in laboratory soil properties and the general empirical nature of Equation 11, the experimentally calculated D_{exp} values were considered only as estimates.

The following explains the three sorption relationships evaluated to calculate the retardation factor (R): linear, Freundlich, and Langmuir. The linear sorption relationship utilizes Equation 3 to calculate R. Two methods were used to calculate K_d values: (1) K_{ow}-K_{oc}-f_{oc} relationship (Equation 2 and Equation 15 see Appendix B Section 8.3.2) where values are found in Table 9 and (2) batch sorption study where values are found in**Error! Reference source not found.** Table 13.

To describe non-linear sorption relationship, the Freundlich and Langmuir isotherms were evaluated. The Langmuir was selected as it provided adequate fit of experimental data (see Section 3.4) and was compatible with the numerical solution methods using the Mathcad™ tool. To calculate the retardation factor, it is necessary to redefine retardation as a function of C as shown in Equation 4. Rearranging the Langmuir equation (Equation 4), where $R(C)$ is defined as the following equation (for the derivation of Equation 12 see Appendix C):

$$R(C) = 1 + \frac{\rho_b}{\phi}\left(\frac{K_L \Gamma_{max}}{1 + K_L C}\right) \tag{12}$$

Values used for Γ_{max} and K_L were obtained from the batch sorption experiments located in Table 15.

The PDEsolve function works best with dimensionless values, therefore, all boundary conditions and initial conditions are converted to dimensionless inputs. The conversion to dimensionless

units for each input is shown in Appendix C. The model uses the PDE solve block to produce dimensionless output of PCE concentration as a function of position and time. The dimensionless output is then converted back to produce an output with dimensions where time is in days and PCE concentration at the top of the soil column is in $mg \cdot L^{-1}$.

The model also is able to produce outputs of PCE concentration at times when sampling points occurred to allow for ease in comparing observed data versus predicted values.

4.3.Results

This section presents the results of the numerical solutions, with the model output displaying PCE concentration at the upper boundary layer over time. The results are presented by applying batch sorption values as inputs to the model and comparing the model output to each respective soil column, starting first with LGS soil (for 3 cm, 6 cm, 11.5 cm) and one field soil (Soil C).

4.3.1. Application to Laboratory Data

The following presents results of the numerical solutions using batch sorption values and other experimental values as inputs (L, ρ_b, D_{exp}, K_d, Γ_{max}, and K_L values) to compare the batch sorption results to the experimental headspace data. The following presents model fitting based on column length and soil type. For fitting the model based on column length LGS experimental data was used, where a linear sorption relationship with input variables L, ρ_b, and D_{exp} were used. For model fitting based on soil type, Soil C experimental data was used (Section 3.3), and compared the linear and Lagmuir sorption model fits where additional input variables, such as K_d, Γ_{max}, and K_L values, were used to produce model output.

Lab Grade Soil

The headspace vial experiment set up laboratory experiments to evaluate contaminant transport for soil columns of varying lengths for LGS. Fitting the model to the different soil lengths will help to determine if the different soil column lengths are scalable. When fitting the model to the experimental data the variable inputs applied are L, ρ_b and D_{exp}. The soil column length, L, had three varying lengths to match the headspace experiment: L = 3 cm, 6 cm, and 11.5 cm. The bulk density, ρ_b, was an experimentally-measured and calculated value of 1.59 $g \cdot mL^{-1}$ (see Appendix D Section 10.1 for bulk density raw data). The bulk density value was then used to calculate the effective diffusion coefficient (see Section 4.2.3 for calculation details), where the experimentally-calculated value for LGS is defined by D_{exp} = 1.23 x 10^{-5} $m^2 \cdot day^{-1}$ (calculations for D_{exp} are found in Appendix B). For LGS, sorption was assumed to be negligible (as discussed in Section 3.3), therefore R = 1.

Figure 29, Figure 30, and Figure 31 display model outputs for column lengths (3 cm, 6 cm, and 11.5 cm respectively). All figures present model outputs based on the experimentally-calculated effective diffusion of PCE D_{exp} = 1.23 x 10^{-5} $m^2 \cdot day^{-1}$ (dotted-green line). **Error! Reference source not found.**Error bars for the experimental LGS data represent the standard deviation based on n = 3.

Figure 29 displays a close fit to the experimental data during early time points for the D_{exp} values for the LGS 3 cm soil column. Day 28 and later sampling events were most likely not captured by the model output due to a lack of understanding of total losses from the headspace vial system. By the last sampling event (Day 193) the model displays the top of the soil at saturated concentrations (set to 200 $mg \cdot L^{-1}$ as suggested by the literature), whereas within the headspace

vial experiment the top of the soil reached only three-quarters of the solubility literature value. The top soil not reaching solubility at the top of the soil column by the end of the experiment is most likely due to leaks from the system.

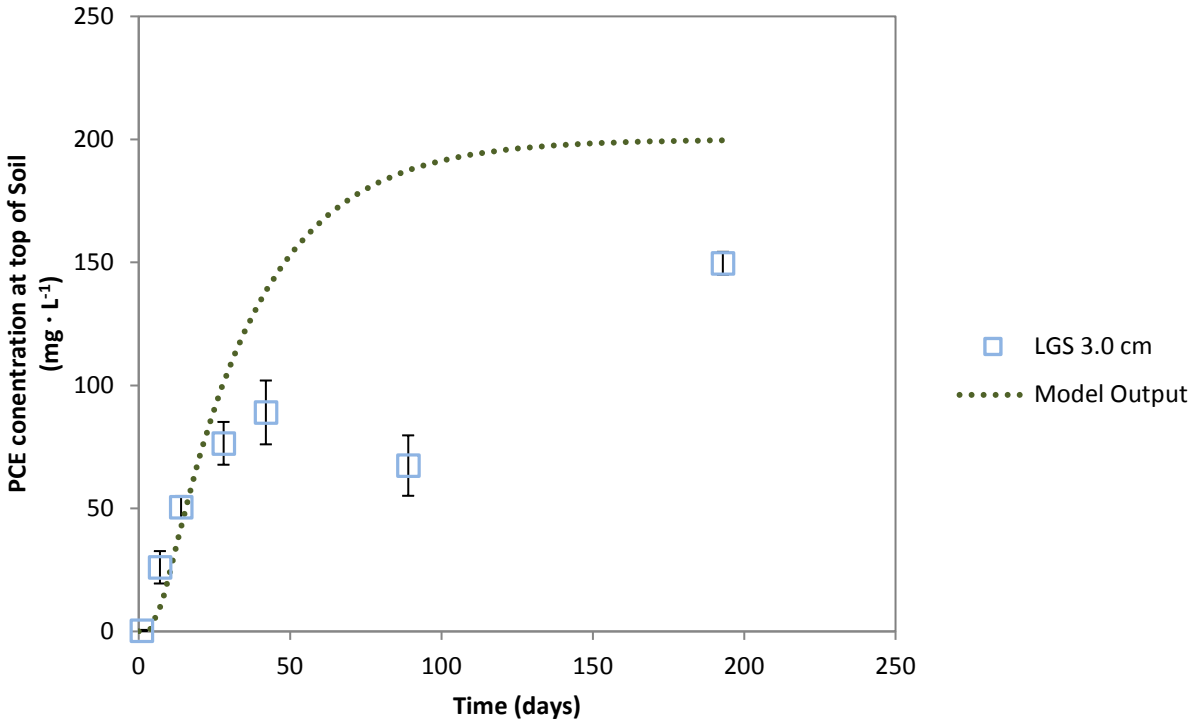

Figure 29. Fitting the model to experimental data: LGS 3 cm with R = 1; D_{exp} = 1.23 x 10^{-5} $m^2 \cdot day^{-1}$

Figure 30 shows the model underestimating the early time points, until Day 193 where the model begins to overestimate the late time point. The faster breakthrough of PCE at the top of the soil column may be due to conduits that may have allowed PCE to diffuse faster through the soil column. It would be prudent to develop a method that would ensure minimal conduit pathways for the constituent of concern to transport through. If the headspace vial method is the preferred route for conducting long-term laboratory studies, it is suggested that the soil column be set up in a way that allows for soil to be compacted that would limit conduits and minimize sore size variation throughout the soil column.

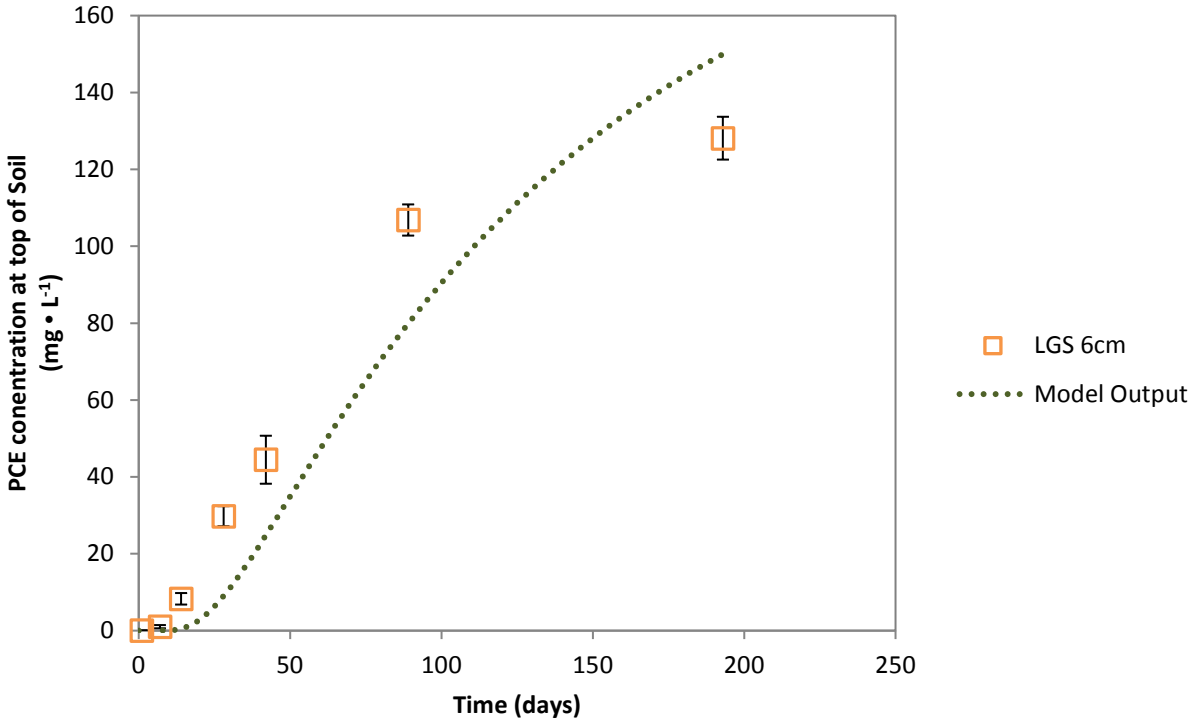

Figure 30. Fitting the model to experimental data: LGS 6 cm column with R = 1; D_{exp} = 1.23 x 10^{-5} $m^2 \cdot day^{-1}$

Figure 31 displays the model output for 11.5 cm column. This figure displays a similar trend of the headspace vial experiment results as the 6.0 cm soil column study, where the headspace vial experiment has consistently higher concentrations of PCE at the top of the soil than the model output. The underestimating of the model is most likely due to the soil column having preferential pathways that were created during the assembly of the soil column. It is noted, that more rigorous methods should be developed in the making of the soil column.

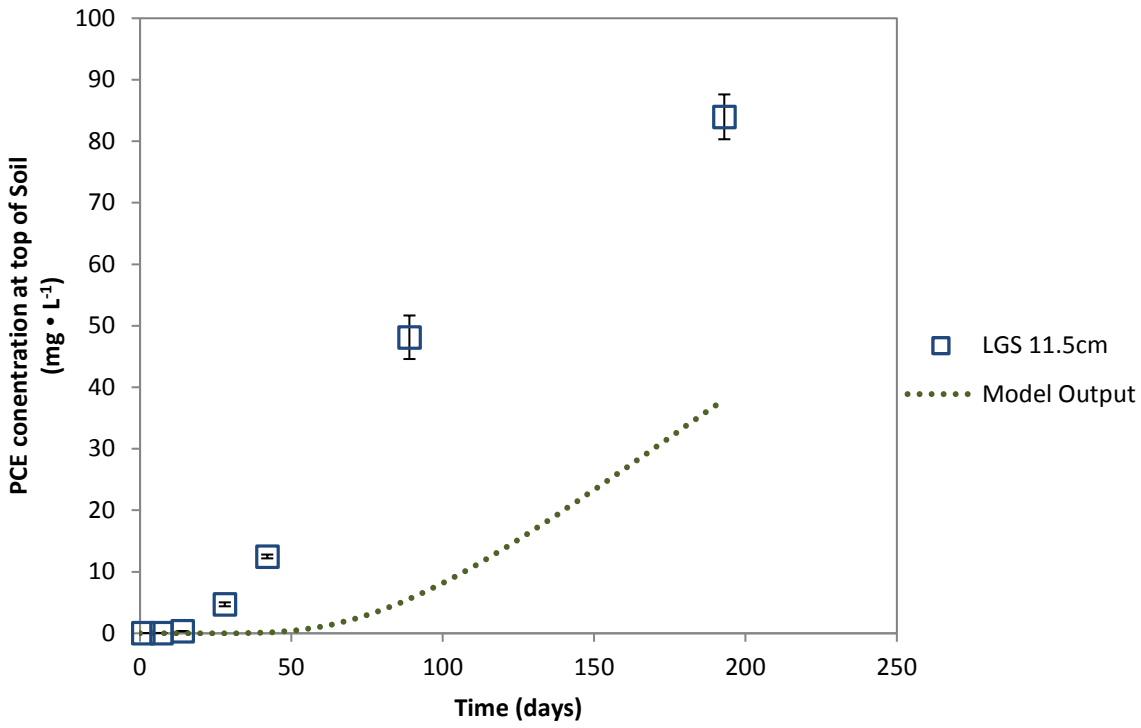

Figure 31. Fitting the model to experimental data: LGS 11.5 cm column with R = 1; D_{exp} = 1.23 x 10^{-5} $m^2 \cdot day^{-1}$

The model output with the closest fit to the headspace experimental data was the 6 cm soil column. Although, the same D_{exp} input value was unable to fit the 3 cm and 11.5 cm headspace experiment soil column data as shown in Figure 29 and Figure 31 of the model output. If the soil columns for the headspace experiment were setup with the exact same porous volume, the soil columns would share the same D_{exp} value and the model would show a closer fit to all three of the varying soil lengths from the experimental data. Due to the inability to use one D_{exp} value to best fit all the soil columns, it is concluded that scaling up soil columns is not a viable option at this time. Although scaling up soil columns is not a viable option, the variances between concentration at the top of the soil column over time for each individual soil column within its respective 3 cm, 6 cm, and 11.5 cm are within a reasonable variance. These small variances in concentration over time show that it is possible to setup soil columns of consistent porosity when

setup to be of the same length. It is necessary to develop more accurate methods in establishing the soil columns effective diffusion to appropriately represent the physical system when using the model to fit to experimental data. Current methods are not to be applied to long term experiments due to indication of leaks from the headspace vial system, potential preferential pathways, and inaccurate physical capture of the D_{exp} value. Before continuing with the headspace vial method establishing the losses that occur due to leaks from the system, establishing a more rigorous method when creating the soil columns are necessary steps before long-term soil column studies can be implemented.

Field Soil

Field soil parameters from the batch study were applied to the model to see the applicability of other inputs, such as sorption, could be represented within the model and compare to the headspace vial data to see if there is a close fit between the data and the model. Soil C was chosen to do initial model fitting since this field soil had the largest difference in contaminant breakthrough (Figure 15), along with finer soil characteristics from the particle distribution analysis (Figure 10 and Figure 11), and the highest sorption potential as measured from the total carbon analysis (Table 8) and batch sorption experiments (**Error! Reference source not found.**Figure 17).

This section will cover two of the common sorption relationships used within numerical modeling: Linear and Langmuir. The input parameters that were held constant throughout each sorption relationship modeling event were ρ_p = 2.65 g·cm^{-3}, ρ_b = 1.695 g·mL^{-1}and the k = 0.00 day^{-1}. The effective diffusion coefficient, D_{exp} = 1.03 x 10^{-5} m^2·day $^{-1}$, that was applied to the model was calculated using the particle and bulk density inputs. The input parameters that were

varied between each of the model fittings was the K_d values that were used to calculate the R, where R is defined by Equation 3 for the linear isotherms and Equation 12 for the Langmuir isotherms. First Soil C will be fitted to the linear sorption numerical model where two different K_d values will be applied as inputs. The first K_d value was obtained through the K_{ow}-K_{oc}-f_{oc} relationship (applied as input only in the linear model) and the second K_d value was obtained from the batch sorption experiments (used in both linear and Langmuir models).

Linear Sorption

The first sorption relationship applied to the model was linear sorption where the K_d values will be used to calculate the retardation factor using Equation 3. The K_d values that will be used as input values for the model were calculated by two methods 1) the K_{ow}-K_{oc}-f_{oc} relationship where values are shown in Table 9 and 2) from the batch sorption isotherm studies where values are shown in**Error! Reference source not found.** Table 13.

Figure 32 shows the model output for using both K_d values as mentioned above. The K_d value calculated with the K_{ow}-K_{oc}-f_{oc} relationship resulted in a K_d value of 1.23 L·kg^{-1} which produced a retardation value of R = 6.83; and the batch isotherm studies resulted in a K_d value of 4.70 L·kg^{-1} producing a retardation value of R = 23.28. The linear sorption model outputs for both of the K_d values was able to capture the early time points, but the model outputs begin to largely underestimate the concentration at the top of the soil starting at day 89 and continuing to increase the gap between the model output versus the headspace vial data through the end of the experiment. The large discrepancies between the experimental data and the model output is most likely due to preferential pathways which allows for the constituent to transport through the soil column at a faster rate. The difference may also be due to inaccurate measurement of D_{exp} value,

as shown through the LGS soil column, which may not accurately represent the physical soil column setup and in turn make the model produce outputs that are not accurately portraying the system.

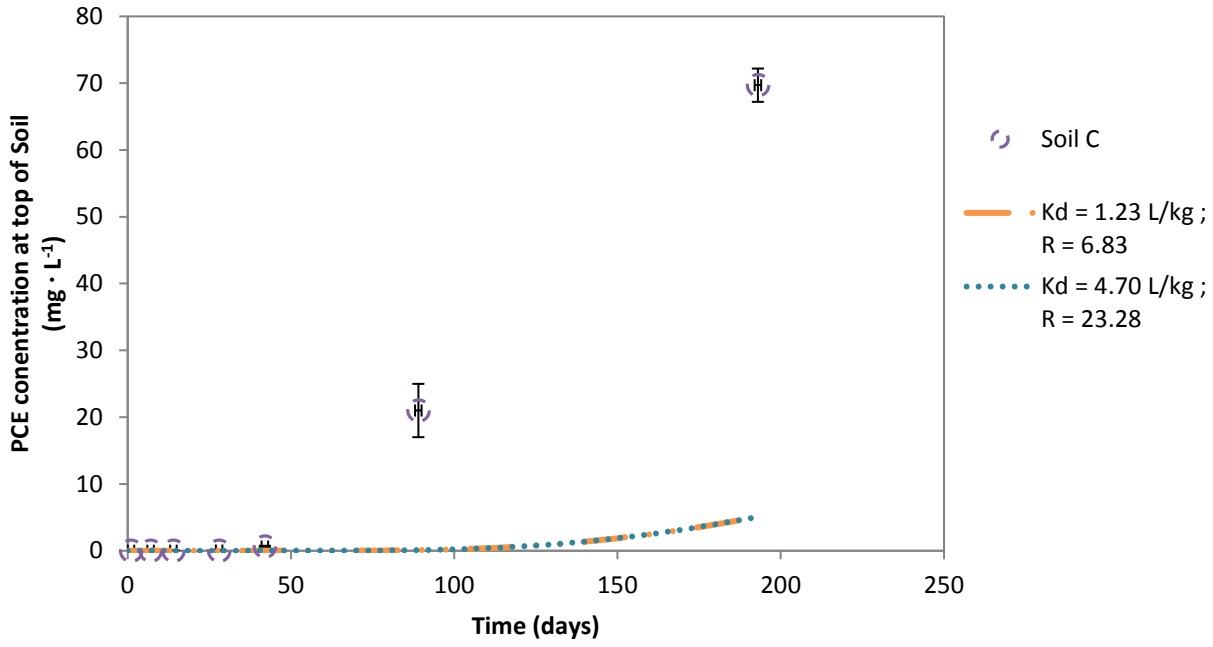

Figure 32. Model output for linear sorption model displaying two different K_d values to calculate the R values

Freundlich Sorption

An attempt was made to solve the governing equation using the Freundlich sorption term. Unfortunately, the Mathcad™ PDE solve algorithm was unable to converge to a correct solution. The inability to converge was most likely due to the exponent within the Freundlich term (Equation 12). It is suggested that for future work alternative modeling approaches be developed to ensure the solution of the Freundlich sorption term to allow for a full and complete comparison of all sorption terms used within the literature.

Langmuir Sorption

The following discusses the application of the Langmuir sorption relationship to calculate retardation factor for the model input. To calculate the retardation factor, the Langmuir equation was rewritten as a function of concentration, *R(C)*, as shown in Equation 16 in the previous methods section. The additional parameter input values that were used for the Langmuir sorption model were Γ_{max} and $K_{L,}$ along with previously used L, ρ_p, and ρ_b inputs used in the linear model.

Figure 33 displays the model output for the Langmuir model and Table 19 shows the parameters that were used as inputs for the model. The Langmuir sorption model was able to capture the early time points but was unable to capture the two later time points (Day 89 and 193), as seen in the linear model as well. One recurring explanation of why the model underestimated the experimental data was due to the D_{exp} value not being representative of the actual column, and due to preferential pathways that may have been created within the column which allow for a higher concentration at the top of the soil column. Another problem could be due to the Γ_{max} and K_L values being estimated at too large of a value causing the model to show an exaggerated amount of sorption within the soil column. The inaccurate D_{exp} value is most likely the case since we saw similar issues with the LGS when comparing the results of the model to the experimental values for the 3 cm and 11.5 cm columns.

Table 19. Model inputs for the Langmuir model

Henry's Dimensionless Value (dimensionless)	**K_L ($L \cdot mg^{-1}$)**	**Γ_{max} ($mg \cdot kg^{-1}$)**	**D_{exp} ($m^2 \cdot day^{-1}$)**
0.712	0.48	51.02	1.03×10^{-5}

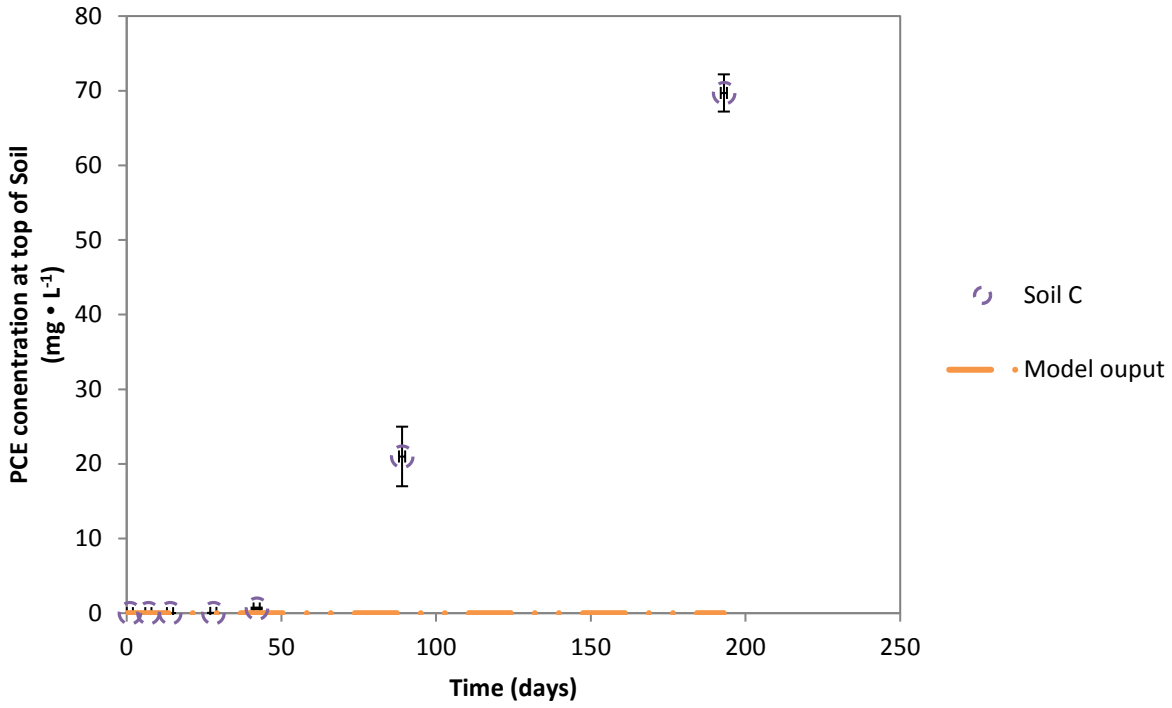

Figure 33. Model output for the Langmuir sorption relationship using K_L = 0.48 L • kg^{-1} and Γ_{max} = 51.02 mg • kg^{-1} values calculated using H_D = 0.712 from batch study experiment

Between the two sorption isotherm model outputs (linear and Langmuir), the linear isotherm was able to closer capture the experimental data as compared to the Langmuir model. Although the linear model output was a closer fit, due to the inability for the model to closely capture the LGS experimental data there is no way to assigning which model technically had the better fit. Applying the numerical model to the headspace experimental data exposes the weaknesses within our method development and allows us to pinpoint issues with the experimental effective diffusion coefficient that is not fully representative of the actual effective diffusion coefficient that is driving the system. For future method development it is suggested to create a more rigorous way to establish the effective diffusion coefficient that more accurately represents the soil column, along with resolving the leaks from the system through the cap. From this exercise

of applying the model to the headspace experimental data it can also be suggested that going to a method that is a more tightly closed system (i.e. ampules) is a more prudent option.

5. SUMMARY AND CONCLUSIONS

The following section is a summary of the key conclusions gathered from each Chapter which includes key results, implications and future work.

5.1. Key Results

In the stability experiment, substantial losses occurred with all the treatments. The treatment with the lowest loss rates occurred with vials that were not lined and were stored underwater with an average loss of 44.1%. Early losses had a higher rate of mass lost in comparison to late losses. Losses are dependent upon initial concentration within the vial, where the difference between early and late losses may be affected by concentration within the system. Loss rates may have been exaggerated due to stir bars being used within the stability experiments. Recommendations for future work include not using the Mininert® vial caps and exploring other options to gather meaningful data on assimilation processes of soil.

In the sorption fiber experiment for the glass fiber filter and the PTFE fiber filter, significant sorption occurred only for the PTFE fiber filter. Due to placement, function, and saturation of the contaminant, the fiber will not have an effect on the diffusive transport of the contaminant. Recommendations for future work suggest carrying out experiments with a range of concentrations, as well as, longer sampling times to observe sorption of each fiber over longer time frames.

In the headspace vial experiment with soil, the control without porous media stayed relatively stable within the range of variability with a starting concentration of 91.0 $mg \cdot L^{-1}$ and an end concentration of 87.4 $mg \cdot L^{-1}$. The key difference between the stability study and the control was

the lack of stir bars used within the headspace vial control. Due to this discrepancy in the two experiments, it is recommended for further investigation into the stability of the headspace vial using Mininert® valves.

The headspace vial experiment, diffusive transport showed lab grade soil followed the trend of breakthrough with 3 cm breaking through first, then 6 cm, a lastly 11.5 cm. When utilizing the headspace method, it is necessary to account for partitioning of the concentration that has accumulated at the top of the soil column. None of the soils reached solubility at the top of the soil column during the 193 day experiment. For field soils, the soil with the slowest transport rate was Soil C, which was supported by the soil characteristics of finer particle distribution and higher fraction of organic carbon compared to all the other field soils.

The batch sorption experiments conducted with the four field soils were used to determine sorption rates and establish parameter values to be used within the model. Only Soil C showed significant sorption as shown by concentrations of PCE decreasing over time. The field soils with higher sorption potential coincided with soil properties with higher organic carbon within the soil, which suggests that sorption to organic carbon is the major sorption mechanism within the field soils used within this study. The batch sorption study also looked at the effects of varying amounts of PCE have on the sorption properties of the field soils. After applying the range of concentrations to the field soils and taking samples at the same 14 day interval, the soil sorption data was then used to find the best fit sorption isotherm for each of the field soils. Soil A and B's sorption data was best fit by the Freundlich Isotherm, Soil C was best fit by the Langmuir isotherm, and Soil D was best fit by the linear isotherm. It was hypothesized that the best fit of isotherms for each field soil may help in establishing the best model type to fit the headspace vial data from the field soil column. To ensure appropriate measurement of sorption

parameters, it is recommended to conduct the sorption experiment with earlier time points to better capture more detail of the soil's sorption properties.

The results from the methanol extraction of the ampules found that recoveries ranged from 93.2% to 101.5% were obtained, with the best recovery occurring with the LGS. Recovery for the methanol extraction of headspace vials ranged from 84.2% to 91.2%, with the best recovery occurring for Soil C. The higher recovery in Soil C may be due to sorption properties of the soil reducing mass lost out of the vials through the Mininert® valve. The higher recovery for ampules shows that this method is the more viable option for long term laboratory studies.

A numerical mathematical model was used to compare the results from the headspace experiment to the batch sorption parameters, in the hopes to assist in understanding data results and critiquing current methods proposed for long-term studies. LGS and Soil C were used to compare batch sorption study parameters to experimental data. The 3-cm LGS model output initially was able to fit closely with the experimental results, but during late time points the model began overestimating experimental results, which most likely was due to leaks from the Mininert® valve that did not allow the headspace vial to reach solubility. The 6-cm and 11.5-cm soil columns model outputs were able to fit initial time points, but during late time points the model began underestimating experimental results. The underestimating is most likely due to preferential pathways occurring within the soil column. The varying model fit to the experimental headspace results for the 3 cm, 6 cm, and 11.5 cm soil column lengths suggest that with current methods the soil columns cannot be scaled up. The data from each soil column group show reasonable variance which suggests that the columns are set up in a way to be duplicated when made at the same length. More rigorous compaction during vial setup is necessary to ensure a more consistent effective diffusion coefficient to allow scaling up to be a

viable option. The varying effective diffusion coefficient may also be driven by losses from the Mininert® valve or sampling techniques. For future efforts, if wanting to carry out the headspace method, it is necessary to ensure losses are kept to a minimum and capturing the physical system through appropriate measurements for D_{exp}.

Soil C obtained a better fit with the linear model than the Langmuir sorption model, which contradicts what the batch sorption study that concluded Soil C best fit with the Langmuir isotherm. The model underestimated the experimental headspace results, which is most likely due to the effective diffusion coefficient not being representative of the physical nature of the soil column. Rigorous methods are necessary to ensure the effective diffusion coefficient is representing the physical properties of the soil column, as well as ensures duplicative efforts for creating the soil columns. The Freundlich sorption relationship could not be applied to the model due to inability for a solution to converge. Future methods should strive to apply all three models in the same numerical manner.

5.2.Implications

The goal of this research was to begin to establish methods to apply to long-term laboratory studies on low-k zones. Preliminary development of sampling methods, experimental design, establishing base line data, and applying preliminary data to a working model were completed within this research document. Current headspace methods were unable to fully contain the PCE mass within the system, and therefore would not be a viable option for long term laboratory studies.

However, the ampules allowed for full capture of the mass within the system using the methanol extraction methods. This method shows the most potential for reducing long term losses out of

the system. For future work, a suggestion of expanding on the ampule method would be to use discretized sampling points to gain understanding of contaminant transport, instead of just mass contained within the whole ampule. In conjunction with the methanol extraction method, exploring a way to recover mass from only the aqueous phase that has not been sorbed by organics to obtain information about the field soils overall sorptive ability should be carried out as well. Potential disadvantages of the ampules may be when reaction is occurring in the vials, where a closed environment may affect the reactivity of the materials producing reaction rates that are not representative of actual rates.

5.3.Future Work

For future work, it is suggested to expand upon the method of utilizing ampules. This would reduce mass losses for long term soil studies and still gain information on long term processes. Some potential problems would need to be addressed prior to starting the long term laboratory experiments. A suggestion for ensure full mass recovery with the method would be to set up ampules with a tracer such as C^{14} to ensure method fully captures total mass. Developing a method to breaking ampules into discretized discs, which would allow for more information to be gathered from the soil on a transport level. Accurately measuring effective diffusion coefficient would also be necessary to achieve understanding of contaminant transport. Once a method is developed to obtain discretized samples from ampules and measurement of effective diffusion coefficient, applying a similar numerical model to the ampules to allow expansion of system to larger realistic systems is necessary for applying to real world scenarios. It is also recommended to further explore how batch sorption studies could be used in conjunction with ampules. Another potential challenge would be the need to have all the ampules set up at the same time for the entire 5-10 year experiment design. A well-developed experimental design, as

well as detailed information of each of the soils used within the system would be necessary to carry out a successful long-term study.

6. REFERENCES

NRC 2004. Contaminants in the Subsurface: Source Zone Assessment and Remediation. The National Academies Press, Washington, DC.

Allen-King, R.M., Grathwohl, P., Ball, W.P., 2002. New modeling paradigms for the sorption of hydrophobic organic chemicals to heterogeneous carbonaceous matter in soils, sediments, and rocks. Advances in Water Resources 25, 985-1016.

Allen-King, R.M., Groenevelt, H., James Warren, C., Mackay, D.M., 1996. Non-linear chlorinated-solvent sorption in four aquitards. Journal of Contaminant Hydrology 22, 203-221.

Allen-King, R.M., McKay, L.D., Trudell, M.R., 1997. Organic Carbon Dominated Trichloroethene Sorption in a Clay-Rich Glacial Deposit. Ground Water 35, 124-130.

ASTM D422-63, 2007. Standard Test Method for Particle-Size Analysis of Soils, ASTM International, West Conshohocken, PA, 2007, www.astm.org

Ball, W.P., Liu, C., Xia, G., Young, D.F., 1997. A diffusion-based interpretation of tetrachloroethene and trichloroethene concentration profiles in a groundwater aquitard. Water Resources Research 33, 2741-2757.

Ball, W.P., Roberts, P.V., 1991. Long-term sorption of halogenated organic chemicals by aquifer material. 2. Intraparticle diffusion. Environmental Science & Technology 25, 1237-1249.

Bear, J., 1988. Dynamics of fluids in porous media.

Bodin, J., Porel, G., Delay, F., 2003. Simulation of solute transport in discrete fracture networks using the time domain random walk method. Earth and Planetary Science Letters 208, 297-304.

Chambon, J.C., Broholm, M.M., Binning, P.J., Bjerg, P.L., 2010. Modeling multi-component transport and enhanced anaerobic dechlorination processes in a single fracture–clay matrix system. Journal of Contaminant Hydrology 112, 77-90.

Chapman, S.W., Parker, B.L., 2005. Plume persistence due to aquitard back diffusion following dense nonaqueous phase liquid source removal or isolation. Water Resources Research 41, n/a-n/a.

Chapman, S.W., Parker, B.L., Sale, T.C., Doner, L.A., 2012. Testing high resolution numerical models for analysis of contaminant storage and release from low permeability zones. Journal of Contaminant Hydrology 136–137, 106-116.

Council, N.R., 2013. Alternatives for Managing the Nation's Complex Contaminated

Groundwater Sites. The National Academies Press, Washington, DC.

Cwiertny, D., Scherer, M., 2010. Abiotic Processes Affecting the Remediation of Chlorinated Solvents, in: Stroo, H.F., Ward, C.H. (Eds.), In Situ Remediation of Chlorinated Solvent Plumes. Springer New York, pp. 69-108.

Falta, R.W., Basu, N., Rao, P.S., 2005. Assessing impacts of partial mass depletion in DNAPL source zones: II. Coupling source strength functions to plume evolution. Journal of Contaminant Hydrology 79, 45-66.

Field, J.A., Sierra-Alvarez, R., 2004. Biodegradability of chlorinated solvents and related chlorinated aliphatic compounds. Reviews in Environmental Science and Bio/Technology 3, 185-254.

Freeze, R.A., Cherry, J.A., 1979. Groundwater. Prentice-Hall.

Geosyntec Consultants, 2004. Assessing the feasibility of DNAPL source zone remediation: Review of case studies.

Goldstein, K.J., Vitolins, A.R., Navon, D., Parker, B.L., Chapman, S., Anderson, G.A., 2004. Characterization and pilot-scale studies for chemical oxidation remediation of fractured shale. Remediation Journal 14, 19-37.

Groisman, L., Rav-Acha, C., Gerstl, Z., Mingelgrin, U., 2004. Sorption of organic compounds of varying hydrophobicities from water and industrial wastewater by long- and short-chain organoclays. Applied Clay Science 24, 159-166.

Johnson, M.D., Huang, W., Weber, W.J., 2001. A Distributed Reactivity Model for Sorption by Soils and Sediments. 13. Simulated Diagenesis of Natural Sediment Organic Matter and Its Impact on Sorption/Desorption Equilibria. Environmental Science & Technology 35, 1680-1687.

Johnson, R.L., Cherry, J.A., Pankow, J.F., 1989. Diffusive contaminant transport in natural clay: a field example and implications for clay-lined waste disposal sites. Environmental Science & Technology 23, 340-349.

Kalinovich, I., Allen-King, R.M., Thomas, K., 2012. Distribution of carbonaceous matter in lithofacies: Impacts on HOC sorption nonlinearity. Journal of Contaminant Hydrology 133, 84-93.

Kriegman-King, M.R., Reinhard, M., 1992. Transformation of carbon tetrachloride in the presence of sulfide, biotite, and vermiculite. Environmental Science & Technology 26, 2198-2206.

Lee, S.Y., Kim, S.J., Chung, S.Y., Jeong, C.H., 2004. Sorption of hydrophobic organic

compounds onto organoclays. Chemosphere 55, 781-785.

Lee, W., Batchelor, B., 2002. Abiotic Reductive Dechlorination of Chlorinated Ethylenes by Iron-Bearing Soil Minerals. 1. Pyrite and Magnetite. Environmental Science & Technology 36, 5147-5154.

Liu, C., Ball, W.P., 2002a. Back Diffusion of Chlorinated Solvent Contaminants from a Natural Aquitard to a Remediated Aquifer Under Well-Controlled Field Conditions: Predictions and Measurements. Ground Water 40, 175-184.

Liu, C., Ball, W.P., 2002b. Back diffusion of chlorinated solvent contaminants from a natural aquitard to a remediated aquifer under well-controlled field conditions: Predictions and measurements. Ground Water 40, 175-184.

Luthy, R.G., Aiken, G.R., Brusseau, M.L., Cunningham, S.D., Gschwend, P.M., Pignatello, J.J., Reinhard, M., Traina, S.J., Weber, W.J., Westall, J.C., 1997. Sequestration of Hydrophobic Organic Contaminants by Geosorbents. Environmental Science & Technology 31, 3341-3347.

Mackay, D.M., Cherry, J.A., 1989. Groundwater contamination: pump-and-treat remediation. Environmental Science & Technology 23, 630-636.

Magar, V.S., Vogel, T., Aelion, C., Leeson, A., 2001. Innovative Methods in Support of Bioremediation, The Sixth International in Situ and On-Site Bioremediation Symposium, San Dieog, CA, p. 197.

McCarty, P.L., 1997. Breathing with Chlorinated Solvents. Science 276, 1521-1522.

Olson, M.R., 2014. Remediation of soil impacted with chlorinated organic compounds: soil missing with zero valent iron and clay. Colorado State University.

Pankow, J.F., Cherry, J.A., 1996. Dense chlorinated solvents and other DNAPLs in groundwater: history, behavior, and remediation. Waterloo Press, 362.

Park, Y., Ayoko, G.A., Horváth, E., Kurdi, R., Kristof, J., Frost, R.L., 2013. Structural characterisation and environmental application of organoclays for the removal of phenolic compounds. Journal of Colloid and Interface Science 393, 319-334.

Parker, B.L., Chapman, S.W., Guilbeault, M.A., 2008. Plume persistence caused by back diffusion from thin clay layers in a sand aquifer following TCE source-zone hydraulic isolation. Journal of Contaminant Hydrology 102, 86-104.

Parker, B.L., Cherry, J.A., Chapman, S.W., 2004. Field study of TCE diffusion profiles below DNAPL to assess aquitard integrity. Journal of Contaminant Hydrology 74, 197-230.

Parker, B.L., Gillham, R.W., Cherry, J.A., 1994. Diffusive Disappearance of Immiscible-Phase Organic Liquids in Fractured Geologic Media. Ground Water 32, 805-820.

Payne, F.C., Quinnan, J.A., Potter, S.T., 2008. Remediation hydraulics. CRC Press, Boca Raton.

Purves, W., Orians, G., Heller, H.C.R., 1994. Life: the Science of Biology, 4th ed. Sinauer Associates Inc.

Saller, K., 2014. Management of contaminants in low permeability media. Colorado State University.

Sale, T.C., Zimbron, J.A., Dandy, D.S., 2008a. Effects of reduced contaminant loading on downgradient water quality in an idealized two-layer granular porous media. Journal of Contaminant Hydrology 102, 72-85.

Sale, T.C., Parker, B.L., Newell, C.J., Devlin, J.F., 2013, Management of contaminants in low permeability media. Colorado State University.

Schwarzenbach, R.P., Gschwend, P.M., Imboden, D.M., 2005. Sorption I: General Introduction and Sorption Processes Involving Organic Matter, Environmental Organic Chemistry. John Wiley & Sons, Inc., pp. 275-330.

Seyedabbasi, M.A., Newell, C.J., Adamson, D.T., Sale, T.C., 2012. Relative contribution of DNAPL dissolution and matrix diffusion to the long-term persistence of chlorinated solvent source zones. Journal of Contaminant Hydrology 134–135, 69-81.

Sheriff, T.S., Sollars, C.J., Montgomery, D., Perry, R., 1987. Modified clays for organic waste disposal. Environmental Technology Letters 8, 501-514.

Stroo, H.F., Leeson, A., Marqusee, J.A., Johnson, P.C., Ward, C.H., Kavanaugh, M.C., Sale, T.C., Newell, C.J., Pennell, K.D., Lebrón, C.A., Unger, M., 2012. Chlorinated Ethene Source Remediation: Lessons Learned. Environmental Science & Technology 46, 6438-6447.

Suthersan, S., Lutes, C., Palmer, P., Lenzo, F., Payne, F., Liles, D., Burdick, J., 2002. Technical Protocol for Using Soluble Carbohydrates to Enhance Reductive Dechlorination of Chlorinated Aliphatic Hydrocarbons. Environmental Security Technology Certification Program (ESTCP), p. 173.

Takeuchi, M., Kawabe, Y., Watanabe, E., Oiwa, T., Takahashi, M., Nanba, K., Kamagata, Y., Hanada, S., Ohko, Y., Komai, T., 2011. Comparative study of microbial dechlorination of chlorinated ethenes in an aquifer and a clayey aquitard. Journal of Contaminant Hydrology 124, 14-24.

Wackett, L.P.,1995. Bacterial co-metabolism of halogenated organic compounds. In: Young YL, Cerniglia CE (ed) Microbial transformation and degradation of toxic organic chemicals.

Wiley-Liss, New York, pp. 217–241

Wahlberg, J., 2013. Retardation and reaction in low permeability layers in groundwater plumes. Colorado State University.

van Genuchten, M.T., Alves, W.J., 1982. Analytical Solutions of the One-Dimensional Convective-Dispersive Solute Transport Equation. United States Department of Agriculture, Economic Research Service.

Yang, M., Annable, M.D., Jawitz, J.W., 2015. Back Diffusion from Thin Low Permeability Zones. Environmental Science & Technology 49, 415-422.

Zeman, Natalie R., 2013. Thermally enhanced bioremediation of LNAPL. Colorado State University.

Zhu, C., Anderson, G., 2002. Environmental Applications of Geochemical Modeling. Cambridge University Press.

7. APPENDIX A – CALIBRATION CURVES AND SUPPORTING DATA

7.1.Headspace Vial Experiment

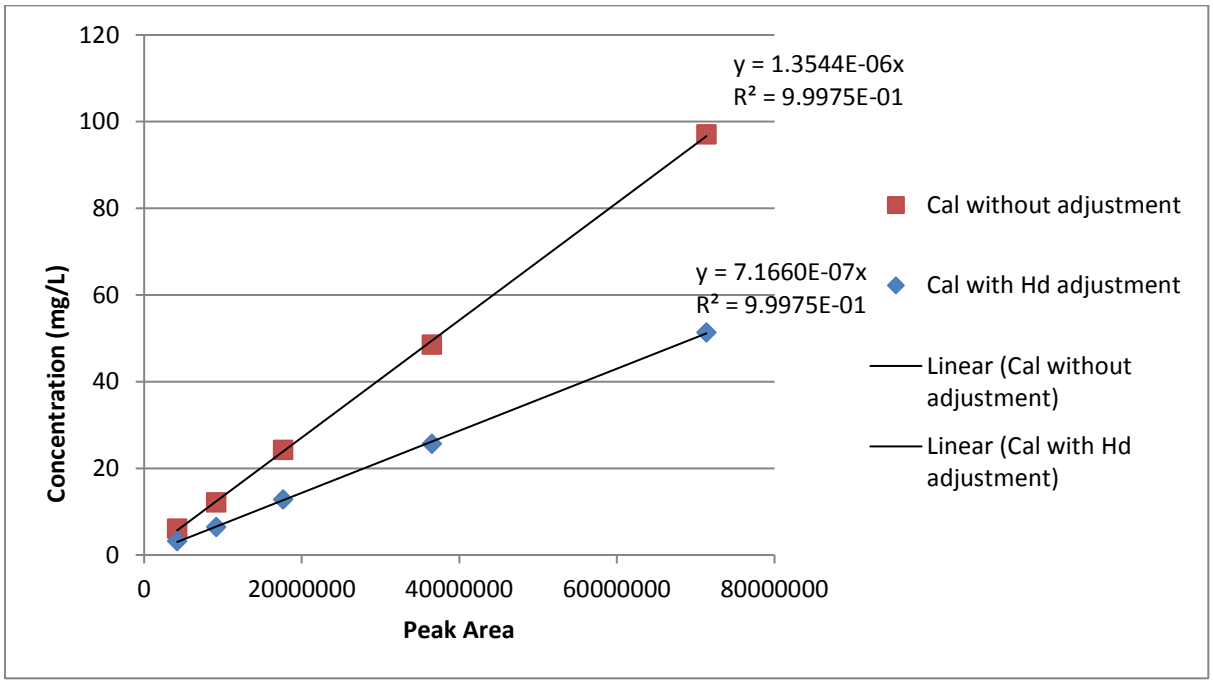

Figure 34. Calibration curve for Diffusion Reactor Headspace Vial gas samples, with GC Peak Area Response versus concentration ($mg \cdot L^{-1}$)

Figure 34 displays the calibration curves and equations, where the Henry's dimensionless (H_d) curve was used to convert GC Peak response times to aqueous concentration of PCE. The concentration calibrations were created with known amounts of Methanol-PCE solution in water (see calculations in Appendix B).

7.2.Sorption Study for Fiber Filters

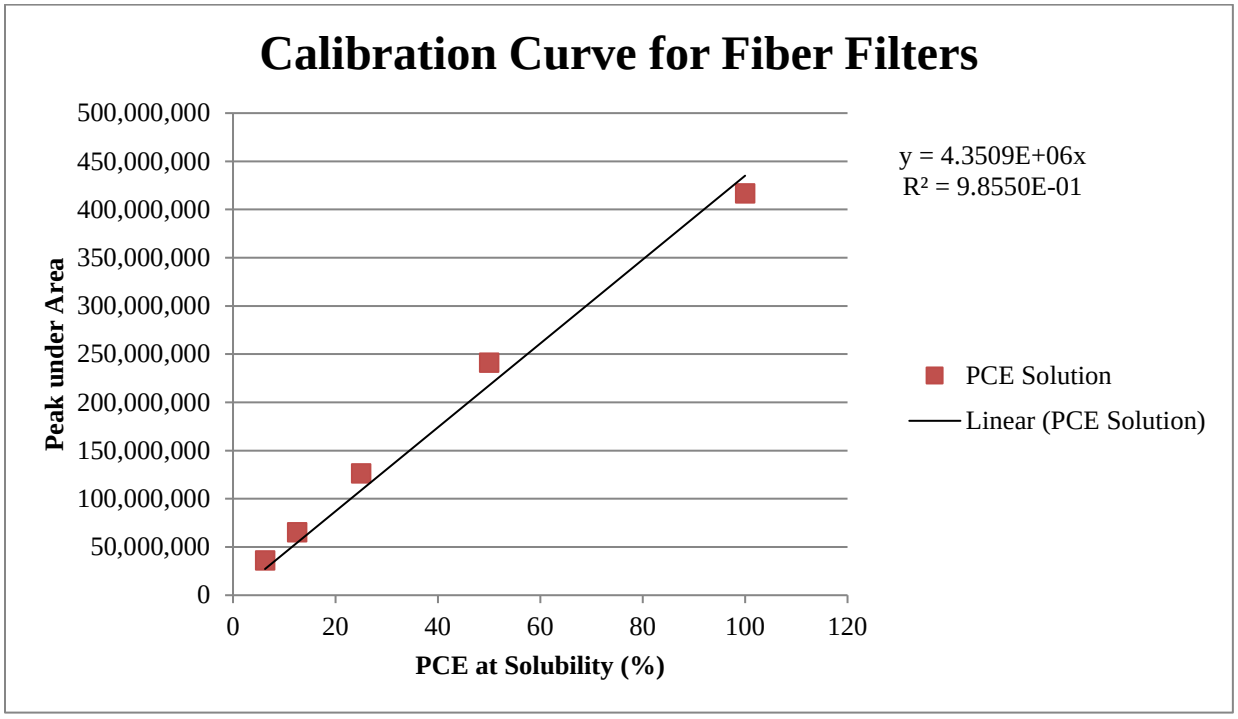

Figure 35. Calibration Curve for sorption study with fiber filters, used to convert GC Peak area to a PCE concentration

7.3.Sorption Study for Soils

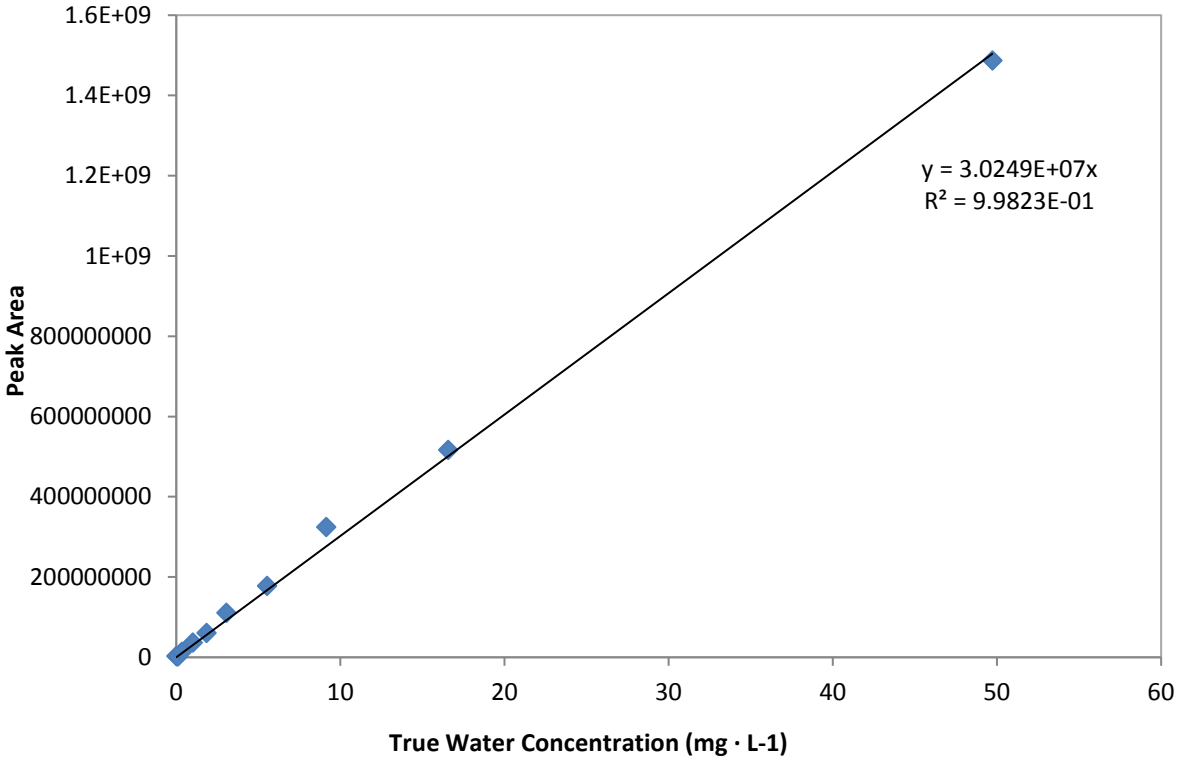

Figure 36. Calibration curve for sorption study of soils using Henry's Dimensionless Coefficient H_D = 0.712

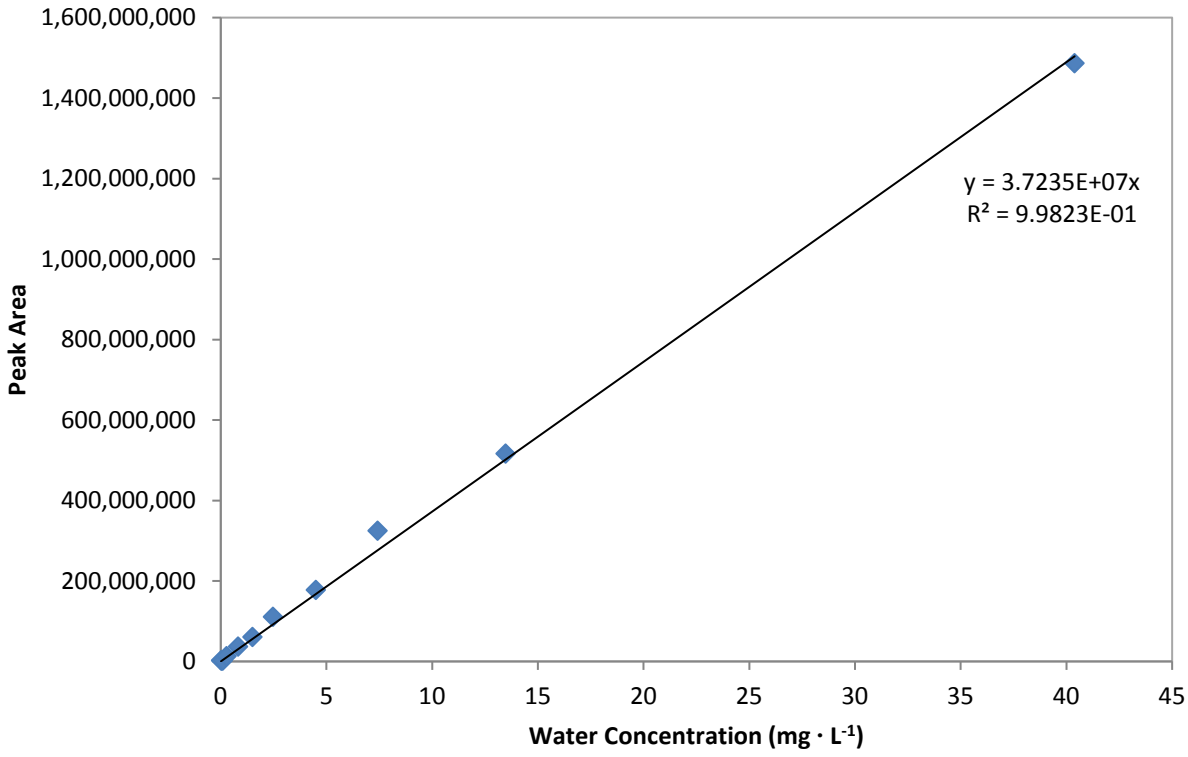

Figure 37. Calibration curve for sorption study of soils using Henry's Dimensionless Coefficient H_d = 1.0832

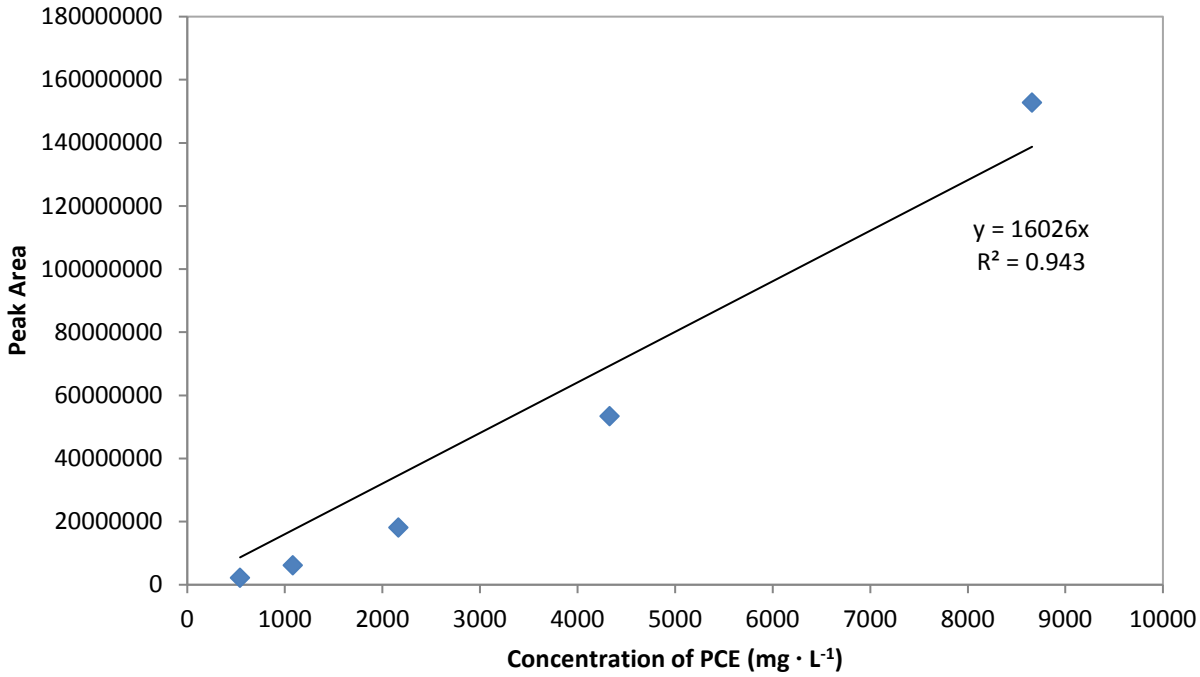

Figure 38. Calibration curve for methanol extraction of ampules using GC/FID

7.4.Methanol Extraction for Ampules

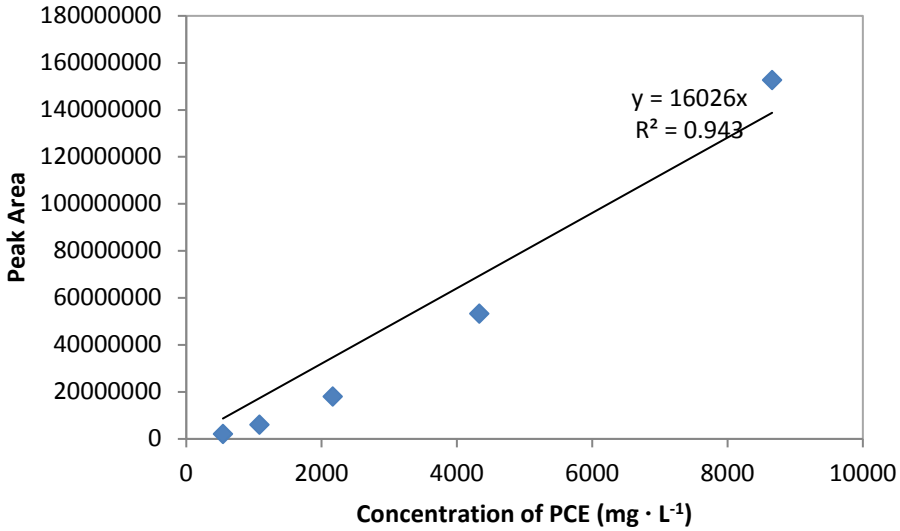

Figure 39. Calibration curve for methanol extraction for ampules.

7.5.Methanol Extraction for Headspace Vials

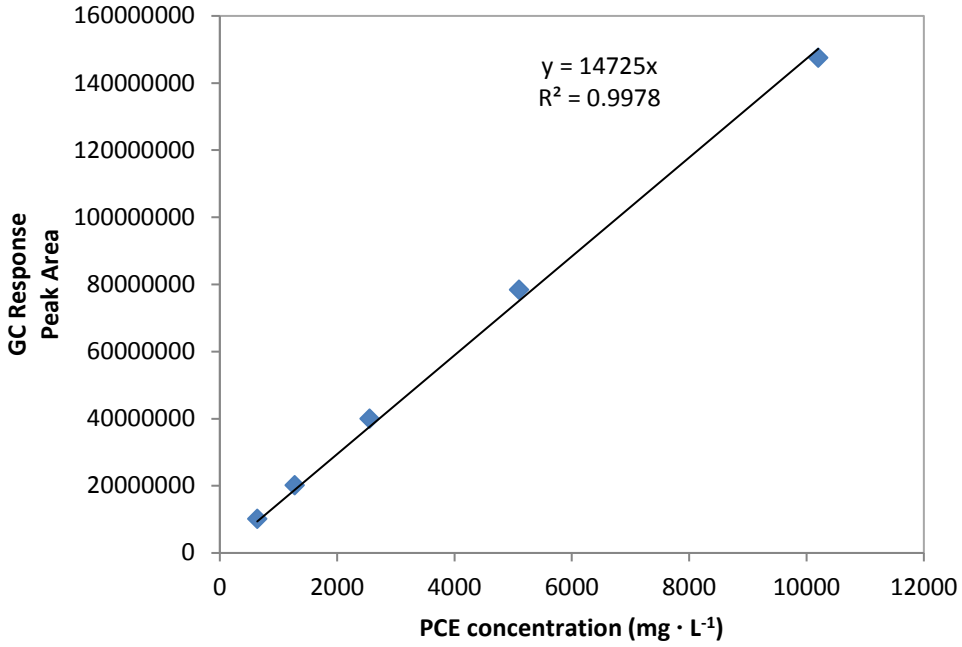

Figure 40. Calibration curve for methanol extraction for headspace vials.

7.6.T-Test: Two-sample assuming Equal Variances

7.6.1. Stability Experiment comparing 1, 10 and 100 mg·L^{-1} PCE concentration within the vials

t-Test: Two-Sample Assuming Equal Variances

Comparing 1 mg/L and 10mg/L

	Variable 1	*Variable 2*
Mean	0.390546	0.46912
Variance	7.88E-06	0.000845
Observations	2	3
Pooled Variance	0.000566	
Hypothesized Mean Difference	0	
df	3	
t Stat	-3.61791	
P(T<=t) one-tail	0.01815	
t Critical one-tail	2.353363	
P(T<=t) two-tail	0.036301	
t Critical two-tail	3.182446	

Reject the null - these are not equal

t-Test: Two-Sample Assuming Equal Variances

Comparing 1 mg/L and 100mg/L

	Variable 1	*Variable 2*
Mean	0.390546	0.291488
Variance	7.88E-06	0.000438
Observations	2	3
Pooled Variance	0.000294	
Hypothesized Mean Difference	0	
df	3	
t Stat	6.324509	
P(T<=t) one-tail	0.003996	
t Critical one-tail	2.353363	
P(T<=t) two-tail	0.007991	
t Critical two-tail	3.182446	

Reject Null

t-Test: Two-Sample Assuming Equal Variances

Comparing 10mg/L and 100mg/L

	Variable 1	*Variable 2*
Mean	0.46912	0.291488
Variance	0.000845	0.000438
Observations	3	3
Pooled Variance	0.000641	
Hypothesized Mean Difference	0	
df	4	
t Stat	8.590506	
P(T<=t) one-tail	0.000504	
t Critical one-tail	2.131847	
P(T<=t) two-tail	0.001009	
t Critical two-tail	2.776445	

Reject Null

7.6.2. Sorption study of Fiber Filters comparing control, glass fiber filters and PTFE filters

Table 20. Results from t-Test analysis using Two Sample Assuming Equal Variances

Control and PTFE Fiber Filter

t-Test: Two-Sample Assuming Equal Variances

	Control	*PTFE Fiber Filter*
Mean	27.00952	22.11925
Variance	1.045864	3.953073
Observations	3	3
Pooled Variance	2.499468	
Hypothesized Mean Difference	0	
df	4	
t Stat	3.78839	
P(T<=t) one-tail	0.009648	
t Critical one-tail	2.131847	
P(T<=t) two-tail	0.019296	
t Critical two-tail	2.776445	

Control and Glass Fiber Filter

t-Test: Two-Sample Assuming Equal Variances

	Control	*Glass Fiber Filter*
Mean	27.00952	25.15178
Variance	1.045864	1.135245
Observations	3	3
Pooled Variance	1.090554	
Hypothesized Mean Difference	0	
df	4	
t Stat	2.178749	
P(T<=t) one-tail	0.047439	
t Critical one-tail	2.131847	
P(T<=t) two-tail	0.094877	
t Critical two-tail	2.776445	

8. APPENDIX B – CALCULATIONS AND DERIVATIONS

8.1.Stability Experiment

Calculations for Stability Experiment - Conducted on 8/27/14

Calculation for High Concentration 100mg/L

$$C_{PCE} := 100\ \frac{mg}{L}$$

$$\rho_{PCE} := 1.62\ \frac{gm}{cm^3}$$

$$V_{water} := 15\ mL$$

$$V_{PCE\_water} := \frac{C_{PCE}}{\rho_{PCE}} \cdot V_{water} = \left(9.259 \cdot 10^{-4}\right)\ mL$$

Finding the amount of PCE to be added to the 4000uL Acetone/PCE solution to acheive 0.925uL of PCE/100uL of Methanol/PCE solution

$$V_{solution} := 0.1\ mL$$

$$V_{stock\_solution} := 4.0\ mL$$

$$V_{PCE\_Acetone} := \frac{V_{PCE\_water}}{V_{solution}} \cdot V_{stock\_solution} = 0.037\ mL$$

Dilution to get to 10mg/L and 1mg/L was conducted through dilutions of the 100mg/L solution. 400 uL of Stock solution into 3600uL of Acetone (D1)

$$C_{stock\_solution} := \frac{V_{PCE\_Acetone}}{V_{stock\_solution}} \cdot \rho_{PCE} = \left(1.5 \cdot 10^4\right)\ \frac{mg}{L}$$

$$D_1 := \frac{C_{stock\_solution}}{3.6\ mL} \cdot 0.4\ mL = \left(1.667 \cdot 10^3\right)\ \frac{mg}{L}$$

Concentration of D1 when 100uL are transferred to 15mL water solution, Dilution 1 (~10 mg/L)

$$C_{D1} := D_1 \cdot \frac{0.1\ mL}{15\ mL} = 11.111\ \frac{mg}{L}$$

$$D_2 := \frac{D_1}{3.6\ mL} \cdot 0.4\ mL = 185.185\ \frac{mg}{L}$$

Concentration of D2 when 100uL are transferred to 15mL water soltuion, Dilution 2 (~1 mg/L)

$$C_{D2} := D_2 \cdot \frac{0.1\ mL}{15\ mL} = 1.235\ \frac{mg}{L}$$

8.2.Headspace vial Experiment

8.2.1. Water Content Conversion Calculations

Converting Water Content (g/g) to volume of water within Headspace Vials and Ampules

Lab Notes 10/23/14 Headspace data raw and calc

LGS water content conversion:

$w_{LGS} := 0.434 \cdot \frac{gm}{gm}$

$\rho_{water} := 1000 \ \frac{kg}{m^3}$

$M_{LGS} := 33.12 \ gm$

$M_{water\_LGS} := w_{LGS} \cdot M_{LGS} = 0.014 \ kg$

$V_{water\_LGS} := \frac{M_{water\_LGS}}{\rho_{water}} = 0.014 \ L$

$M_{PCE\_LGS} := 0.436667 \ gm$

$C_{PCE\_LGS} := \frac{M_{PCE\_LGS}}{V_{water\_LGS}} = (3.038 \cdot 10^4) \ \frac{mg}{L}$

$V_{Extract} := V_{water\_LGS} + 80 \ mL = 0.094 \ L$

$C_{PCE\_LGS\_Extract} := \frac{M_{PCE\_LGS}}{V_{Extract}} = (4.627 \cdot 10^3) \ \frac{mg}{L}$

$Ratio_{MeOH\_Water} := \frac{V_{water\_LGS}}{80 \ mL} = 0.18$

Soil A water content conversion:

$w_{soilA} := 0.262 \cdot \frac{gm}{gm}$

$\rho_{water} := 1000 \ \frac{kg}{m^3}$

$M_{soilA} := 38.945 \ gm$

$M_{water\_soilA} := w_{soilA} \cdot M_{soilA} = 0.01 \ kg$

$V_{water\_soilA} := \frac{M_{water\_soilA}}{\rho_{water}} = 0.01 \ L$

$M_{PCE\_soilA} := 0.5 \ gm$

$C_{PCE\_soilA} := \frac{M_{PCE\_soilA}}{V_{water\_soilA}} = (4.9 \cdot 10^4) \ \frac{mg}{L}$

$$V_{Extract} := V_{water\_soilA} + 80\ mL$$

$$C_{PCE\_soilA\_Extract} := \frac{M_{PCE\_soilA}}{V_{Extract}} = (5.543 \cdot 10^{3})\ \frac{mg}{L}$$

$$Ratio_{MeOH\_Water} := \frac{V_{water\_soilA}}{80\ mL} = 0.128$$

Soil D water content conversion:

$$w_{soilD} := 0.358 \cdot \frac{gm}{gm}$$

$$\rho_{water} := 1000\ \frac{kg}{m^{3}}$$

$$M_{soilD} := 35.59\ gm$$

$$M_{water\_soilD} := w_{soilD} \cdot M_{soilD} = 0.013\ kg$$

$$V_{water\_soilD} := \frac{M_{water\_soilD}}{\rho_{water}} = 0.013\ L$$

$$M_{PCE\_soilD} := 0.45\ gm$$

$$C_{PCE\_soilD} := \frac{M_{PCE\_soilD}}{V_{water\_soilD}} = (3.532 \cdot 10^{4})\ \frac{mg}{L}$$

$$V_{Extract} := V_{water\_soilD} + 80\ mL$$

$$C_{PCE\_soilD\_Extract} := \frac{M_{PCE\_soilD}}{V_{Extract}} = (4.852 \cdot 10^{3})\ \frac{mg}{L}$$

$$Ratio_{MeOH\_Water} := \frac{V_{water\_soilD}}{80\ mL} = 0.159$$

8.2.2. Calculations for estimating saturation of soils

The definition of water saturation of soils (S_w):

$$S_w = \frac{V_w}{V_T} = \frac{\theta}{\phi}$$

Where, V_w is the volume of water (L^3), V_T is the total volume (L^3), θ is the water content ($L^3 \cdot L^{-3}$) and ϕ is the porosity ($L^3 \cdot L^{-3}$). Porosity was calculated using the following equation:

$$\phi = 1 - \frac{\rho_b}{\rho_p}$$

Where, ρ_b is bulk density and ρ_p is the particle density which was assumed to be 2.65 $g \cdot cm^{-3}$.

Using the measured water content and calculated porosity (Appendix D) during experimental setup the saturation of the soils are able to be calculated. Saturated soil values are found in Table 21.

Table 21. Values used to estimate saturated soil for each field soil

Soil Type	Bulk Density ρ_b	Particle Density ρ_p	Porosity ϕ	Water Content θ	Water Saturation of Soil S_w
	($g \cdot mL^{-1}$)	($g \cdot cm^{-3}$)	(dimensionless)	(dimensionless)	(dimensionless)
LGS	1.59	2.65	0.40	0.43	1.09
Soil A	2.06	2.65	0.22	0.26	1.18
Soil B	1.92	2.65	0.28	0.33	1.18
Soil C	1.70	2.65	0.36	0.43	1.19
Soil D	1.79	2.65	0.32	0.36	1.11

8.2.3. Calibration Curve

Calculations for Calibration Curve for Headspace Vials Experiment from 10/17/14

$M_{vial} := 5.7731\ gm$

$M_{vial\_MeOH} := 8.6776\ gm$

$M_{vial\_PCE} := 8.7552\ gm$

$M_{PCE} := M_{vial\_PCE} - M_{vial\_MeOH} = (7.76 \cdot 10^{-5})\ kg$

$\rho_{PCE} := 1620\ \frac{mg}{cm^3}$ $V_{MeOH} := 3.950\ mL$

$V_{solution} := V_{MeOH} + \frac{M_{PCE}}{\rho_{PCE}} = 3.998\ mL$

Volume of PCE in the PCE /Methanol solution

$V_{PCE} := \frac{M_{PCE}}{V_{solution} \cdot \rho_{PCE}} = 0.012\ \frac{mL}{mL}$ **PCE/ PCE-Methanol Solution**

Calculation for determining actual concentration of PCE injected into 4mL vials containing 2mL of Water

$V_{water} := 2\ mL$ $V_{extracted\_solution} := 0.01\ mL$

$C_{PCEinWater} := \frac{V_{PCE} \cdot V_{extracted\_solution}}{V_{water}} \cdot \rho_{PCE} = 97.051\ \frac{mg}{L}$

8.2.4. Derivation for Partitioning Equation

The conservation of mass equation is defined as:

$$M_{total} = M_g + M_w$$

Where M_{total} is the total mass within the system (M), M_g is the mass within the gas phase (M), and M_w is the mass within the water phase (M). The total mass is known, but with two unknowns another equation is needed to solve for the mass in the two different phases. The Henry's dimensionless equation will be used to help find the two unknowns

Definition of Henry's dimensionless coefficient (H_D):

$$H_D = \frac{\frac{M_g}{V_g}}{\frac{M_w}{V_w}}$$

Where, *M* is the mass (M), *V* is the volume (L^3). The volume of the air and water are known. Reordering the equation to separate the two phases.

$$\frac{M_g}{V_g} = \frac{M_w}{V_w} \cdot H_D$$

And redefining the mass in the gas phase in terms of total mass and mass in the water phase minimizes our unknowns to only one variable.

$$\frac{M_{total} - M_w}{V_g} = \frac{M_w}{V_w} \cdot H_D$$

$$M_w = \frac{M_{total}}{\left(\left(\frac{V_g}{V_w} \cdot H_D\right) + 1\right)}$$

8.2.5. Concentration of Control

Calculations for Control for Headspace Vial Experiment

Lab notes 10/24/14

$Mass.vial\_MeOH := 8.6685\ gm$
$Mass.vial\_PCE := 8.8173\ gm$

$M.PCE := Mass.vial\_PCE - Mass.vial\_MeOH = (1.488 \cdot 10^{-4})\ kg$

$\rho.PCE := 1620\ \frac{mg}{cm^3}$ $V.MeOH := 3.910\ mL$

$V.solution := V.MeOH + \frac{M.PCE}{\rho.PCE} = 0.004\ L$

$V.water := 36.90\ mL$
$PCE\_solubility := 200\ \frac{mg}{L}$

$C.Stock := \frac{M.PCE}{V.solution} = (3.718 \cdot 10^{4})\ \frac{mg}{L}$

$C.water := \frac{C.Stock}{V.water} \cdot 0.1\ mL = 100.766\ \frac{mg}{L}$

$Solubility\_Percent := \frac{C.water}{PCE\_solubility} = 0.504$

8.3.Batch Sorption Study for Field Soil - PCE concentration in vials

8.3.1. PCE Concentration in Vials

Methanol and PCE solution for Batch Sorption Experiment for Field Soils
Calculating Injection concentration from Stock Solution of 90mg/L

$M_{vial} := 5.5887\ gm$

$M_{vial\_MeOH} := 8.4780\ gm$

$M_{vial\_PCE} := 8.8347\ gm$

$M_{PCE} := M_{vial\_PCE} - M_{vial\_MeOH} = (3.567 \cdot 10^{-4})\ kg$

$\rho_{PCE} := 1620\ \frac{mg}{cm^3}$ $V_{MeOH} := 3.778\ mL$

$V_{solution} := V_{MeOH} + \frac{M_{PCE}}{\rho_{PCE}} = 3.998\ mL$

Volume of PCE in the PCE /Methanol solution

$$V_{PCE} := \frac{M_{PCE}}{V_{solution} \cdot \rho_{PCE}} = 0.055 \ \frac{mL}{mL}$$

PCE/ PCE-Methanol Solution

Calculation for determining actual concentration of PCE injected into vials containing 10mL of Water

$V_{water} := 10 \ mL \qquad V_{extracted\_solution} := 0.01 \ mL$

$$C_{PCEinWater} := \frac{V_{PCE} \cdot V_{extracted\_solution}}{V_{water}} \cdot \rho_{PCE} = 89.215 \ \frac{mg}{L}$$

Highest Concentration ~90mg/L

Calculations for dilutions (~30 mg/L, 10 mg/L, 3.33 mg/L, 1.11 mg/L)

$$D_1 := \frac{V_{PCE} \cdot 1.0 \ mL}{3.0 \ mL} = 0.018$$

$$C_{D1} := \frac{D_1 \cdot V_{extracted\_solution}}{V_{water}} \cdot \rho_{PCE} = 29.738 \ \frac{mg}{L}$$

$$D_2 := \frac{D_1 \cdot 1.0 \ mL}{3.0 \ mL} = 0.006$$

$$C_{D2} := \frac{D_2 \cdot V_{extracted\_solution}}{V_{water}} \cdot \rho_{PCE} = 9.913 \ \frac{mg}{L}$$

$$D_3 := \frac{D_2 \cdot 1.0 \ mL}{3.0 \ mL} = 0.002$$

8.3.2. Estimating K_d value using K_{oc} and f_{oc}

Using the LFER for natural organic carbon –water partition coefficient and octanol-water partition constant (Schwarzenbach et al. 2003):

$$\log(K_{oc}) = a \log(K_{ow}) + b \qquad (14)$$

Where, *a* is the slope and *b* is the intercept which is derived from groups of organic compounds. The contaminant of concern is PCE, an apolar halocarbon (where one or

more carbon atoms are linked by covalent bonds with one or more halogen atoms), values for a = 0.57 and b = 0.66, and log K_{ow} = 2.88.

$$K_{oc} = 10^{[0.57(2.88)+0.66]}$$

$$K_{oc} = 10^{2.3016}$$

Using Equation 2, apply the calculated K_{oc} value and the f_{oc} values from Table 8 to calculate the K_d value for each field soil:

$$K_{\mathrm{d}} = 10^{2.3016} f_{oc} \qquad (15)$$

8.3.3. Converting Henry's constant to Henry's dimensionless

Henry's constant (*H*) for PCE = 0.017atm·m^3·mol^{-1} as defined by Pankow and Cherry (1996) was used to estimate partitioning of PCE. To convert Henry's constant to Henry's dimensionless (H_D) form the following equation was used:

$$H_D = \frac{H}{RT}$$

Where, the gas constant, R= 0.080206 L·atm·mol^{-1}·K^{-1} and temperature, T, is assumed to be 298.15 K. The conversion from Henry's constant to dimensionless produced the value H_D = 0.712, and was used throughout this research.

8.3.4. Calculating PCE mass sorbed onto field soils using Henry's dimensionless, H_D = 0.712

Calculating Mass of True water Concentration using Henry's Dimensionless number-
(Cali PT Graphs)

$C_{injected\_theoretical} := 89.2286 \ \frac{mg}{L}$ $\quad$ $H_D := 0.712$

$M_{total} := C_{injected\_theoretical} \cdot 10 \ mL$ $\quad$ $V_{water} := 10 \ mL$

$M_{total} = 0.89229 \ mg$ $\quad$ $V_{headspace\_vial} := 20.845 \ mL$

$$V_{soil} := \frac{5 \ gm}{2.65 \ \frac{gm}{cm^3}} = 1.88679 \ mL$$

$$V_{gas\_phase} := V_{headspace\_vial} - V_{water} - V_{soil} = 8.95821 \ mL$$

$$M_{water} := \frac{M_{total}}{\frac{V_{water}}{V_{gas\_phase}} \cdot H_D + 1} = 0.49715 \ mg$$

Calculating Mass of Gas using Henry's Dimensionless 0.712 for (H=0.712 Tab comparing SJ5 data)

$C_{t\_water} := 51.7759855 \ \frac{mg}{L}$

$M_{total\_injected} := 0.892155 \ mg$ **From total Mass injected PCE (mg)**

$M_{t\_water} := C_{t\_water} \cdot 10 \ mL = 0.51776 \ mg$ **Multiplying by how much volume of water was in vial**

$M_{gas} := \frac{V_{gas\_phase} \cdot H_D \cdot M_{t\_water}}{V_{water}} = 0.33024 \ mg$

$M_{sorbed} := M_{total\_injected} - M_{t\_water} - M_{gas} = 0.04416 \ mg$

$C_{soil} := \frac{M_{sorbed}}{5 \ gm} = 8.83106 \ \frac{mg}{kg}$

8.3.5. Henry's dimensionless constant corrected for salt

To calculate the effects of salt on the partitioning of PCE from the different phases we accounted for salting-out effects. The range of salt water concentration is between 100 $mg \cdot L^{-1}$ and >50,000$mg \cdot L^{-1}$, where salt water concentrations found in the ocean fall within approximately 36,000$m \cdot L^{-1}$ (Division of Water Quality 2010, Greenberg et al. 1973). To calculate for the "salting out" effect we applied the Henry's dimensionless constant used to the following equation found in Schwarzenbach (2003):

$$K_{ilw,salt} = K_{il} \cdot 10^{K_i^s [salt]_{total}}$$

Where, $K_{ilw,salt}$ is the partitioning coefficient of a compound (i) in a water to liquid interaction that accounts for salinity, K_{ilw} is the partitioning coefficient of the compound in water to a liquid (l) with the liquid in our case being air, K_i^s is the *Setschenow* or salting constant (unit M^{-1}) and $[salt]_{total}$ is the total molar salt concentration. Here we assume that the $K_i^s = 0.19$ (assuming all salt ions are NaCl ions and since benzene is the

closest compound to PCE due to being non-polar, small in size, and relatively stable compound). The K_{il} for PCE was determined to be 0.712 since K_{il} and Henry's dimensionless (H_D) are interchangeable. Lastly, we will assume the water is the same concentration as ocean salt concentration where $[salt]_{total}$ = 0.615 M

$$K_{ilw,salt} = 0.712 \cdot 10^{(0.19 \cdot 0.615)}$$

$$K_{ilw,salt} = 0.932$$

The value calculated is for the extreme condition of ocean salt water concentration. We see that there is an increase in the partitioning coefficient but for our case we do not expect waters to get to that high of concentrations and therefore will most likely not expect to see that drastic of a change in the partitioning coefficient.

8.4. Ampules Calibration Curve

Calculations for Calibration Curve for Closed Ampules on the GC/ECD analysis

Stock solution from 3/5/15

$M_{vial} := 5.5846\ gm$

$M_{vial\_MeOH} := 8.6356\ gm$

$M_{vial\_PCE} := 8.6766\ gm$

$M_{PCE} := M_{vial\_PCE} - M_{vial\_MeOH} = (4.1 \cdot 10^{-5})\ kg$

$\rho_{PCE} := 1620\ \frac{mg}{cm^3}$ $V_{MeOH} := 3.975\ mL$

$V_{solution} := V_{MeOH} + \frac{M_{PCE}}{\rho_{PCE}} = 4\ mL$

Volume of PCE in the PCE /Methanol solution

$V_{PCE} := \frac{M_{PCE}}{V_{solution} \cdot \rho_{PCE}} = 0.006\ \frac{mL}{mL}$ **PCE/ PCE-Methanol Solution**

$C_{stock} := \frac{M_{PCE}}{V_{solution}} = (1.025 \cdot 10^4)\ \frac{mg}{L}$

Calculations for dilutions

$$D_1 := \frac{C_{stock} \cdot 0.040\ mL}{4.000\ mL} = 102.492\ \frac{mg}{L}$$ **Also Known as C0**

$$C_1 := \frac{D_1 \cdot 1.0\ mL}{2.0\ mL} = 51.246\ \frac{mg}{L}$$

$$C_2 := \frac{C_1 \cdot 1.0\ mL}{2.0\ mL} = 25.623\ \frac{mg}{L}$$

$$C_3 := \frac{C_2 \cdot 1.0\ mL}{2.0\ mL} = 12.812\ \frac{mg}{L}$$

$$C_4 := \frac{C_3 \cdot 1.0\ mL}{2.0\ mL} = 6.406\ \frac{mg}{L}$$

$$C_5 := \frac{C_4 \cdot 1.0\ mL}{2.0\ mL} = 3.203\ \frac{mg}{L}$$

$$C_6 := \frac{C_5 \cdot 1.0\ mL}{2.0\ mL} = 1.601\ \frac{mg}{L}$$

$$C_7 := \frac{C_6 \cdot 1.0\ mL}{2.0\ mL} = 0.801\ \frac{mg}{L}$$

8.5.Calibration curve for methanol extraction for headspace vials

Calculations for Calibration Curve for Headspace vials extraction on the GC/FID

Stock solution from 5/13/15

$M.vial := 5.5234\ gm$

$M.vial\_MeOH := 8.6286\ gm$

$M.vial\_PCE := 8.6694\ gm$

$M.PCE := M.vial\_PCE - M.vial\_MeOH = (4.08 \cdot 10^{-5})\ kg$

$\rho.PCE := 1620\ \frac{mg}{cm^3}$ $V.MeOH := 3.975\ mL$

$V.solution := V.MeOH + \frac{M.PCE}{\rho.PCE} = 4\ mL$

Volume of PCE in the PCE/Methanol solution

$V.PCE := \frac{M.PCE}{V.solution \cdot \rho.PCE} = 0.006\ \frac{mL}{mL}$ **PCE/PCE-Methanol Solution**

$C.stock := \frac{M.PCE}{V.solution} = (1.02 \cdot 10^4)\ \frac{mg}{L}$

Calculations for dilutions for calibration curve

$C.2 := \frac{C.stock \cdot 1.0\ mL}{2.0\ mL} = (5.1 \cdot 10^3)\ \frac{mg}{L}$

$C.3 := \frac{C.2 \cdot 1.0\ mL}{2.0\ mL} = (2.55 \cdot 10^3)\ \frac{mg}{L}$

$C.4 := \frac{C.3 \cdot 1.0\ mL}{2.0\ mL} = (1.275 \cdot 10^3)\ \frac{mg}{L}$

$C.5 := \frac{C.4 \cdot 1.0\ mL}{2.0\ mL} = 637.47\ \frac{mg}{L}$

9. APPENDIX C – NUMERICAL MODEL

9.1.Conversion to dimensionless form

For the numerical model to properly solve within the PDE solve block all parameters must be converted to a dimensionless form. The following parameters that were converted were time and the degradation coefficient.

9.1.1. Time

First, to convert time, t (T) to dimensionless time, τ (dimensionless), and the following equation was used:

$$\tau = t\left(\frac{D_{PCE}\ *}{L_C^2}\right)$$

Where, L_C (L) is the column length, and D ($L^2 \cdot T^{-1}$) is the effective diffusion. To get the proper output, the equation is rearranged and the dimensionless time is converted back to time, one just rearranges the equation.

9.1.2. Degradation coefficient

To convert the degradation coefficient, k (T^{-1}) to dimensionless degradation coefficient, D_2 (dimensionless), the following equation was used:

$$D_2 = \frac{L_C}{D_{PCE}} k_{PCE}$$

Where the variable definitions and dimensions are the same as above in the Time section.

9.2.Relating retardation factor and the Langmuir equation

The following definitions for the partitioning coefficient (Equation 1), the Langmuir equation (Equation 3) and retardation factor (Equation 5) to get to the retardation factor as a function of the aqueous concentration as shown in Equation 12.

Rearranging Equation 1, we have a new definition for K_d:

$$K_d = \frac{C_s}{C_w} \tag{1a}$$

Starting with Equation 4, and rearranging the equation in terms of $C_s \cdot C_w^{-1}$:

$$C_s = \frac{\Gamma_{max} K_L C_w}{1 + K_L C_w} \tag{4}$$

$$C_s(1 + K_L C_w) = \Gamma_{max} K_L C_w \tag{4a}$$

$$\frac{C_s}{C_w} = \frac{\Gamma_{max} K_L}{1 + K_L C_w} \tag{4b}$$

Apply Equation 1a to Equation 4b:

$$K_d = \frac{\Gamma_{max} K_L}{1 + K_L C_w} \tag{4c}$$

Then insert Equation 4c into Equation 3:

$$R = 1 + \frac{\rho_b}{\phi}\left(\frac{\Gamma_{max} K_L}{1 + K_L C_w}\right) \tag{12}$$

10. APPENDIX D – RAW DATA

10.1. Bulk density

Soil Type	ID#	Weight of vials (g)	Weight of vial with Soil (g)	Weight of vial with water added (g)	Weight of soil (g)	Weight of water added (g)	Water Difference (mL)	Bulk Density (g/mL)	Average (g/mL)	Std Dev (g/mL)
LGS	1	16.3	23.99	42.04	7.69	18.05	4.75	1.61894737	1.591445	0.039408
LGS	2	16.57	25.6	42.52	9.03	16.92	5.88	1.53571429		
LGS	3	16.49	26.37	43.07	9.88	16.7	6.1	1.61967213		
LGS	4	16.38	21.71	-	5.33	-	-	-		
Soil A	1	16.76	25.48	44.21	8.72	18.73	4.07	2.14250614	2.063769	0.095623
Soil A	2	16.32	25.31	43.45	8.99	18.14	4.66	1.92918455		
Soil A	3	16.32	25.18	43.8	8.86	18.62	4.18	2.11961722		
Soil A	4	16.28	22.61	42.78	6.33	20.17	2.63	2.40684411		
Soil B	1	16.71	23.03	42.19	6.32	19.16	3.64	1.73626374	1.916122	0.154182
Soil B	2	16.43	24.54	43.07	8.11	18.53	4.27	1.89929742		
Soil B	3	16.44	23.37	42.89	6.93	19.52	3.28	2.11280488		
Soil B	4	16.35	21.45	42.12	5.1	20.67	2.13	2.3943662		
Soil C	1	16.68	23.69	42.65	7.01	18.96	3.84	1.82552083	1.695269	0.104175
Soil C	2	16.34	26.25	42.74	9.91	16.49	6.31	1.57052298		
Soil C	3	16.28	27.01	43.46	10.73	16.45	6.35	1.68976378		
Soil C	4	16.71	23.02	42.13	6.31	19.11	3.69	1.7100271		
Soil D	1	16.37	26.66	42.61	10.29	15.95	6.85	1.50218978	1.79344	0.220573
Soil D	2	16.35	25.23	43.21	8.88	17.98	4.82	1.84232365		
Soil D	3	16.81	24.77	43.66	7.96	18.89	3.91	2.03580563		
Soil D	4	16.56	22.56	41.75	6	19.19	3.61	1.66204986		
WATER		16.56		39.36		22.8				

10.2. Water Content

Soil Moisture Content			10/23-24/14				
				After Baking			
Soil Type	ID #	Weight of jar+lid (g)	Weight of jar+lid+soil (g)	weight of jar +lid - water (g)	Soil +water Mass (g)	Water mass (g)	water content (g/g)
LGS	1	146.88	165.34	157.27	18.46	8.07	0.437161
LGS	2	154.71	177.67	167.6	22.96	10.07	0.438589
LGS	3	145.73	176.68	163.17	30.95	13.51	0.436511
LGS	4	165.4	186.18	177.35	20.78	8.83	0.424928
Soil A	1	137.36	150.84	147.26	13.48	3.58	0.265579
Soil A	2	140.8	121.83	148.43	-	-	-
Soil A	3	135.35	155.9	150.5	20.55	5.4	0.262774
Soil A	4	162.61	210.34	198.05	47.73	12.29	0.25749
Soil B	1	150.02	164.27	159.6	14.25	4.67	0.327719
Soil B	2	145.28	161.77	156.38	16.49	5.39	0.326865
Soil B	3	149.79	164.62	159.7	14.83	4.92	0.33176
Soil B	4	165.68	179.49	175.04	13.81	4.45	0.32223
Soil C	1	148.47	163.33	156.89	14.86	6.44	0.433378
Soil C	2	132.97	157.19	146.74	24.22	10.45	0.431462
Soil C	3	134.2	160.48	149.32	26.28	11.16	0.424658
Soil C	4	164.95	188.45	178.54	23.5	9.91	0.421702
Soil D	1	146.08	163.9	157.56	17.82	6.34	0.35578
Soil D	2	150.14	170.99	163.49	20.85	7.5	0.359712
Soil D	3	150.96	172.69	164.88	21.73	7.81	0.359411
Soil D	4	163.57	179.87	174.06	16.3	5.81	0.356442

10.3. Headspace Vial

Headspace Experiment Setup				10/23-24/14							
Soil	Vol Type	ID #	Weight of Vial +Glass Beads +Water (g)	Weight of vial with PCE (g)	Weight of vial with soil (g)	Mass of PCE (g)	Vol of PCE (µL)	Mass of Soil and Water added (g)		Estimated volume of MeOH (L)	MeOH (mL)
LGS	1	1	32.08	32.59	54.98	0.51	314.8148	22.39		0.084584615	84.58462
LGS	1	2	33.51	34.05	57.82	0.54	333.3333	23.77		0.088953846	88.95385
LGS	1	3	32.05	32.51	55.52	0.46	283.9506	23.01		0.085415385	85.41538
LGS	2	1	41.75	42.26	93.4	0.51	314.8148	51.14		0.143692308	143.6923
LGS	2	2	42.61	43.19	96	0.58	358.0247	52.81		0.147692308	147.6923
LGS	2	3	41.49	41.98	92.2	0.49	302.4691	50.22		0.141846154	141.8462
LGS	3	1	52.79	53.24	137.75	0.45	277.7778	84.51		0.211923077	211.9231
LGS	3	2	53.83	54.28	136.94	0.45	277.7778	82.66		0.210676923	210.6769
LGS	3	3	54.45	54.93	138.2	0.48	296.2963	83.27		0.212615385	212.6154
Soil A	2	1	42.28	42.8	100.91	0.52	320.9877	58.11		0.155246154	155.2462
Soil A	2	2	42.46	43	102.73	0.54	333.3333	59.73		0.158046154	158.0462
Soil A	2	3	42.72	43.18	102.93	0.46	283.9506	59.75		0.158353846	158.3538
Soil B	2	1	42.41	42.85	98.35	0.44	271.6049	55.5		0.151307692	151.3077
Soil B	2	2	-	-	97.51	-	-	-		0.150015385	150.0154
Soil B	2	3	42.01	42.48	97.11	0.47	290.1235	54.63		0.1494	149.4
Soil C	2	1	42.34	42.81	93.72	0.47	290.1235	50.91		0.144184615	144.1846
Soil C	2	2	41.48	41.93	92.24	0.45	277.7778	50.31		0.141907692	141.9077
Soil C	2	3	42.76	43.21	93.65	0.45	277.7778	50.44		0.144076923	144.0769
Soil D	2	1	42.42	42.9	98.34	0.48	296.2963	55.44		0.151292308	151.2923
Soil D	2	2	42.34	42.83	97.61	0.49	302.4691	54.78		0.150169231	150.1692
Soil D	2	3	42.32	42.76	98.17	0.44	271.6049	55.41		0.151030769	151.0308

10.4. Ampules

Closed Glass Ampules							
Soil Type	ID #	Weight of vial + GB +water (g)	Weight of vial with PCE (g)	Weight of vial with added Soil (g)	Mass of PCE (g)	Volume of PCE (µL)	Mass of Soil+Water (g)
LGS	1	18.52	18.86	51.64	0.34	209.8765	32.78
LGS	2	18.58	19.07	52.61	0.49	302.4691	33.54
LGS	3	18.7	19.18	52.22	0.48	296.2963	33.04
Soil A	1	18.53	19.02	57.78	0.49	302.4691	38.76
Soil A	2	18.49	19.01	57.35	0.52	320.9877	38.34
Soil A	3	18.53	19.02	57.18	0.49	302.4691	38.16
Soil A	4	18.57	19.06	59.58	0.49	302.4691	40.52
Soil B	1	18.57	19.06	56.5	0.49	302.4691	37.44
Soil B	2	18.6	19.06	56.65	0.46	283.9506	37.59
Soil B	3	18.68	19.16	56.04	0.48	296.2963	36.88
Soil C	1	18.45	18.88	52.32	0.43	265.4321	33.44
Soil C	2	18.45	18.92	52.47	0.47	290.1235	33.55
Soil C	3	18.36	18.8	52.07	0.44	271.6049	33.27
Soil D	1	-	19	54.9	-	-	35.9
Soil D	2	18.42	18.89	53.91	0.47	290.1235	35.02
Soil D	3	18.51	18.94	54.79	0.43	265.4321	35.85

10.5. Tray used for Headspace Vial Storage

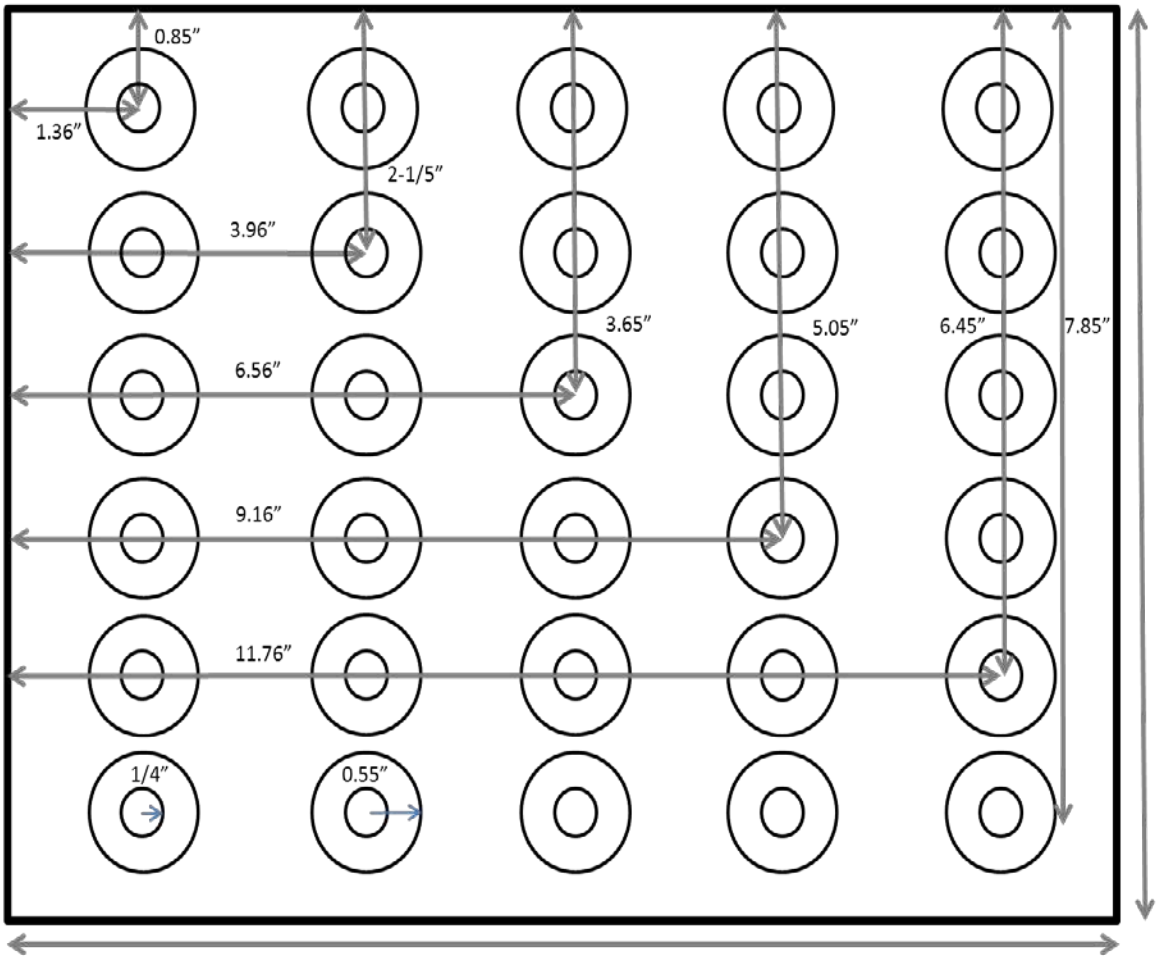

Side view – Tray